Enhancing Focused Ultrasound Therapy Using Nanoscale Agents

by

Moslem SadeghiGoughari

A thesis

presented to the University of Waterloo

in fulfillment of the

thesis requirement for the degree of

Doctor of Philosophy

in

Mechanical and Mechatronics Engineering department

Waterloo, Ontario, Canada, 2020

Examining committee membership:

The following served on the Examining Committee for this thesis. The decision of the Examining Committee is by majority vote.

External Examiner:	Tamie Poepping Associate Professor, Physics and Astronomy, University of Western Ontario
Supervisor(s):	Hyock Ju Kwon, and Soo Jeon Associate Professor, Dept. of Mechanical and Mechatronics Engineering, University of Waterloo
Internal Member:	John Wen Associate Professor, Dept. of Mechanical and Mechatronics Engineering, University of Waterloo
Internal Member:	James Tung Assistant Professor, Dept. of Mechanical and Mechatronics Engineering, University of Waterloo
Internal-External Member:	Alfred Yu Professor, Dept. of Electrical and Computer Engineering, University of Waterloo

I hereby declare that I am the sole author of this thesis. This is a true copy of the thesis, including any required final revisions, as accepted by my examiners.

I understand that my thesis may be made electronically available to the public.

Abstract

Focused ultrasound therapy, also known as high intensity focused ultrasound (HIFU), is a new energy-based method that uses ultrasonic energy to treat a range of health disorders and tumors. Despite the great potential for cancer treatment, the HIFU therapies for the breast and abdominal regions have not yet been granted FDA approval. One of major challenges of HIFU is the collateral damage due to the use of high ultrasonic energy during the thermal treatment. One promising strategy to enhance the heating mechanism of HIFU, and consequently to reduce its side effects, is to employ nanoparticles (NPs) as ultrasound absorption agents. To improve the therapeutic mechanism of NP-enhanced HIFU, it is essential to better understand the physics of the interaction between ultrasonic waves and NPs, and to clarify the effects of crucial parameters that can affect HIFU's heating mechanism.

This thesis includes experimental and numerical analyses i) to develop an analytical and numerical model that can simulate the physics of NP-enhanced HIFU, ii) to examine the effects of NP features, including the NP size and volume concentration, on the thermal mechanism of HIFU, and iii) to investigate the feasibility of using carbon nanotubes (CNTs) as new ultrasound absorption agents during HIFU to enhance heating at low powers.

In an effort to describe the physics of the interaction between ultrasonic waves and NPs, a set of HIFU equations governing the temperature variation during the NP-enhanced HIFU thermal procedure was derived based on the principle of energy conservation for heat transfer. The accuracy of the numerical model was verified by performing a series of HIFU experiments on phantoms embedded with magnetic NPs (MNPs). A quantitative comparison with experimental results demonstrated the potential of the numerical model to accurately predict the heating mechanism of HIFU mediated by NPs. The results showed that the transport processes that occur

at the boundaries between NPs and the surrounding medium play a major role in the temperature rise during NP-enhanced HIFU.

Based on the results from the numerical simulation and experiments, the effects of MNP features, including the size and volume concentration, on the HIFU heating mechanism were examined, and the performance of NPs was studied when exposed to ultrasonic fields at different ranges of powers and frequencies. It was proved that the increase of MNP size and volume concentration greatly enhanced the HIFU parameters; the effects of MNPs were further improved by increasing the power and frequency of the ultrasonic field.

In addition, an experimental analysis was conducted to assess the utility of CNTs as new ultrasound absorption agents during the HIFU thermal therapy using phantoms embedded with CNTs. The results showed the improving effects of CNTs on the HIFU thermal ablation became more pronounced by increasing the absorption rate of acoustic energy and temperature. It was also demonstrated that the effects of CNTs for increasing temperature were improved by amplifying the power and frequency, as well as by increasing the CNT concentration.

Acknowledgements

First and foremost, I would like to express my sincere appreciation to my supervisors Prof. Hyock-Ju Kwon and Prof. Soo Jeon for their inspirations and guidance throughout my PhD study. Their tolerance as a supervisor and never-ending energy for bringing novel technical ideas should be highly appreciated. So truly THANK YOU for everything.

I also would like to acknowledge the financial support provided by Government of Ontario through the Ontario Trillium Scholarship. I extend my appreciation to my internal members of my dissertation committee, Prof. Alfred Yu from Electrical and Computer Engineering Department, and Prof. John Wen and Prof. James Tung from Mechanical and Mechatronics Engineering Department. Each has been a great source of input and constructive comments. I highly appreciate my external examiner, Prof. Tamie Poepping from University of Western Ontario for reviewing my thesis.

My sincere thanks also go to my colleagues and friends Hassan Askari, Mehran Zamani, Ehsan Asadi, Yanjun Qian, Jeong-Woo Han, Salman Lari, Bonghun Shin, and Shiyi Yang for their support and assistance during my studies at the University of Waterloo.

I am also extremely grateful to my uncle, Sohrab Sadeghi, for all of his encouragement, support and inspirations. He has been my inspiration since I was a little boy, in so much of what I do, and what I desire to become. He has been really involved in every step of my PhD study with his endless support and encouraging words.

Finally, I would like to express my deepest gratitude to my parents, Jahangir SadeghiGoughari and Tarlan KarimiGoughari for their love, prayers, caring and continuing support for educating and preparing me for my future. My appreciation likewise extends to my

family members Naser, Mohsen, Fatemeh, Masoumeh, Leila, Maryam, Simin, Ebrahim, Davood, Hossein, and Vahid for true love and support throughout my life.

Dedication

To my beloved parents and my uncle, Sohrab.

Table of Contents

List of Tables

List of Figures

Nomenclature

B/A	nonlinearity parameter
C_b	specific heat of blood (J/kg.℃)
C_p	specific heat of medium (J/kg.℃)
$C_{P_{mn}}$	specific heat of medium embedded with NPs (J/kg.℃)
$C_{p_{NP}}$	specific heat of NPs (J/kg.℃)
c	speed of sound in medium (m/s)
c_l	local propagation speed of sound in medium (m/s)
c_{mn}	speed of sound in medium embedded with NPs (m/s)
c_{NP}	speed of sound in NPs (m/s)
f	frequency (Hz)
I	intensity (W/m^2)
I_{max}	maximum intensity (W/m^2)
I_o	initial intensity (W/m^2)
k	thermal conductivity of medium (W/m.℃)
k_{mn}	thermal conductivity of medium embedded with NPs (W/m.℃)
k_{NP}	thermal conductivity of NPs (W/m.℃)
p	acoustic pressure (Pa)
Q	rate of absorbed energy per unit volume (W/m^3)
q_c	rate of diffusion of energy per unit volume due to conduction (W/m^3)
q_h	rate of change in energy density of medium (W/m^3)
q_i	rate of heat generated per unit volume due to the intrinsic wave absorption mechanism (W/m^3)
q_p	rate of diffusion of energy per unit volume due to perfusion (W/m^3)

q_t	rate of heat generated per unit volume through the thermal wave absorption mechanism (W/m^3)
q_{tv}	rate of heat generated per unit volume due to the thermal and viscous absorption processes (W/m^3)
q_v	rate of heat generated per unit volume due to the viscous wave absorption mechanism (W/m^3)
q_w	rate of heat generated per unit volume due to the temperature gradient process around NPs (W/m^3)
R	radius of NPs (m)
r	radial axis (m)
$\vec{\boldsymbol{r}}$	spatial coordinate (m)
SAR	specific absorption rate (W/kg)
T	temperature (℃)
$\bar{T}$	mean temperature (℃)
T_b	temperature of blood flow (℃)
T_o	heat-wave parameter (℃)
t	time (s)
u	particle velocity (m/s)
w_b	perfusion rate of blood flow (1/s)
z	beam axis (m)
α	attenuation coefficient (Np/m)
α_a	absorption coefficient of medium (Np/m)
α_i	intrinsic absorption coefficient of medium embedded with NPs (Np/m)
α_{NP}	intrinsic absorption coefficient of NPs (Np/m)
α_o	absorption coefficient of medium at frequency of $f_o = 1\ MHz$ (Np/m)
α_t	thermal wave absorption coefficient (Np/m)

α_{tv}	absorption coefficient for the viscous and thermal processes (Np/m)
α_v	viscous wave absorption coefficient (Np/m)
β	coefficient of nonlinearity
ϑ_m	kinematic viscosity of medium (m^2/s)
γ	thermal expansion coefficient of medium (1/ K)
γ_{NP}	thermal expansion coefficient of NPs (1/ K)
ρ	density of medium (kg/m^3)
ρ_b	density of blood (kg/m^3)
ρ_{mn}	density of medium embedded with NPs (kg/m^3)
ρ_{NP}	density of NPs (kg/m^3)
φ	volume concentration of NPs
τ	KZK time (s)
ω	angular frequency (rad/s)

Chapter 1

Introduction

Focused ultrasound therapy, often referred to as high intensity focused ultrasound (HIFU), is a new type of noninvasive therapeutics which has been recognized for broad spectrum of treatments including thermal ablation of tumor [1–3], thrombolysis [4–6], kidney stone comminution [7–9], and drug delivery through sonoporation [10–12]. HIFU allows the local treatment of an abnormality inside the body by focusing ultrasonic beams from an extracorporeal source to the target area [13]. The main effect of ultrasound therapy is tissue heating, induced through the absorption of acoustic energy and its conversion to heat. During HIFU, the temperature at the focal region can effectively rise over 60℃, resulting in irreversible biological damages, such as necrosis and cell apoptosis [14]. Due to the non-invasive nature, HIFU can offer safer and lower-cost therapy with better precision and shorter recovery time, compared to invasive surgical approaches [1]. As a result, nowadays, the HIFU treatment guided by advanced imaging techniques has been applied to treat various benign and malignant tumors, including those of prostate [15–17], liver [18–20], breast [21–23], brain [24–26], bone [27–29], and kidney [30–32].

1.1. Motivation

Despite the great potential of HIFU for cancer treatment, there exist several challenges that impede its application to tumors of large size and highly vascularized structure [1]. First, since a single HIFU insonation ablates only a small portion of tumor, a number of focal applications are required to cover the entire tumor, thus the treatment time becomes longer as the size of tumor increases.

Furthermore, a few cancer cells may survive after the HIFU ablation in the spaces between the small focal regions [1]. On the other hand, tumors with highly vascularized structures or those that are formed in vascularized tissues tend to be more resistant to HIFU, as blood vessels can dissipate the generated heat [33, 34]. To reduce the treatment time and blood perfusion effects, it is necessary to make the deposition of acoustic energy at the targeted area as efficient as possible [35]. Traditionally, a high level of ultrasonic power is employed during the HIFU insonation to this end, however, it may cause several adverse effects such as the overheating of surrounding normal tissue and skin burns, as reported in several clinical studies [36, 37]. Due to these concerns, the HIFU therapies for the breast and abdominal regions have not been approved yet by the Food and Drug Administration (FDA) in the U.S [35].

One of the strategies that can decrease the likelihood of adverse effects of ultrasound heating is to adopt ultrasound absorption agents that make acoustic energy deposition at the tumor region more efficient [35, 38]. The use of ultrasound agents can enhance the heating mechanism of HIFU by increasing the conversion rate of acoustic energy to heat, and consequently reduce the concerns regarding the treatment time and blood perfusion effects. To this end, various materials have been considered, such as porphyrin [39], iodized oil [40], microbubbles [41], and most recently nanoparticles (NPs) [42]. Among them, NPs have gained increasing popularity due to their nanoscale-size effects and unique properties, allowing them to easily pass through capillaries to accumulate in a tumor site and consequently enhance hyperthermal mechanisms in tumorous tissues [43]. During the last decade, a number of studies have been reported on the potential benefits of gold NPs (AuNPs) [35, 44, 45], and magnetic NPs (MNPs) [42, 46, 47] to enhance the therapeutic mechanism of HIFU and consequently to reduce the adverse effects of HIFU. A

comprehensive review on the state of the art in the area of the NP-mediated HIFU will be provided in Chapter 2.

To improve the performance of NPs during the HIFU treatment for the purpose of making the thermal ablation process safer and more efficient, it is essential to clarify the effects of important factors regarding the NP-enhanced focused ultrasound therapy by understanding the interaction mechanism of ultrasonic waves with NPs. In an attempt to accomplish this objective, this research studies the physics of NP-enhanced HIFU and examines the influence of key parameters that can affect the therapeutic mechanism of HIFU.

1.2. Thesis Objectives

The principal objectives of this PhD work are to:

O1) Develop an analytical model that can precisely simulate the physics of interaction between ultrasonic waves and NPs, the consequent energy absorption, and the heat transfer during the NP-enhanced HIFU thermal procedure;

O2) Investigate the effects of NP features including the size and volume concentration, as well as the NP dose on the HIFU thermal mechanism;

O3) Demonstrate the feasibility of using carbon nanotubes (CNTs) as new ultrasound absorption agents for HIFU to enhance heating at low powers, and consequently to reduce the adverse effects of HIFU.

1.3. Contributions of the Field

Based on the experimental and numerical analyses presented in this PhD thesis, the main contributions of the field are as follows:

C1) An analytical modeling of the thermal mechanism of HIFU in the presence of NP as ultrasound absorption agents was developed. To deeply understand the performance mechanism of NPs during HIFU, and to clarify the influence of key parameters that can affect therapeutic results, it is essential to develop a mathematical model that can explore the physics behind the problem. To this end, a set of mathematical equations governing the temperature variation during the HIFU thermal procedure was derived by simulating the physics of the interaction between ultrasonic waves and NPs, leading to the heat transfer. The accuracy of developed model was verified by performing a series of in vitro studies.

C2) The effect of NP features, specifically NP size, on the heating mechanism of HIFU was examined. The heat transfer during NP-enhanced HIFU depends on the transport processes occurring at the boundary between the NPs and the surrounding medium; since the NP size can define that interface area, it is crucial to examine the effects of NP size on HIFU's heating results, and to determine the corresponding optimized values for better performance of NPs. To this end, HIFU experiments were performed by developing an experimental setup including phantoms with uniform distribution of MNPs with different sizes and volume concentrations and the effect of NP features on the thermal mechanism of HIFU was examined.

C3) The effect of NP dose when injected locally at the focused region was investigated. In the clinical application of NPs using intratumoral injection [48, 49], where NPs are injected directly into the tumor site, the dose of NPs (the volume of injected NPs) is the key parameter that can affect the efficiency of treatment; therefore, developing a study that examines the effect of NP dose when delivered locally to the focused region is necessary

for making the thermal ablation process more efficient and safer. To this end, an experimental setup was developed to precisely inject AuNPs at the focused region of a tissue-mimicking phantom in order to examine the effect of NP at different doses on HIFU's heating results.

C4) The potential of CNTs as new nanoscale agents for the HIFU thermal therapy was investigated. A key advantage of CNTs over MNPs and AuNPs is their ability to act as temperature sensors for monitoring the temperature rise to ensure that a sufficient amount of thermal dose is delivered to the targeted area [50, 51]. As a result, CNTs have the potential to be considered as effective agents for hyperthermia treatment; however, their performance mechanism as ultrasound absorption agents during the HIFU thermal therapy has not yet been reported. To this end, an experimental examination was conducted using phantoms with uniform distribution of CNTs with different volume concentrations to investigate the effect of CNTs on thermal mechanism of HIFU, as well as to examine their performance when exposed to ultrasonic fields at different ranges of powers and frequencies.

The research contributions presented in this PhD thesis not only can help with deeper understanding of the mechanism of NPs during HIFU treatment, but can also be useful for the purpose of the treatment design. A key challenge of the extracorporeal use of HIFU, limiting its clinical application, is the collateral damage due to the use of high levels of ultrasonic energy during the thermal treatment. To reduce the adverse effects of HIFU, it is essential for the practitioners to have a presurgical planning tool that enables them to select characteristics of HIFU treatment, including the power, frequency and exposure time, as well as the dose of NPs as therapeutic agents. Therefore, development of a numerical model that can simulate the therapeutic

mechanism of HIFU is useful for this purpose. Although the numerical simulation provided in this PhD work was based on simplified models of biological tissue and NPs distribution, it has the potential to be further improved for preclinical purposes if imaging data are available, which provide information on the structure of biological tissue and the distribution of NPs inside the targeted tissue.

In addition, the contributions of this PhD work can help with the design of new nanoscale agents for HIFU treatment. A key factor in the design of NPs is their shape and size in order to determine optimized values for effective results. The numerical modeling, as well as the experimental data presented in this PhD works can help the researchers along this direction. Another important factor in the design of agents for HIFU is the discovery of new ultrasound agents which can offer better performance than currently available agents. This PhD dissertation proposes CNTs as new ultrasound absorption agents for HIFU. CNTs not only have the potential to enhance HIFU's heating mechanism, but also can be used as temperature sensors that indicate the temperature during thermal treatment

1.4. Thesis Structure

This PhD thesis includes six chapters, structured as follows:

- Chapter 1 illustrates the research motivation, objectives, main contributions, and thesis structure.
- Chapter 2 provides a comprehensive review on the state of the art in the area of HIFU and NPs as agents for cancer treatment. Section 2.1 reviews the mechanism, advantages, clinical application and limitations of HIFU treatment, and illustrates the importance of using ultrasound agents for the HIFU thermal treatment. The application of NPs for cancer

treatment is reviewed in Section 2.2, and the potential of NPs as agents for HIFU treatment is discussed in Section 2.3. Section 2.4 provides a comprehensive review on existing thermal model for simulating HIFU's thermal mechanism.

- Chapter 3 illustrates the mathematical modeling developed for the simulation of HIFU heating mechanism. Section 3.1 presents the linear and nonlinear thermal models of HIFU used for the validation of the experimental setup. Section 3.2 presents the mathematical equations derived for modeling the HIFU mechanism in the presence of NPs. The solution procedure developed to solve the governing equations is described in Section 3.3.
- Chapter 4 is focused on the design and development of the HIFU experimental setup. The components of HIFU setup are explained in Section 4.1, and the tissue mimicking phantoms for simulating the biological tissue are illustrated in Section 4.2. Section 4.3 discusses the temperature measurement system used for monitoring the HIFU thermal mechanism.
- Chapter 5 presents the results form both experiments and numerical simulations. Section 5.1 shows the linear and nonlinear thermal results developed for the validation of the HIFU experimental setup. In Section 5.2, the effects of AuNPs, MNPs, and CNTs on the HIFU thermal mechanism are presented and the feasibility of the developed mathematical model for the simulation of NP-enhanced HIFU is investigated.
- Chapter 6 presents conclusions and future work.

Chapter 2

Literature Review

2.1. Focused Ultrasound Therapy

Focused ultrasound therapy, also known as high intensity focused ultrasound (HIFU), is a new energy-based therapeutic method that uses ultrasonic energy to treat a range of disorders and tumors [1]. Compared to diagnostic ultrasound, HIFU employs higher time-averaged intensities at focused regions. Typical diagnostic ultrasound transducers produce ultrasonic waves with time-averaged intensities of $0.1 - 100 \ \frac{\mathrm{mW}}{\mathrm{cm}^2}$ which can induce compression and rarefaction pressures in the range of $0.001 - 0.003$ MPa. By contrast, HIFU transducers are able to deliver ultrasound with time-averaged intensities of $100 - 10{,}000 \ \frac{\mathrm{W}}{\mathrm{cm}^2}$ to a focused area, with peak compression pressures of up to 30 MPa and peak rarefaction pressures up to 10 MPa [52].

2.1.1. HIFU Mechanism

HIFU allows the local treatment of an abnormality inside the body by focusing ultrasonic beams from an extracorporeal source to the target area [14], as show in Figure 2-1. When ultrasonic waves propagate through the tissue, the medium particles start to vibrate, resulting in alternating cycles of compression and rarefaction pressure inside the tissue. Due to the concave shape of transducer, the ultrasonic beams converge into a focal area where the resulting acoustic pressure reaches the highest amplitude [1]. This process induces tissue heating and corresponding temperature rise in the focal region that would be associated with irreversible biological effects such as necrosis and cell apoptosis [53].

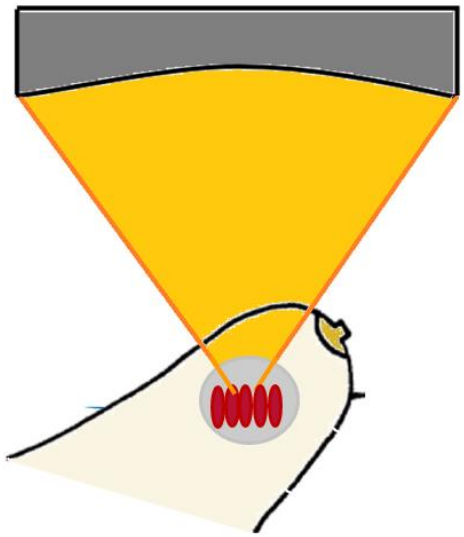

Figure 2-1 The HIFU mechanism for local treatment of a tumor.

A single HIFU exposure ablates a small volume, so in order to achieve the complete necrosis, the ablation treatment needs to be applied to the entire volume of tumor [1]. Practically, many ablated lesions must be placed side by side to paint out the entire tumor. The size of a focused region depends on many factors, such as the characteristics of the transducer and the acoustic properties of the targeted tissue, but typically a single insonation covers a cigar shape region with approximate dimensions in the order of $8-15$ mm (along beam axis) by $1-3$ mm (transverse direction). The postoperative imaging data show that two weeks following focused ultrasound therapy, the periphery of the ablated regions would be replaced by proliferative repair tissue [1].

Two predominant effects of HIFU, which lead to the desired therapeutic results, are the conversion of acoustic energy to heat (thermal effect) and the cavitation (mechanical effect) [54]. The major effect is tissue heating, induced through the absorption of acoustic energy and its conversion to heat. During HIFU, the temperature at the focused region can rise efficiently over 80°C, which even for a very short exposure time, should lead to the effective thermal toxicity [55].

In addition, the cavitation mechanism can also cause some deleterious mechanical bioeffects during HIFU [56]. Acoustic cavitation contains a range of complex phenomena including the creation, oscillation, growth and collapse of bubbles in an acoustic field. Cavitation occurs when the molecular structure of tissue is subjected to an ultrasonic field at a relatively high intensity level. If, during the rarefaction, the expansion pressure applied to the tissue is of sufficient magnitude, gas can be drawn out of the tissue to form bubbles (Figure 2-2) [1]. The exposure of the bubbles to the existed ultrasonic field can result in either stable or inertial cavitation.

During stable cavitation, the bubbles pulsate over many cycles and remain physically intact, while the inertial cavitation includes the violent oscillation, rapid growth, and collapse of the bubbles. The oscillation of bubbles can lead to effective therapeutic results when the inertial cavitation occurs against a solid surface in tissue [14]. The collapse of bubbles near a solid surface can create high-velocity liquid jets, leading to a force sufficient to damage cell membranes. For the inertial cavitation near a cell membrane, the mechanical effect is the predominant reason for damage to the cell [57].

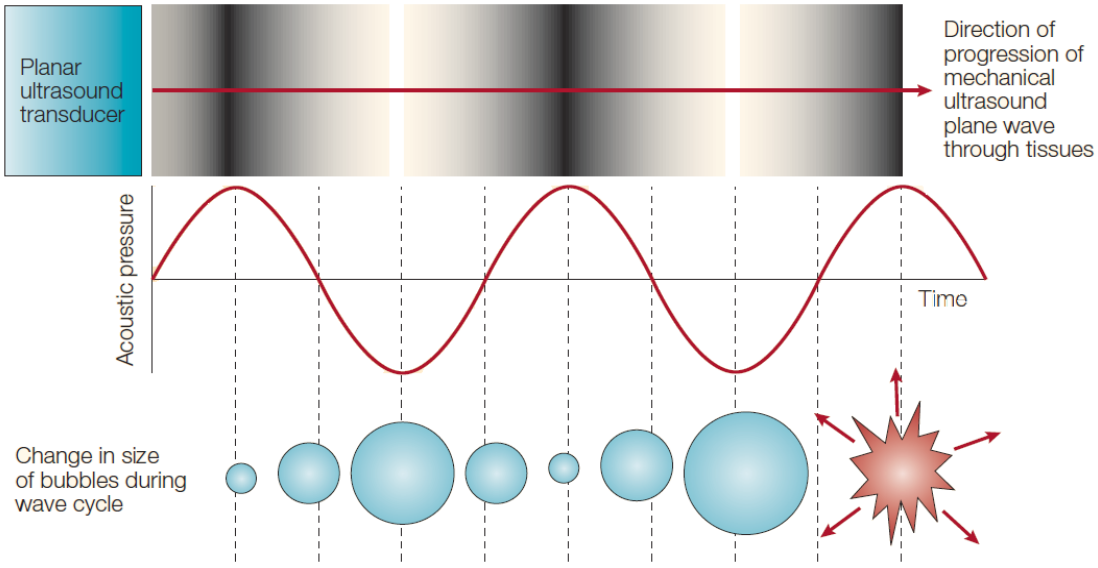

Figure 2-2 The principle of bubble generation during HIFU (Reprinted with permission from Ref. [1] copyright 2020 Springer Nature).

2.1.2. Clinical Application

The most recent studies on medical applications of HIFU have been motivated by the great advantages of this method over other surgical approaches. Among available therapeutic methods, HIFU is the only one that is truly noninvasive, and can ablate the targeted area without need for any surgical removals [22]. Compared to invasive surgical practices that may promote metastases by a variety of mechanisms, the HIFU treatment has little risk of metastasis or tumor seeding, as it is performed noninvasively by an external energy source [58]. Unlike radiotherapy and chemotherapy, which are only applicable to some kinds of tumors, the mechanism of HIFU is independent of tumor type, thus it can be applied to almost all types of tumors [1]. Finally, since ultrasound is non-ionizing, tissue in the entry and exit path of the HIFU beam is not injured, thus the HIFU treatment can be repeated multiple times with minor effects on healthy tissues [59].

Studies on the clinical applications of HIFU have been growing rapidly. The main use of HIFU is for the non-invasive treatment of solid tumors [1, 60]. Typically, it is performed clinically to treat benign and malignant tumors, including those of the liver [20, 61], prostate [15, 62], brain [63, 64], and breast [22, 65]. In addition, HIFU can also be carried out to achieve hemostasis [19, 66]. HIFU is promoted in several clinical centres around the world as a clinical method to control bleeding, both from individual vessels, as well as from gross damage to the capillary bed.

The first studies on focused ultrasound therapy date back to the 1920s and 1930s, when researchers discovered that ultrasound at high intensity levels could cause some physical, chemical and biological effects [67–69]. In 1944, an initial study on animal cases proposed the focused ultrasound as a potential method that could produce regions with high localized biological effect [70]. HIFU was first used for clinical application in the 1950s to treat neurologic disorders such as Parkinson’s disease [71]. Despite some success, the treatment required craniotomy and the results

were short-lived. In 1970, ultrasound hyperthermia was suggested for the treatment of cancer tumors; however, lack of imaging methods for controlling the ablation procedure prevented this strategy from progressing to clinical applications, and during subsequent decades, the investigation and applications of HIFU were relegated to laboratory level experiments [14]. In the 1990s, this method emerged again for clinical research due to the advent of imaging methods for guiding HIFU. Furthermore, the understanding of the ability of HIFU to cause immediate cell death by coagulation necrosis has made it a great candidate for the rapid and direct treatment of cancer tumors [14]. As a result, in present day, HIFU treatment guided by advanced imaging techniques has been clinically used in the treatment of different kinds of cancers [1, 60].

2.1.3. Ultrasound Absorption Agent

Despite the enormous potential of HIFU, there are several challenges of treating the tumors of large size and with vascularized structure [1]. First, a single HIFU insonation typically ablates a small cigar-shaped volume of tumor with approximate dimensions in the order of $8-15$ mm long by $1-3$ mm diameter; thus a number of HIFU sonications are required to ablate the entire tumor. This results in long treatment time, particularly for large tumors, and also increases the risk of cancer cell survival in the spaces between the focal regions after the treatment [1]. Additionally, the mechanism of HIFU is not perfectly effective in the treatment of tumors located in vascularized tissues, as blood vessels can act as thermal sinks for the heat produced by focused ultrasound [33].

To reduce the exposure time for each HIFU insonation and the blood perfusion effect, it is required to enhance the heating mechanism of HIFU by increasing the conversion rate of acoustic energy to heat. It is obvious that enhancing the heating mechanism can significantly increase the temperature rise and consequently reduce the exposure time for the HIFU insonation. In addition, it has been reported that decreasing the HIFU exposure time can significantly reduce the blood

perfusion effects [33]. Early studies have shown that the HIFU mechanism for very short exposures (<3 seconds) is independent of the blood perfusion effect [1]. As a result, developing a mechanism that can enhance the heating effects of HIFU is crucial to address the concerns regarding the long treatment time and blood perfusion. In typical HIFU devices, a high level of ultrasonic power is employed to address these concerns by increasing the thermal dose converted from acoustic energy; however, this can result in several adverse effects such as overheating of normal tissues and skin burns, as reported in several clinical studies [36, 37]. Furusawa et al. [36] performed MRI-guided HIFU on 30 patients with biopsy-confirmed breast cancer to evaluate the safety and effectiveness of HIFU during and after the ablation. Although successful in treatment, a third-degree skin burn was discovered at the end of treatment in 3% of the patients. Li et al. [37] performed HIFU treatment on 17 patients with recurrent and metastatic abdominal tumors, and discussed the adverse effects due to high ultrasonic power during HIFU. They reported skin burns in all 17 patients and mild enteroparalysis in 15 of them. Partly due to these issues, the FDA has not yet granted approval to HIFU for breast and abdominal procedures [35]. Therefore, there is a critical need to eliminate the risks involved in focused ultrasound therapy by enhancing the delivery of thermal energy to the tumor site, while reducing the ultrasonic power for the HIFU mechanism.

One of the strategies that can decrease the likelihood of adverse effects of ultrasound heating is to adopt ultrasound absorption agents to make acoustic energy deposition at the tumor region more efficient [35]. The aim of agents for the HIFU ablation therapy is to change the attenuation mechanism of the medium in order to enhance the absorption rate of acoustic energy. To this end, various organic and inorganic materials have been considered such as iodized oil [40], porphyrin [39], microbubbles [41], and most recently nanoparticles (NPs) [35]. Among them, NPs have

gained increasing popularity as potential agents for the focused ultrasound therapy of solid tumors due to their nanoscale-size and unique hyperthermal properties [43].

2.2. Nanoparticles

NPs are considered as microscopic particles with at least one dimension less than 100 nm [72]. The small size of NPs compared to biological molecules such as nucleic acids and proteins has made them great candidates for different biomedical applications to be used as drug carriers and therapeutic agents [73]. NPs have been recognized as possible agents for gene, antibiotic and drug delivery due to their unique properties allowing them to easily pass through the capillaries to reach the target site.

2.2.1. NP-Targeted Tumor Site

NPs can be delivered to the target tumor location by injecting them directly into the tumor structure intravenously [74], or by making use of the blood circulation system [75]. The NPs injected via intravascular (IV) method are mostly accumulated in the tumor site rather than in healthy tissue due to the enhanced permeability and retention effect (EPR) [76]. Compared to the normal blood vessels with tight junctions that are impermeable to molecules size greater than $2-4$ nm, the blood vessels formed in the tumor site are highly disorganized with numerous pores and wide gap junctions between endothelial cells. Thus, blood vessels around the tumor site allow particles with nanoscale size to pass through tumor vascular endothelial cell gaps and to accumulate in the tumor site while they stay out of the healthy area [77]. Generally, both organic and inorganic NPs can be delivered via the cardiovascular system; however, inorganic NPs need to be covered with organic coating materials, such as polyethylene glycol (PEG) and dextran polymers, to become more biocompatible and to consequently increase the delivery efficiency [78]. The NPs that are

biocompatible with the bloodstream are able to circulate for a longer time during IV application, resulting in more accumulation of NPs in the tumor site [75]. Recently, a new generation of NPs has been developed that can be used for active targeting delivery. A number of markers are attached to the NP surface to bind them directly to the cancer cells. Active targeting allows more localised delivery of NPs to the targeted area and thus can make the delivery more efficient [75].

2.2.2. NP-Assisted Thermal Therapy

Beside using NPs for targeting cancer cells, magnetic NPs (MNPs) and gold NPs (AuNPs) have been recognized as effective agents for hyperthermia applications due to their high potential to generate heat when they are stimulated by an external energy source such as magnetic, infrared, radiofrequency and ultrasonic fields [78]. Magnetic fluid hyperthermia (MFH) is a form of NP-assisted thermal therapy which uses MNPs to generate heat at the targeted area in the presence of an alternating magnetic field [79, 80]. The magnetic energy emitted from an external field is converted to internal energy within MNPs, resulting in heating and temperature rise for therapeutic purposes. Since the magnetic energy is not susceptible to attenuation, MFH can be used for the treatment of the deeply located tumors such as liver tumors [81]. AuNPs also are suited for thermal ablation treatment due to their potential to convert light energy to heat [82, 83]. AuNP-mediated thermal therapy can only be used for the treatment of subcutaneous tumors since the light energy is susceptible to attenuation by the tissue [84].

NP-assisted radiofrequency heating is another form of thermal ablation which uses the heat generated by the interaction between radiofrequency electromagnetic radiation waves and NPs for ablation of tumors [85, 86]. Radiofrequency electromagnetic radiation treatment is an invasive method in which several electrodes are placed within the tumor to ablate cancer cells. AuNPs and MNPs can be used in the radiofrequency thermal therapy in which adding them can increase the

efficiency of radiofrequency treatment by enhancing heating process [85]. Recently, a number of studies have shown promising potential of MNPs and AuNPs as ultrasound agents during HIFU by enhancing thermal and mechanical effects.

2.3. NP-Mediated HIFU

In addition to potential benefits of MNPs and AuNPs for hyperthermia treatment with magnetic, infrared, and radiofrequency radiation, there have been studies that investigated their feasibility for use in HIFU treatment. As one of the first studies, Smith and his coworkers [87] performed an experimental examination on water containing MNPs to study their effect on the degree of inertial cavitation induced by the HIFU insonation. They measured the inertial cavitation dose in the absence and presence of NPs and showed that MNPs could increase the inertial cavitation effect induced by HIFU. Ho et al. [88], in another study, investigated the effects of MNPs on the inertial cavitation dose when they were injected into tumor spheroids and showed the high potential benefit of MNPs in enhancing the therapeutic mechanism of cavitation. Sun et al. [89] developed superparamagnetic poly (lactic-co-glycolic acid) (PLGA)-iron oxide microcapsules and investigated the utility of these microcapsules during HIFU. They performed the HIFU tests on rabbits bearing breast cancer and showed that the composite microcapsules could efficiently enhance the HIFU ablation of breast cancer. Dibaji et al. [42] examined the potential of MNPs to enhance the heating mechanism during HIFU at low acoustic powers. They developed phantoms embedded with MNPs to investigate the effects of MNP concentrations and showed that the temperature at focal region and thermal dose increased with the rise in concentration of MNPs. Sun et al. [47] investigated the effects of MNPs on the thermal therapy of liver cancer using HIFU. Superparamagnetic PLGA-coated Fe_3O_4 microcapsules were fabricated using a modified double

emulsion evaporation method to be utilized for in vivo studies. They showed that the fabricated microcapsules could enhance the ablation process of liver tumor using HIFU. You et al. [90] developed multifunctional Fe_3O_4-PLGA nanocapsules with magnetic properties and investigated their potential in the treatment of hepatocellular carcinoma (HCC) using HIFU. The treatment of large and deep tumors, such as HCC, requires a high operating energy and long treatment duration. They showed that the presence of MNPs in the tumor region could effectively enhance the HCC treatment outcome.

In response to the potential of AuNPs for HIFU treatment, Devarakonda et al. [35] used MRI-guided HIFU to investigate the effects of AuNPs on the heating mechanism of HIFU. They performed the thermal tests on the phantoms embedded with AuNPs, and showed that AuNPs could significantly improve the HIFU thermal ablation by increasing temperature rise and lesion volume. McLaughlan et al. [45] developed a new approach for the monitoring and the enhancement of HIFU mechanism for the nucleation of cavitation activity using AuNPs and pulsed laser illumination. They showed the high potential of the proposed technique in both the monitoring of HIFU and enhancing the cavitation mechanism. Coluccia et al. [91] used MRI-guided HIFU to investigate the potential of Cisplatin-conjugated gold NP (GNP-UP-Cis) to treat glioblastoma tumor. They showed that the combination of HIFU and AuNPs with Cisplatin could enhance the treatment of glioblastoma tumor by allowing a high dose of Cisplatin to penetrate into the blood brain barrier.

As seen from the above literature review, MNPs and AuNPs have some potential to significantly improve the HIFU mechanism by enhancing the heating and cavitation effects. However, the exact mechanism of interaction between NPs and ultrasonic wave propagation during the NP-enhanced HIFU has not been clearly understood to the level that we can make

selective use of NPs for desirable clinical outcomes. Likewise, the effects of key parameters that can affect the efficiency of therapeutic results have not been well investigated yet.

2.4. Thermal Models of HIFU

This section provides a review on excising thermal models for predicting the temperature rise process during HIFU. In an early attempt to predict the thermal mechanism of HIFU, Fry et al. [92, 93] developed an analytical model by simulating the absorbed acoustic energy as a heat source term. They provided a linear function for temperature rise during HIFU that can only be valid for the HIFU process for a short exposure time, when the conduction and blood perfusion are not factors.

Lele [94] extended the work done by Fry et al. [92, 93], and developed a thermal model for HIFU that includes a term for the conduction and thus can be used for HIFU insonation time that is longer than the thermal diffusion time. To accurately model the conduction factor in prediction of temperature rise, it is required to first determine the acoustic intensity distribution at the focused region. Parker [95] developed an analytical solution to the model proposed by Lele [94] by assuming a Gaussian radial profile for the intensity distribution at the focused region. However, for accurate simulation of HIFU heating mechanism, a model with more details of heat source generated by wave propagation is required. In this case, an analytical modeling of HIFU is not valid and numerical simulation is instead required.

Another important diffusion factor that needs to be consider in thermal modeling of the HIFU is heat perfusion due to the blood vessels presented in biological tissue. To this end, two thermal models have been used in the HIFU thermal planning: the Pennes bioheat transfer equation (BHTE) [96], and the scalar effective thermal conductivity equation (ETCE) [97]. A review of

exiting models for blood perfusion effects can be found in Ref [98]. Recent experimental studies support the feasibility of both BHTE and ETCE models [99, 100]; however, these models can only simulate the heat diffusion from capillary vessels, not that from large blood vessels [33].

The perfusion heat by large blood vessels can usually be modelled by using a forced heat convection term in the regions of blood flow [101, 102]. However, this simplified model for blood vessels is not able to simulate the effect of acoustic streaming due to the propagation of the ultrasonic waves in the blood flow regions. In an effort to simulate the HIFU heating process in tissue containing large blood vessels when the acoustic streaming is considered, Huang et al. [33] developed a numerical model that combines the ultrasound propagation, acoustic streaming, blood cooling and ultrasound heating in viscous medium. They also provided a verification of model prediction by conducting a serious of in vitro experiments. In another study on modeling the HIFU in the presence of large blood vessels, Solovchuk et al. [34] proposed a 3D acoustics-thermal-fluid coupling model to examine the effects of convective cooling and acoustic streaming on the temperature field during HIFU. Their model was developed based on the bioheat equations and the Navier–Stokes equations for the blood vessels.

Regarding the physics of NP-mediated HIFU, there have been studies that provided mathematical models to simulate the heating mechanism of HIFU in the presence of NPs. Bera et al. [103] developed a theoretical analysis to study the mechanism of MNP energy transfer during HIFU. They used the heat transfer equation for solid spheres suspended in a fluid-based medium to predict the temperature rise process during the HIFU insonation. Kaczmarek et al. [38] developed a mathematical model based on Pennes' bio-heat equation to simulate the effects of MNPs on the heat transfer mechanism during the ultrasound hyperthermia. They used a Gaussian distribution function to model the heat generated by ultrasound hyperthermia and showed the

effects of MNP concentration and ultrasonic frequency on the temperature rise process during the HIFU insonation.

Chapter 3

Modeling and Numerical Studies

Some parts of the thesis are published in three journals: i) Sadeghi-Goughari, Moslem, Soo Jeon, and Hyock-Ju Kwon. "Enhancing Thermal Effect of Focused Ultrasound Therapy Using Gold Nanoparticles." IEEE transactions on nanobioscience 18.4 (2019): 661-668; ii) Sadeghi-Goughari, Moslem, Soo Jeon, and Hyock-Ju Kwon. "Magnetic nanoparticles-enhanced focused ultrasound heating: size effect, mechanism, and performance analysis." Nanotechnology 31.24 (2020): 245101; iii) Sadeghi-Goughari, Moslem, Soo Jeon, and Hyock-Ju Kwon. "Analytical and Numerical Model of High Intensity Focused Ultrasound Enhanced with Nanoparticles." IEEE Transactions on Biomedical Engineering (2020).

This chapter presents numerical analyses to simulate the heat transfer induced by HIFU, and more importantly to provide a thermal model of NP-enhanced HIFU. First, a thermal model of HIFU in the absence of NPs was developed to investigate the effects of linear and nonlinear wave propagations on the thermal mechanism of HIFU. Second, the physics of HIFU in the presence of NPs has been studied, which led to the derivation of a mathematical equation representing the temperature rise profile during the NP-enhanced HIFU. Using the developed model, the effects of NP features including the size and volume concentration on the thermal mechanism of HIFU were examined. In particular, the performance of NPs was investigated when exposed to ultrasonic fields at different ranges of powers and frequencies.

3.1. Linear and Nonlinear Thermal Models of HIFU

In this section, a HIFU model in the absence of NPs was developed to examine the effects of linearity and nonlinearity during the HIFU insonation. To this end, a set of mathematical equations describing the HIFU thermal procedure was combined. The physics of HIFU involves three main mechanisms: the nonlinear wave propagation, acoustic energy absorption, and heat transfer.

3.1.1. Nonlinear Wave Propagation

As ultrasonic waves propagate through the tissue, particles in the medium start to oscillate around their equilibrium position. The displacement of particles changes the density and pressure in the medium (Figure 3-1). Determining the acoustic pressure distribution induced by wave propagation is essential for modeling ultrasound physics [104].

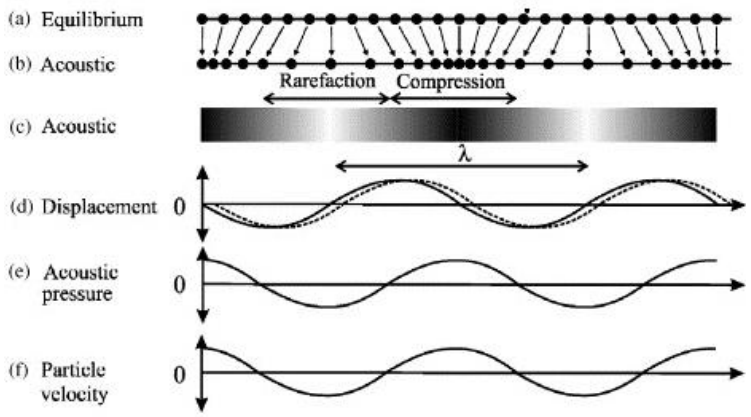

Figure 3-1 Schematic of one-dimensional longitudinal acoustic wave propagation (Reprinted with permission from Ref. [104] copyright 2020 Elsevier).

If we assume that ultrasonic waves propagate with a constant velocity and there is a linear relationship between the density and the pressure of the medium, the wave equation can be used to model ultrasonic wave propagation during HIFU [105].

$$\nabla^2 p = \frac{1}{c^2}\frac{\partial^2 p}{\partial t^2} \tag{3-1}$$

where p is acoustic pressure, t is time, and c is linear acoustic speed of sound. However, the linear wave equation is unable to predict the physics of ultrasound for most HIFU applications as nonlinear phenomenon may arise with large pressure magnitudes [104]. When the ultrasonic waves are propagating through a biological medium, it exhibits nonlinear behaviors from two factors. The first one is the material's nonlinear properties (i.e. stiffness of biological tissue is nonlinear and the pressure stimulus required to compress the medium increases nonlinearly as a function of density). The second one is the convective nature of acoustic wave propagation (i.e. the wave is transported by particle motion) [104]. In nonlinear wave propagation, the local propagation speed of sound, c_l, is dependent on the particle velocity, u, [106]

$$c_l = c + \beta u \tag{3-2}$$

where β is the coefficient of nonlinearity given by

$$\beta = 1 + \frac{B}{2A} \tag{3-3}$$

and B/A is a nonlinearity parameter that characterizes the nonlinear properties of the medium. Typical values of B/A vary from 5 for water to 10 for fatty tissue [106].

Nonlinearities may cause the initial ultrasonic waves to be distorted as they propagate through the medium since the waves propagate faster in compression regions (with positive particle velocity) than rarefaction regions (with negative particle velocity), as shown in Figure 3-2. The distortion of ultrasonic waves in the time domain may generate additional frequencies for waveform and harmonics of the initial frequency. This can result in increasing wave attenuation leading to enhanced heating and streaming effects [106].

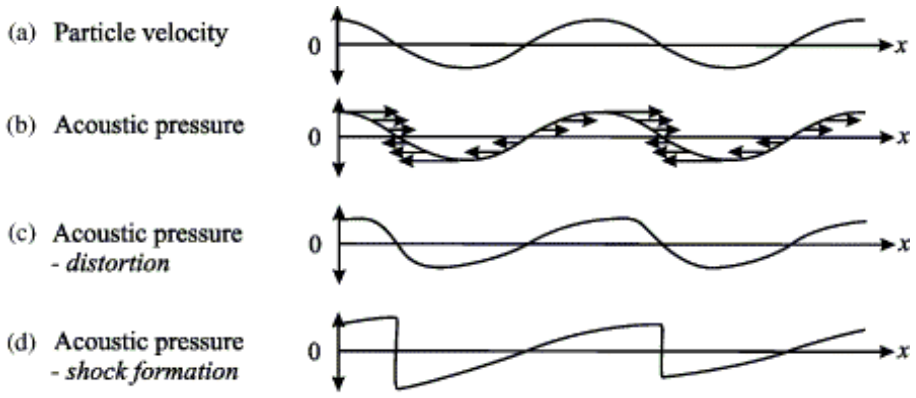

Figure 3-2 The effects of nonlinearity on wave distortion (Reprinted with permission from Ref. [104] copyright 2020 Elsevier).

Nonlinear ultrasound propagation in a biological medium can be simulated by the Kuznetsov, Zabolotskaya and Khokhlov (KZK) equation [107]

$$\frac{\partial^2 p}{\partial \tau \partial z} - \frac{c}{2}\nabla_{\perp}^2 = \frac{1}{2c^3\rho}\frac{\partial}{\partial \tau}\left[\delta\frac{\partial^2 p}{\partial \tau^2} + \beta\frac{\partial p^2}{\partial \tau}\right] \tag{3-4}$$

where $\tau = (t - \frac{z}{c})$, z denotes the beam axis, $\nabla_{\perp}$ is the transverse Laplacian, and ρ is density. Here, the first term inside bracket on the right hand side accounts for the attenuation from thermoviscous effects in which the acoustic diffusivity (δ) is related to the acoustic absorption coefficient (α_a) by $\delta = \frac{2c^3\alpha_a}{\omega^2}$ with ω being the angular frequency.

Once the acoustic pressure distribution is derived by solving Eq. (3-4), the following equation can be used to determine the rate of energy per unit area transported by ultrasonic waves [106]

$$I = \frac{p^2}{2\rho c} \tag{3-5}$$

where I is the intensity, i.e., the acoustic power per unit area.

3.1.2. Wave Absorption

Ultrasonic waves propagating through a tissue medium get attenuated as they proceed due to the intrinsic absorption properties of the medium. For an ultrasonic wave traveling in the z-direction, the acoustic intensity, I, with respect to the distance is known to decay exponentially as [106]

$$I = I_o e^{-2\alpha z} \tag{3-6}$$

where I_o is the initial intensity and $\alpha = \alpha_a + \alpha_s$ is the total attenuation coefficient in which α_s is the scattering coefficient. For waves propagating through homogeneous media, the ultrasound energy is mostly attenuated by the absorption mechanism. Hence, scattering can be ignored, so that $\alpha = \alpha_a$ [106].

It is known that the absorption coefficient is directly related to frequency, Eq. (3-7), and ultrasound waves with higher frequency are attenuated more by the medium. For a thermoviscous medium, the following relation can be used to consider the dependency of absorption coefficient to frequency, f

$$\alpha_a = \alpha_o \left(\frac{f}{f_0}\right)^n \tag{3-7}$$

where α_o is the absorption coefficient at frequency of $f_o = 1$ MHz, and $n = 1$ for tissue, and 2 for water [106].

The rate of absorbed energy converted to heat per unit volume can be defined as the rate of drop in acoustic intensity as the ultrasonic wave propagates through the medium [106], and can be expressed as

$$Q = -\frac{\partial I}{\partial z} = -\frac{\partial}{\partial z}(I_o e^{-2\alpha_a z}) = 2\alpha_a I \tag{3-8}$$

3.1.3. Heat Transfer

In order to combine the acoustic pressure field derived from the wave equation with thermal analysis, and to model the thermal transport during focused ultrasound, the absorbed acoustic energy per unit volume can be considered as a heat source for the Pennes bioheat transfer equation [96]

$$\rho C_p \frac{\partial T}{\partial t} = \nabla(k\nabla T) - \rho_b C_b w_b (T - T_b) + Q, \tag{3-9}$$

where $T(t, \vec{r})$ is temperature distribution with $\vec{r}$ being spatial coordinate, C_p is specific heat, and k denotes thermal conductivity of the medium. ρ_b, C_b, w_b, and T_b refer to the density, specific heat, perfusion rate and temperature of the blood flowing, respectively. A combination of Eqs. (3-4), (3-8), and (3-9) describes the thermal mechanism of HIFU including nonlinear wave propagation, acoustic energy absorption and heat transfer.

3.2. Thermal Model of NP-Enhanced HIFU

In this section, a thermal model of HIFU in the presence of NPs as ultrasound absorption agents is presented. First, the physics behind the problem is discussed to gain a deeper understanding of the interaction mechanism between ultrasonic waves and NPs, and then a mathematical analysis is performed to determine a set of equations for describing the temperature rise profile during the NP-enhanced HIFU insonation.

3.2.1. Physics

The HIFU-induced heat generation in a biological tissue embedded with NPs depends on the intrinsic absorption properties of the medium, as well as on the transport processes taking place at the boundaries between the NPs and the surrounding medium (Figure 3-3) [103, 108]. The heat

conversion mechanisms involved with HIFU procedure can be identified by multiple effects as follows (identified as M1 through M6 and depicted in Figure 3-4). The intrinsic wave absorption in a biological tissue occurs due to the viscous properties of the medium that causes the energy dissipation. The energy absorbed by the medium during the ultrasound propagation is converted to heat, resulting in the rise of temperature in the tissue (M1) [106]. The other mechanisms causing the energy transfer during the HIFU procedure are involved with the presence of NPs and their oscillating motion under the acoustic pressure [108]. First, the relative motion of NPs in a tissue medium with viscous properties forms layers of viscous waves around the NPs and at their interface with suspending medium. The generated viscous waves affect the attenuation of ultrasonic waves and cause higher amounts of acoustic energy to be absorbed through the interaction between the ultrasonic and viscous waves (M2) [108]. In another mechanism induced by NPs, a temperature gradient is generated around NPs due to the work done by their oscillation under acoustic pressure, inducing a heat flow, as well as a temperature rise, in the surrounding tissue (M3) [108]. The produced temperature gradient also forms layers of thermal waves around NPs in which their interaction with ultrasonic waves leads to the higher absorption of acoustic energy and consequently higher temperature rise (M4) [108].

The heat generated during the NP-enhanced HIFU insonation can be diffused through two mechanisms in a biological tissue: conduction and perfusion [33]. The conduction is viewed as the heat transfer from more energetic to less energetic particles of the medium due to the interaction between particles (M5). On the other hand, the perfusion refers to the energy exchange between the medium's particles and blood flow acting as a sink of the thermal energy produced during HIFU (M6) [109].

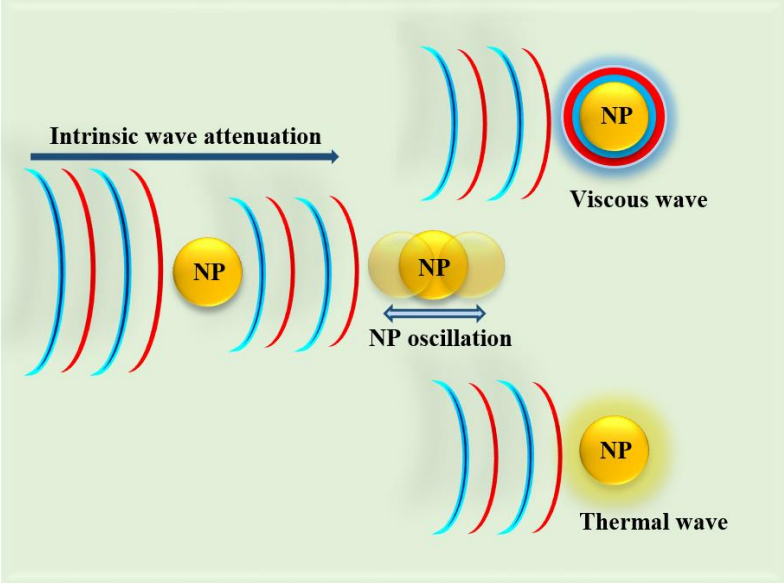

Figure 3-3 The interaction mechanism between ultrasonic waves and embedded NPs, leading to the higher wave absorption.

3.2.2. Mathematics

A major objective of the thermal analyses of HIFU is to derive the time-dependent temperature field in the medium during the insonation. A set of differential equations governing the temperature distribution can be determined by applying the principle of conservation of energy (the first law of thermodynamics) to a infinitesimal control volume of a tissue medium embedded with NPs [109]. Considering the heat flowchart presented in Figure 3-4, the rate of energy transfer per unit volume during the NP-enhanced HIFU can be given as

$$q_h = q_i + q_v + q_w + q_t - q_c - q_p \tag{3-10}$$

The term in the left side, q_h, represents the rate of change in energy density of the control volume during the HIFU process. The first term in the right hand side, q_i, denotes the rate of heat generated per unit volume due to the intrinsic wave absorption mechanism (M1). The terms q_v and q_t denote the rate of heat generated per unit volume due to the absorption mechanisms of ultrasonic waves caused by their interaction with viscous (M2) and thermal waves (M4), respectively; q_w represents

the rate of heat generated per unit volume due to the temperature gradient process around NPs (M3). Finally, the last two terms, q_c and q_p, are related to the rate of diffusion of energy per unit volume due to the conduction (M5) and blood flow perfusion (M6), respectively.

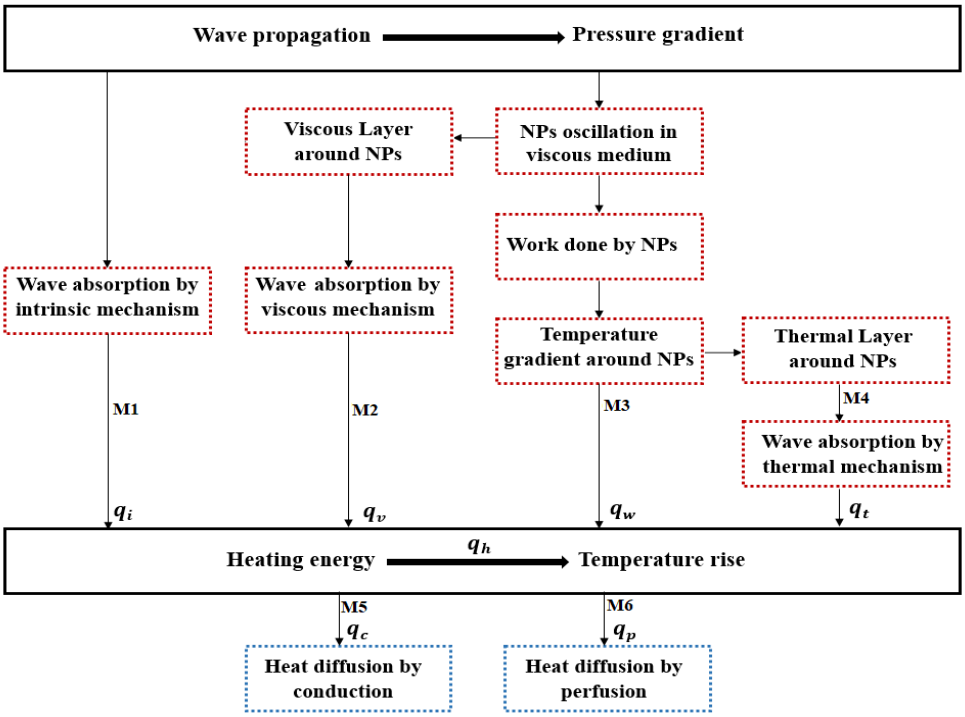

Figure 3-4 A flowchart diagram of temperature rise mechanism during NP-mediated HIFU.

3.2.2.1.Intrinsic wave absorption

The rate of heat generated per unit volume due to the intrinsic wave absorption mechanism can be expressed using Eq. (3-8), applied to q_i

$$q_i = 2\alpha_i I \tag{3-11}$$

Here, α_i is the intrinsic absorption coefficient which for a tissue medium embedded with NPs can be described as $\alpha_i = (1-\varphi)\alpha_a + \varphi\ \alpha_{NP}$ in which α_{NP} is the intrinsic absorption coefficients of the NPs, and φ is the volume concentration of NPs (%v/v) [103]. The intrinsic absorption coefficient of a material differs by the nature of the physical processes leading to the loss of energy and is usually determined by experimental observation [106].

3.2.2.2. Thermal and viscous wave absorption

The amount of acoustic energy absorbed at the surface of NPs depends on the thermal and viscous properties of both NP and suspending medium, as well as on the features of NPs including the size and volume concentration [103]. By introducing the absorption coefficient, α_{tv}, for the viscous and thermal processes occurring at the surface of NPs, the rate of absorbed energy per unit volume due to those processes can be presented as below

$$q_{tv} = q_{t+}q_v = 2\,\alpha_{tv}\,I \tag{3-12}$$

In practice for ultrasonic waves traveling in a biological tissue, α_{tv} can be divided into two terms as $\alpha_{tv} = \alpha_t + \alpha_v$ [108], where the first and second terms are the thermal wave and viscous wave absorption coefficients, respectively. Allegeral et al. [108] reported a set of analytical relations of α_t and α_v for the suspension of small-size particles by solving the wave equations for the propagation of compressional, viscous, and thermal waves in spherical coordinates in terms of series expansions of Bessel Functions. Based on their results, the following equations can be employed to describe acoustic absorption coefficients for thermal and viscous waves during the NP-enhanced HIFU ablation process [108]

$$\frac{\alpha_v}{\varphi} = \frac{18\left(\frac{\omega}{c}\right)\left(1-\frac{\rho}{\rho_{NP}}\right)^2 Y^2(Y+1)}{4Y^4\left(\frac{\rho}{\rho_{NP}}+2\right)^2 + 36Y^3\left(\frac{\rho}{\rho_{NP}}+2\right) + 162\left(\frac{\rho}{\rho_{NP}}\right)^2 Y(Y+1) + 81\left(\frac{\rho}{\rho_{NP}}\right)^2}$$

$$\frac{\alpha_t}{\varphi} = \frac{1}{6}\omega^2 R^2 c\, T_o\, \rho\, {\rho_{NP}}^2 {C_p}_{NP}^{\,2}\left(\frac{\gamma}{\rho C_p} - \frac{\gamma_{NP}}{\rho_{NP} {C_p}_{NP}}\right)^2 \frac{1}{k_{NP}}\left(\frac{1}{5}+\frac{k_{NP}}{k}\right) \tag{3-13}$$

where ρ_{NP}, ${C_p}_{NP}$, γ_{NP}, and k_{NP} denote the density, specific heat, thermal expansion coefficient, and thermal conductivity of NPs. T_o is a heat-wave parameter related to the temperature, γ is the

thermal expansion of the suspending medium, R is the radius of NPs, and Y is defined as $\left(\frac{\omega}{2\vartheta_m}\right)^{\frac{1}{2}} R$, where ϑ_m is the kinematic viscosity of the suspending medium.

3.2.2.3.Temperature gradient due to the NPs oscillation

The temperature gradient generated at the boundary of NPs due to the work done by their motion depends on the amplitude of acoustic pressure (which defines the domain of NPs oscillation), as well as on the thermal properties of the surrounding medium, such as the thermal expansion coefficient (which represents the tendency of the medium for volume change in response to the temperature rise). Using the heat transfer equation for solid spheres suspended in a fluidic-based medium, the rate of heat generated per unit volume due to the temperature gradient process around NPs can be given as below [103]

$$q_w = T_o\, \gamma\, (\alpha_v + \alpha_t)\;\, c_{mn}\, p \tag{3-14}$$

where c_{mn} is the speed of sound in the medium embedded with NPs which can be defined as $c_{mn} = (1-\varphi)c + \varphi c_{NP}$ [103],

Eq. (3-14) can be rewritten in the term of acoustic intensity using Eq. (3-5) which describes *I* in term of p as

$$q_w = \; T_0\, \gamma(\alpha_v + \alpha_t)\, c_{mn} \sqrt{2\, \rho_{mn}\, c_{mn}}\, \sqrt{I} \tag{3-15}$$

where ρ_{mn} is the density of the medium containing NPs which can be described as $\rho_{mn} = (1-\varphi)\rho + \varphi\, \rho_{NP}$.

3.2.2.4. Heat diffusion mechanism: conduction and perfusion

The heat generated by the interaction mechanisms between NPs and the HIFU waves can be diffused through the conduction and perfusion. The rate of diffusion of energy per unit volume can

be describe by Fourier's law for conduction, and an empirical model proposed by Pennes [109] for perfusion:

$$q_c = k_{mn}\nabla^2 T$$
$$q_p = \rho_b C_b w_b (T - T_b) \tag{3-16}$$

where k_{mn} is the thermal conductivity of the medium embedded with NPs, which can be given by $\frac{1}{k_{mn}} = \frac{\varphi}{k_{NP}} + \frac{(1-\varphi)}{k}$.

3.2.2.5. NP-enhanced HIFU heat equation

By substituting Eqs. (3-11), (3-12), (3-15) , and (3-16) into Eq. (3-10) and considering Eq. (3-13), the final form of HIFU heating equation in the presence of NPs can be obtained as below:

$$\rho_{mn} C_{P_{mn}} \frac{\partial T}{\partial t} = 2(\alpha_i + \alpha_v + \alpha_t) I + T_0\, \gamma\, (\alpha_v + \alpha_t)\, c_{mn} \sqrt{2\, \rho_{mn}\, c_{mn}}\, \sqrt{I} + k_{mn}\nabla^2 T + \rho_b C_b w_b (T - T_b) \tag{3-17}$$

where for a tissue medium embedded with NPs, $C_{P_{mn}} = (1-\varphi)C_p + \varphi C_{NP}$.

3.3. Solution Procedure

3.3.1. Numerical Solution

To simulate the heating mechanism induced by ultrasound absorption and to calculate the acoustic pressure and consequent temperature rise during NP-enhanced HIFU, we need to solve the equations regarding wave propagation (Eq. (3-4)) and heat transfer (Eq. (3-17)). In general forms, there is no analytical solution for these equations; however, numerical methods such as finite difference method (FDM) and finite element analysis (FEA), can be used to solve the problem.

In the current study, a numerical simulation has been conducted to model the NP-enhanced HIFU mechanism. There exists a free software package released by the FDA [110] for simulating

axisymmetric HIFU by solving the KZK equation. Based on this package, a Matlab code has been developed to derive the acoustic features of nonlinear wave propagation, as well as the temperature rise due to the wave absorption. Figure 3-5 shows the geometry of the HIFU model employed for the computational simulation. Dimensions of the transducer and the tissue phantom in the model were compatible with the experimental setup to verify the validity of the numerical simulation. The phantom and the transducer were arranged coaxially to form a simplified 2D axisymmetric model to reduce the computational load of the simulation.

In the numerical modeling, the acoustic pressure simulation was applied to all domains, whereas the heat transfer analysis was performed only in the phantom domain. To apply boundary conditions to the acoustic pressure analysis, the transducer was driven at the frequency of f and the power of P, turned on 15 s of insonation, and then turned off for cooling. Three perfectly matched layers (P1, P2 and P3) were defined at the edges of the computational domains for absorbing outgoing waves. For the heat transfer analysis, the medium surfaces were considered to be fixed at the initial temperature of 20 ℃. The acoustic and thermal properties of the materials used in the numerical simulation are listed in Table 3-1.

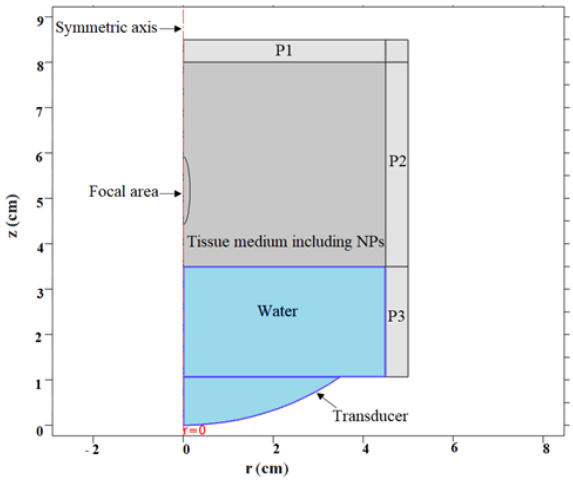

Figure 3-5 Axisymmetric HIFU simulation model containing water and tissue domains; P1, P2, and P3 denote perfectly matched layers.

Table 3-1 Material properties for computational analysis of NP-enhanced HIFU.

Material	MNPs [103]	Agar Phantom	Water
Density (kg/m^3)	5.17×10^3	1044	1000
Speed of sound (m/s)	4897	1568	1482
Specific Heat ($J/kg\ ℃$)	651.26	3710	NA
Thermal conductivity ($W/m\ ℃$)	7	0.59	NA
Thermal expansion coefficient (K^{-1})	11.8×10^{-6}	2.75×10^{-4}	NA

3.3.2. Analytical Solution

An analytical solution to the HIFU heat equation in the absence of NPs (Eq. (3-9)) can be determined if the pattern of ultrasonic wave absorption (heating term, Q) is known. It has been proven that for small elliptically shaped focal zones where the aspect ratio of the axial to lateral beam width is greater than two, the heat transfer is dominated by radial conduction. Accordingly, the heating term (Q) in Eq. (3-9) can be approximated by a 1D radial Gaussian [111]

$$Q = 2\,\alpha_a I_{max}.\exp\left(-\frac{r^2}{{r_0}^2}\right) \tag{3-18}$$

where r denotes the radial coordinate in the axisymmetric HIFU model, I_{max} is intensity at $r = 0$ and r_0 is a measure of the focal width.

Under above assumption, the following analytical solution for temperature rise profile during HIFU can be obtained [111]

$$\begin{aligned}\Delta T(r=0,t) &= \left(\frac{2\alpha_a I_{max}}{\rho C_p}\right)\left(\frac{{r_0}^2}{4k}\right)\mathrm{In}(1+4kt/{r_0}^2)\\ \Delta T(r\neq 0,t) &= \left(\frac{2\alpha_a I_{max}}{\rho C_p}\right)\left(\frac{{r_0}^2}{4k}\right)\left[\mathrm{Ei}\left(\frac{-r^2}{{r_0}^2}\right)-\mathrm{Ei}\left(\frac{-r^2}{{r_0}^2(1+4kt/{r_0}^2)}\right)\right]\end{aligned} \tag{3-19}$$

where $\mathrm{Ei}(\cdot)$ is the exponential integral given by

$$\mathrm{Ei}(x) = -\int_{-x}^{\infty} \frac{e^{-\varphi}}{\varphi} d\varphi \tag{3-20}$$

Chapter 4

Experimental Design

Some parts of the thesis are published in three journals: i) Sadeghi-Goughari, Moslem, Soo Jeon, and Hyock-Ju Kwon. "Enhancing Thermal Effect of Focused Ultrasound Therapy Using Gold Nanoparticles." IEEE transactions on nanobioscience 18.4 (2019): 661-668; ii) Sadeghi-Goughari, Moslem, Soo Jeon, and Hyock-Ju Kwon. "Magnetic nanoparticles-enhanced focused ultrasound heating: size effect, mechanism, and performance analysis." Nanotechnology 31.24 (2020): 245101; iii) Sadeghi-Goughari, Moslem, Soo Jeon, and Hyock-Ju Kwon. "Analytical and Numerical Model of High Intensity Focused Ultrasound Enhanced with Nanoparticles." IEEE Transactions on Biomedical Engineering (2020).

A HIFU experimental setup was developed to validate HIFU's thermal mechanism in a tissue-mimicking phantom. Agar-based phantoms were fabricated to simulate the acoustic and thermal properties of biological tissue, and thus to serve as a medium for hosting NPs. A schematic diagram of the experimental setup is shown in Figure 4-1. The setup consists of three main components including ultrasound generation system, tissue-mimicking phantom, and temperature measurement system. A function generator and a RF amplifier were used to run the HIFU transducer for focusing ultrasound beams into a tissue phantom. Both HIFU transducer and the phantom were immersed in degassed water contained in a tank to provide a coupling region between them. A thermocouple was embedded in the phantom to measure the temperature rise in the focal region. The outputs were connected to a computer to monitor temperature rise using LabVIEW. Detailed descriptions of components are presented in subsequent sections.

4.1. HIFU Setup

In the ultrasound generation system, a single-element transducer having a concave shape (Model H-101, Sonic Concepts, Woodinville, WA) was used to generate HIFU. The H-101 transducer has an active diameter of 64.0 mm, and a focal depth of 51.74 mm, measured from the exit plane of transducer housing rim to the geometric focus. The required signal to drive the transducer at a desired frequency was produced by a function generator (33210A Function/ Arbitrary Waveform Generator, 10 MHz, Hewlett Packard) and amplified by a RF amplifier (A-500, 60 dB fixed gain, Electronic Navigation Industries, Rochester, NY). The amplified signal passed through an acoustic matching network (Sonic Concepts, Woodinville, WA) designed to realize output resistance of 50 Ω before being routed to the transducer. Finally, a three-dimensional positioning system (CNC, Sherline, US) was assembled to the setup to move the transducer along the beam axis as well as other orthogonal directions. Figure 4-2 displays the elements used in the ultrasound generation system. For the experiments, the HIFU transducer was driven at various levels of powers of 2, 4.5, 8 , 12.5 W, and of frequencies of 1, 1.1, 1.15, 1.2 and 1.3 MHz. It needs to be mentioned that the values monitored for powers are simply electrical powers generated by the RF amplifier circuit. Due to the loss during transmission and conversion to acoustic energy, the electrical power is generally higher than the acoustic power emitted from the transducer's surface.

(a)

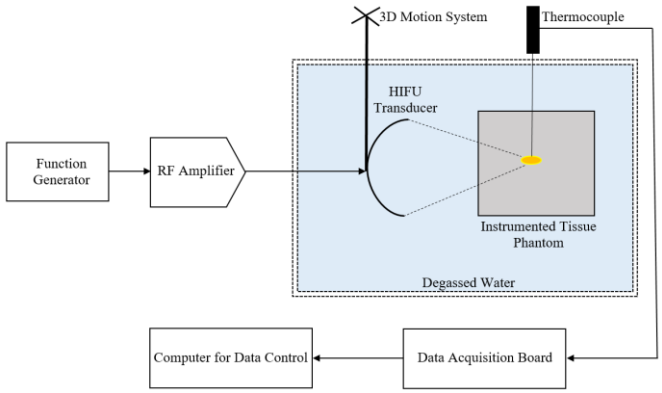

(b)

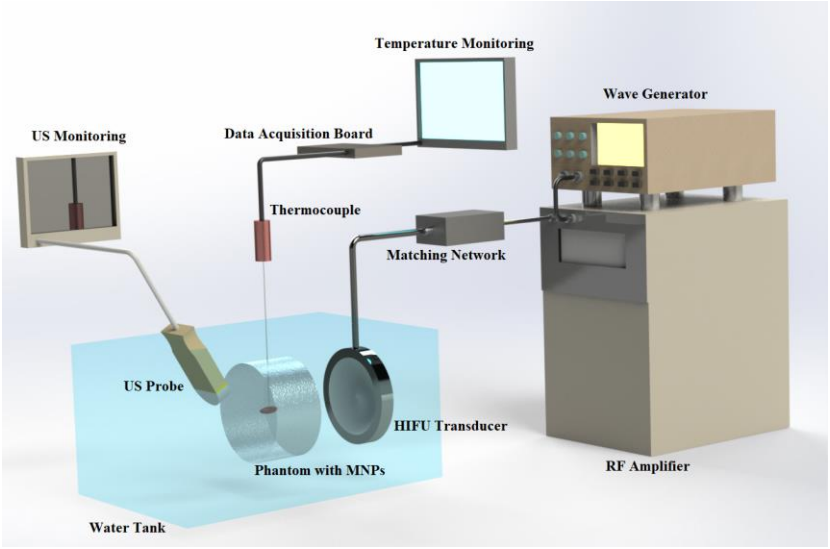

Figure 4-1 Experimental HIFU setup **(a)** a schematic, and **(b)** a 3D model.

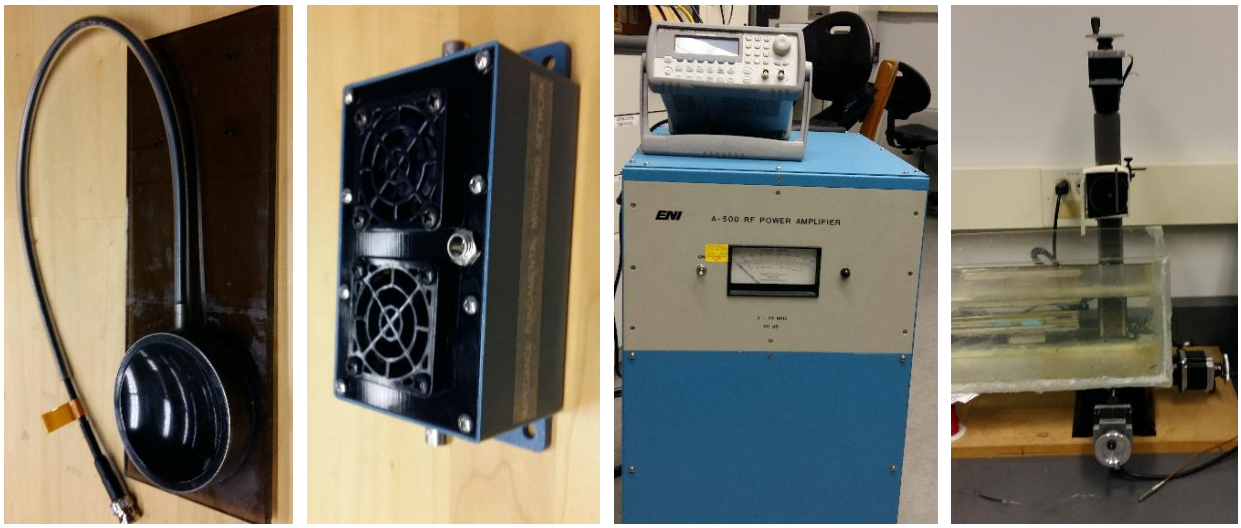

(a) **(b)** **(c)** **(d)**

Figure 4-2 HIFU setup elements: **(a)** HIFU transducer; **(b)** acoustic matching network; **(c)** function generator and RF amplifier; **(d)** 3D motion system.

4.2. In Vitro Phantom

Agar-based phantoms as in vitro media were developed to monitor the heating mechanism of HIFU and also to host NPs with different features. Agar phantoms have similar porous structures and thermo-acoustic properties to biological tissues and have been widely used in literature for nanodrug delivery and hyperthermia studies [33, 56]. For the experiments, three different recipes for phantom models were developed: (i) phantoms with similar thermal and absorption properties to the biological tissue for examining the applicability of the designed HIFU setup; (ii) low-absorption phantoms for monitoring the thermocouple artifact effect; (iii) phantoms containing NPs for studying their feature effects. Detailed descriptions of each recipe are presented in the following subsections.

4.2.1. Tissue-Mimicking Phantom

Tissue-mimicking phantoms were fabricated consisting of water, agar, graphite powder, methyl paraben and 1-propanol to simulate the thermal and acoustic properties of biological tissue [33]. The process to make phantoms is illustrated in Figure 4-3. First, water was heated to a temperature about 90 ℃, and then methyl paraben (analytical standard 47889, Sigma-Aldrich, Canada) and agar (Agar A7002, Sigma-Aldrich, Canada) were mixed to make a solution. As the mixture cooled, the graphite powder (282863, powder <20 μm, Sigma-Aldrich, Canada) and 1-propanol (279544, Sigma-Aldrich, Canada) were added to the solution at temperatures of about 80°C and 70°C, respectively. The mixture was finally poured into a cylindrical mold and kept for 1 day at room temperature to ensure complete solidification of the phantom (Figure 4-4(a)). The acoustic features of phantom, such as the speed of sound and the attenuation coefficient, were controlled by the amount of 1-propanol (acting as an agent to tune the speed of sound) and graphite powder (acting

as a scatterer) added to the mixture. Table 4-1 lists the recipe for making the phantom, and Table 4-2 shows the acoustic and thermal properties of the developed phantom as well as the corresponding value for human tissue from reference [56].

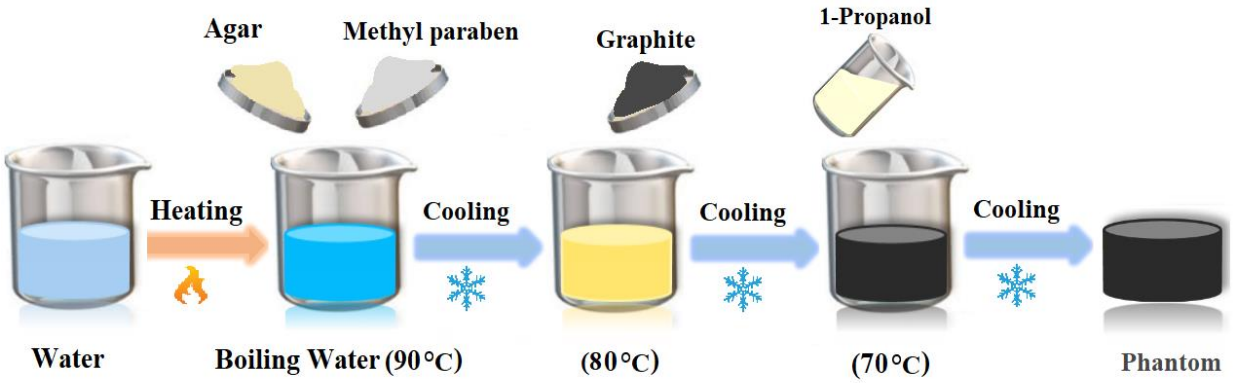

Figure 4-3 Schematic of preparation process of the tissue-mimicking phantom.

Table 4-1 Tissue-mimicking phantom recipe.

Component	Amount
Water	600 ml
Agar	18 g
methyl paraben	0.75 g
Graphite	54 g
1-propanol	50 ml

Table 4-2 Acoustic and thermal properties of phantom and human tissue [33]

Properties	Phantom	Human tissue
Density (kg/m^3)	1045	1000-1100
Speed of Sound (m/s)	1551	1450-1640
Attenuation($Np/m/MHz$)	10.17	4.03-17.27
Specific Heat ($J/kg.℃$)	3710	3600-3890
Thermal conductivity ($J/m.℃$)	0.59	0.45-0.56

The developed tissue-mimicking phantoms were also used for studying the mechanism of NPs when injected locally to the focused region during the NP-enhanced HIFU procedure. To investigate the dose effects of NPs, a stabilized suspension of AuNPs (in citrate buffer, ~3.5E+10 particles/mL NPs concentration, Sigma Aldrich, Canada) was utilized. AuNPs are usually provided as a colloidal suspension of nanoparticles of gold in a fluid medium, such as water and citrate buffer. To consider the presence of AuNPs during the HIFU ablation, a gauge needle was used to inject the buffer solution containing AuNPs (Figure 4-4(b)) into the targeted area. The size of the AuNPs injected into the phantom was $50\,\mathrm{nm}$. To ensure that AuNPs were delivered correctly to the target area, an ultrasound imaging was conducted using the medical ultrasound scanner (Ultrasonic Scanner Accuvix XQ, Korea). It is known that AuNPs are weak contrast agents and can not be detected via B-mode image; instead, the ultrasound imaging was conducted to guide the needle used for the injection of AuNPs, as shown in Figure 4-5, to ensure that the needle was positioned accurately in the focused region, where the thermal ablation would be applied and the temperature would be monitored by a thermocouple.

4.2.2. Low-Absorption Phantom

Low-absorption phantoms were fabricated using a mixture of water and agar to check any artificial effects due to the presence of the thermocouple inside the phantom. Since pure agar gel has a negligible absorption coefficient, any rises of temperature by the thermocouple during the HIFU insonation may be attributed to the artificial heating effect. The details on the low absorption phantoms and measurement of thermocouple artifact effects will be explained in Section 4.3. Figure 4-6 shows a low absorption phantom after solidification.

(a)

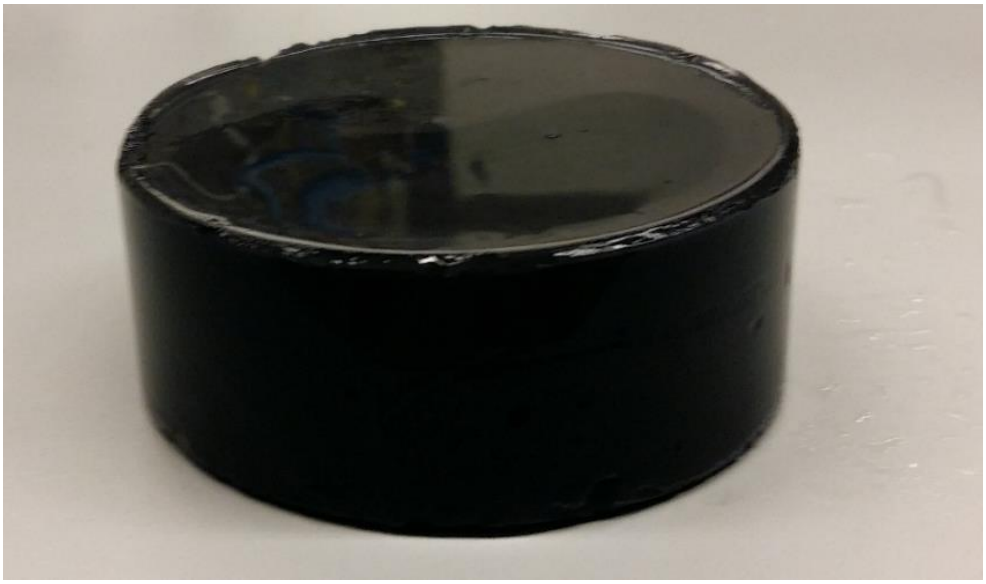

(b)

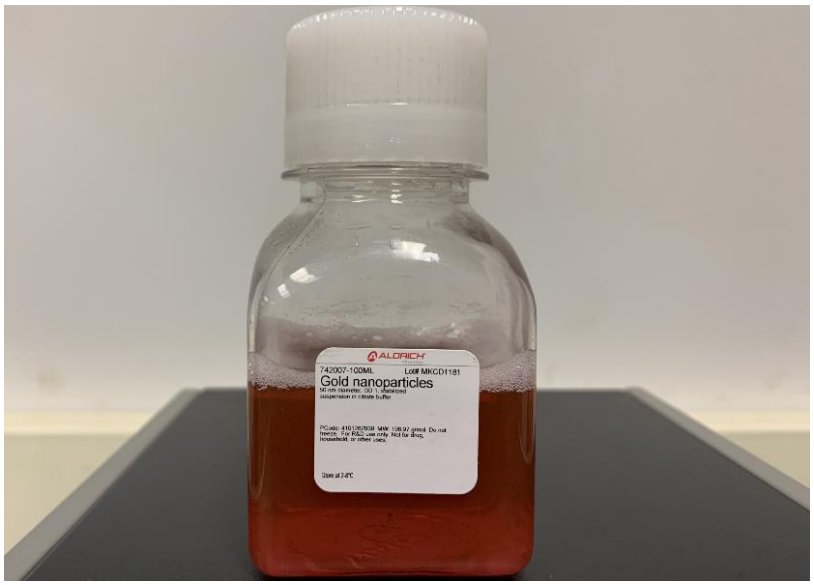

Figure 4-4 (a) Tissue-mimicking phantom after solidification, **(b)** AuNPs for injection to the focal area.

Figure 4-5 US image of phantoms for guiding the injection of NPs into the focal area where the temperature was monitored by a thermocouple.

Figure 4-6 A low-absorption phantom after solidification.

4.2.3. Phantom Embedded with NPs

Agar-based phantoms embedded with NPs were fabricated for in vitro experiments on NP-enhanced HIFU. The fabricated phantoms were used to take control of the distribution of NPs inside the suspending medium. They form realistic tissue models with well-defined thermo-acoustic properties so as to investigate the feature effects of NPs.

First, phantoms containing MNPs with different sizes and volume concentrations (%v/v) were developed to examine the feature effects of MNPs on HIFU's thermal mechanism. It has been reported that MNPs have much greater effect than AuNPs in enhancing the thermal mechanism of HIFU and consequently are better agents for the HIFU hyperthermia [46]. To fabricate a phantom with MNPs, a solution of agar gel was prepared by dissolving agar powder (Agar A7002, Sigma-Aldrich, Canada) in the boiling water, and then a suspension of iron oxide Fe_3O_4 (Ferromagnetic nanoparticles, purity of 98%, Dark Black, U.S. Research Nanomaterials, Inc., US) was added to the solution at a desired temperature. The mixture was stirred for 1 hour using a magnetic stir bar to achieve uniform distribution of MNPs inside the phantom, and then was kept for 12 hours at room temperature for solidification. For the experiments, I developed four types of phantoms contained MNPs with the size of 100 and $200\,\mathrm{nm}$, and volume concentration ($\%\,\mathrm{v/v}$) of 0.5% and 0.75%, respectively (Figure 4-7). It is known that the absorption of ultrasonic waves in pure agar gel (without MNPs) is extremely small [33], and accordingly no temperature rise was expected for all ranges of powers and frequencies used during the experiments.

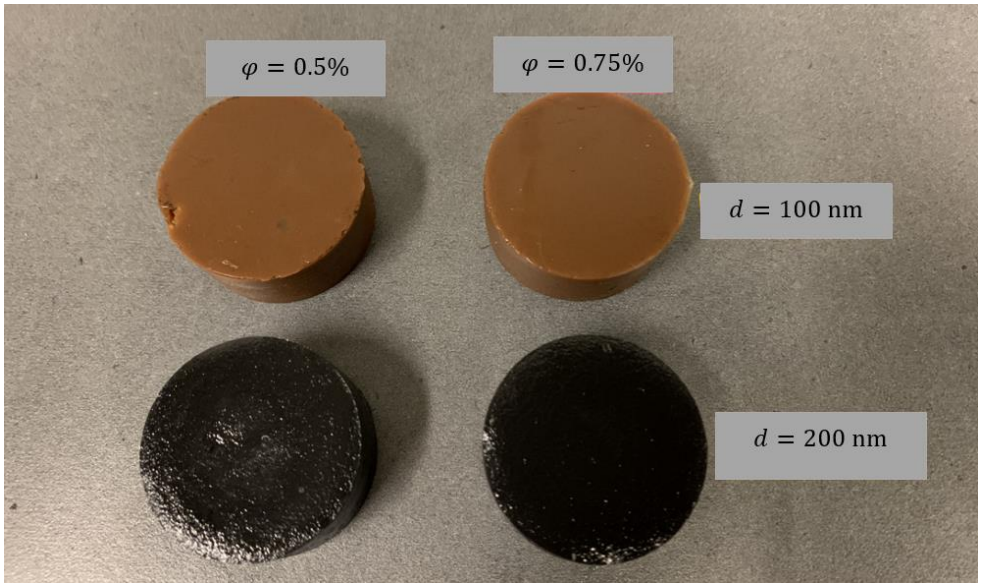

Figure 4-7 Phantoms containing MNPs with different NP sizes and volume concentrations.

The same recipe was also used to develop phantoms containing CNTs to investigate the feasibility of using them as new ultrasound absorption agents during the HIFU thermal ablation to enhance the heating at low power. To this end, a solution of agar gel was mixed with CNT powder (Short MWCNTs, >95%, OD: $50 - 80$ nm, U.S. Research Nanomaterials, Inc., US) and the mixture was stirred for 1 hour using a magnetic stir bar to achieve uniform distribution of CNTs. Three phantoms were fabricated with volume concentration (% v/v) of 0.25%, 0.5%, and 1% in order to consider the effects of CNT features during the HIFU ablation (Figure 4-8).

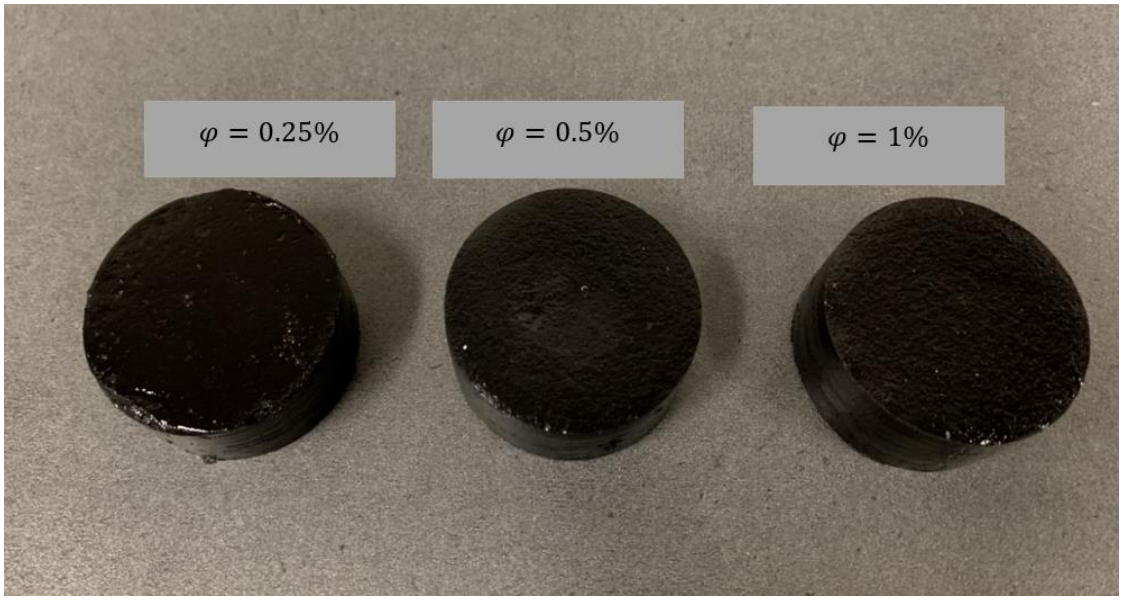

Figure 4-8 Phantoms containing CNTs with different concentrations.

Finally, a temperature measurement was performed to check the proper distribution of NPs inside the phantom medium and to ensure that NP aggregation did not occur after the phantom solidification. For each experiment with a given constant power and ultrasonic frequency, I slightly moved the location of the focused region inside the phantom and monitored the temperature rise during the HIFU insonation. We can hypothesize that if NPs were distributed uniformly inside the phantom medium, no dramatic differences in temperature rise would be seen for different focused regions inside the phantom.

4.3. Temperature Measurement Method

To measure the temperature and monitor the heating mechanism of HIFU, a thermocouple (Type K, grounded junction, 250 μm diameter, Omega Engineering Inc., Stamford, CT, Canada) was installed at the focused region. A data-acquisition board (NI USB-6210, National Instruments, US) was used to monitor temperature. Figure 4-9 shows the thermocouple, the data-acquisition board, and a tissue-mimicking phantom with an embedded thermocouple. To ensure that the cavitation

did not occur during the thermal ablation, temperature rise was carefully monitored during the HIFU insonation, as the occurrence of cavitation might cause a sudden jump in the temperature profile [33].

(a)

(b)

(c)

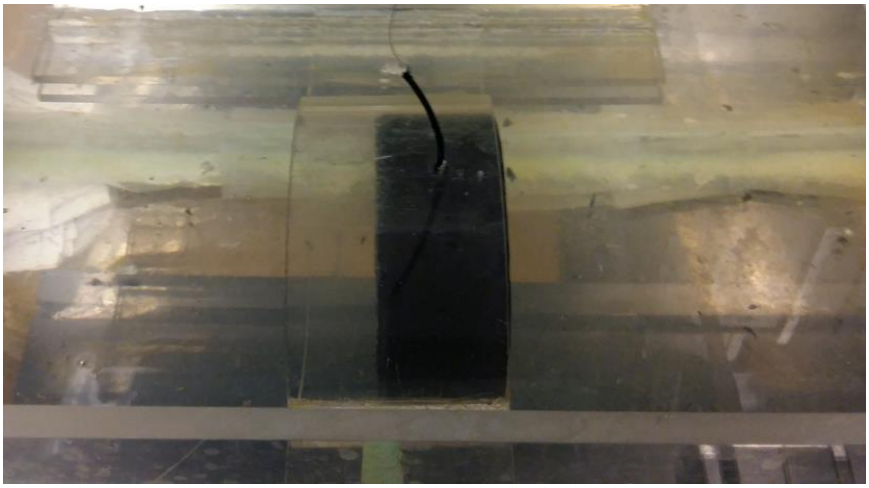

Figure 4-9 (a) Thermocouple, **(b)** data-acquisition board, **(c)** tissue-mimicking phantom with an embedded thermocouple.

To consider an error bar for a temperature rise, each experiment (with a constant power, frequency and phantom model) was repeated four times, while the location of focused region was changed inside the phantom for each trial. A mean value for temperature rise was calculated from temperature data collected through four trials ($N = 4$). Then, the standard deviation function, s, was used to quantify the variability of the measured data

$$s = \sqrt{\frac{\sum_{i=1}^{N}(T_i - \bar{T})}{N-1}}. \tag{4-1}$$

Using Eq. (4-1), the results can be reported as $\bar{T} \pm s$, in which $\bar{T}$ denotes the mean temperature rise.

A thermal analysis was performed to ensure that the thermocouple was accurately positioned at the focused area. The transducer has its focal depth of $51.74\,\text{mm}$, so the thermocouple was positioned accurately at this depth using the 3D motion system (CNC Deluxe Mill, Vista, US). The temperature profile has been measured multiple times on different points around the presumable focal point. Then, the point with the highest temperature has been taken as the focal point. The 3D motion system was used to move the transducer to change the position of focused area inside the phantom around the presumable focal point, and the temperature rise profile at each position was carefully monitored. The result showed that the temperature rise at the original location was the highest; thus it was regarded as the true focal point.

It should be mentioned here that the *in situ* temperature measurement using the thermocouple can result in some artifact effects, causing errors in monitoring the HIFU parameters. Firstly, positioning the thermocouple inside the phantom can result in wave distortion, as a thermocouple with diameter equal to or greater than the wavelength can affect the wave propagation, and thus distort the ultrasonic field [112]. However, the thermocouple used for the

experiments had much smaller diameter (250 μm) than the wavelength (≈ 1.4 mm); therefore, it was unlikely to cause distractive effects on wave propagation [56]. Secondly, the ultrasonic wave propagation can cause a relative motion of the surrounding medium with respect to the thermocouple surface, leading to heating of the thermocouple and consequently higher temperature measurement than that of the surrounding tissue, which called viscous artifact effect.

To address any concerns regarding the thermocouple artifact effects, the method proposed in [56] was followed, and the measured data were modified by considering any temperature rises in pure agar gel in the presence of the thermocouple. An agar phantom without NPs was fabricated, as a low-absorption medium, and the temperature profile was monitored during the HIFU insonation for all ranges of powers and frequencies used for the experiments. Since pure agar gel has a negligible absorption coefficient, any rises of temperature monitored by the thermocouple should be attributed to the artifact heating effect. It was originally postulated that temperature rises would be observed due to the presence of thermocouple. However, no temperature rise was observed in the focal area during the insonation period for all experiments. This may be attributed to the low ranges of powers used for the experiments (2, 4.5, 8, and 12.5 W). As discussed above, the movement of medium around the thermocouple's surface due to the acoustic pressure is the main reason for heating artifacts; therefore, when the powers are high (causing high pressure gradients), the thermocouple artifacts can be significant [33], while it may not be crucial for the HIFU insonation with low ranges of powers.

In addition to temperature monitoring, the rate of absorbed energy per unit volume was also determined. Using the HIFU heat equation (3-17), the absorption rate can be measured by considering the slope of temperature change at the beginning of the insonation when the heat transfer due to the conduction is negligible. Thus, the rate of temperature change during HIFU can

be related to the rate of absorbed energy per unit volume, Q, and specific absorption rate (SAR) by [35]

$$\rho_{mn} C_{P\,mn} \left.\frac{dT}{dt}\right|_{t=0^+} = Q, \tag{4-2}$$

$$SAR = \frac{Q}{\rho_{mn}} = C_{P\,mn} \left.\frac{dT}{dt}\right|_{t=0^+}.$$

To estimate the temperature slope at time zero ($\left.\frac{dT}{dt}\right|_{t=0^+}$), the temperature values, measured by the thermocouple, can be approximated to a function obtained from the solution of the HIFU heat transfer equation by assuming a Gaussian profile for the focal region [35]. The solution can be used for cases where focal zones have small elliptical shapes, where the axial dimension is much greater than the radial dimension. The profile of temperature at the focal point during HIFU as a function of time, is given by [111]:

$$\Delta T = \left(\frac{2\alpha I_{max}}{\rho C_p}\right)\left(\frac{{r_0}^2}{4k}\right) \mathrm{In}(1 + 4kt/{r_0}^2), \tag{4-3}$$

Chapter 5

Results and Discussions

Some parts of the thesis are published in three journals: i) Sadeghi-Goughari, Moslem, Soo Jeon, and Hyock-Ju Kwon. "Enhancing Thermal Effect of Focused Ultrasound Therapy Using Gold Nanoparticles." IEEE transactions on nanobioscience 18.4 (2019): 661-668; ii) Sadeghi-Goughari, Moslem, Soo Jeon, and Hyock-Ju Kwon. "Magnetic nanoparticles-enhanced focused ultrasound heating: size effect, mechanism, and performance analysis." Nanotechnology 31.24 (2020): 245101; iii) Sadeghi-Goughari, Moslem, Soo Jeon, and Hyock-Ju Kwon. "Analytical and Numerical Model of High Intensity Focused Ultrasound Enhanced with Nanoparticles." IEEE Transactions on Biomedical Engineering (2020).

This chapter summarizes the results form the numerical and experimental studies introduced in the previous chapters. First, the results of HIFU on tissue-mimicking phantoms in the absence of NPs are provided in Section 5.1 to better understand HIFU's heating mechanism and to investigate the effect of nonlinearity on the wave propagation and heat transfer. Then, the results from the experiments and numerical modeling on NP-enhanced HIFU are presented in section 5.2 to show the effects of NPs, including AuNPs, MNPs and CNTs, on the thermal mechanism of HIFU.

5.1. Thermal Effect of HIFU

5.1.1. Linear and Nonlinear Effects

This section presents the results from numerical modeling for the linear and nonlinear HIFU analyses (Eq. (3-4)). Figure 5-1 shows the intensity profile along the beam axis when the

transducer was driven at frequency of 1.1 MHz with powers of $10, 50, 100$, and 150 W. The oscillating pattern of wave propagation during HIFU is obvious in the intensity profile in which the highest amplitude of intensity occurs at the focused region with approximate length of 2 cm along the beam axis (i.e., $6 \leq z \leq 8$ cm). A comparison between linear and nonlinear results clearly shows the effects of nonlinearity in higher intensity amplitude. This increase in intensity is induced by the generation of harmonic pressures during the nonlinear wave propagation. Another effect of nonlinearity on the wave distribution can also be detected in the intensity profiles. As we can see, the nonlinearity tends to shift the focal point, where the highest amplitude occurs, to a deeper point inside the phantom. In the intensity diagram for $P = 150$ W, the nonlinearity causes the focal point to shift from 6.2 cm to a deeper point at 6.6 cm. It is also obvious that the nonlinearity depends on the power since the intensity amplitude increases by amplifying the transducer's power.

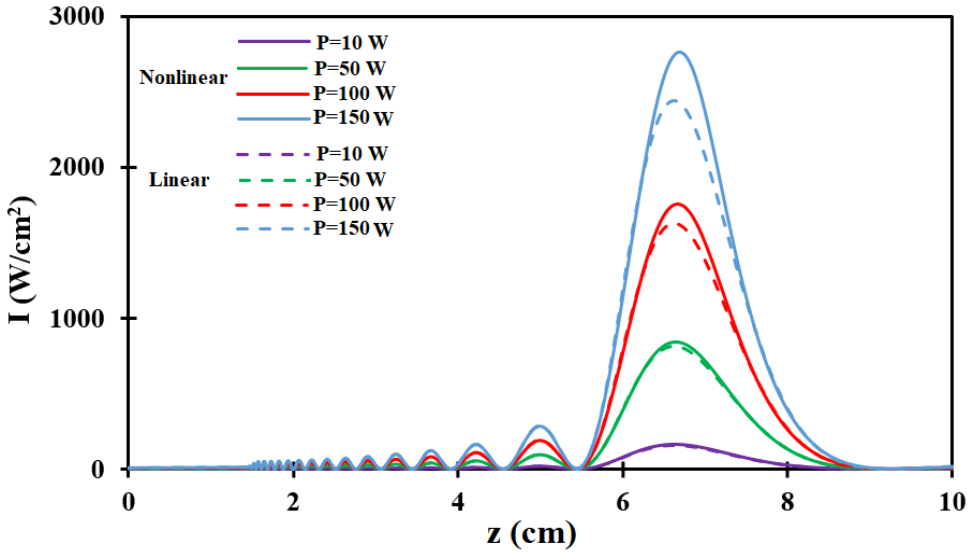

Figure 5-1 Acoustic intensity profile along beam axis derived from linear and nonlinear analyses when the tissue mimicking phantom was used as the computational domain and the transducer was driven at the frequency of 1.1 MHz.

Figure 5-2 shows the maximum intensity of focal point as a function of the power. The results achieved from the nonlinear and linear analyses are compared to show the effects of nonlinearity. As we can see, when the transducer is driven at relatively low powers, the relation between the intensity at focal point and power is linear and the effect of nonlinearity is less significant. However, as the power is increased, the nonlinearity in wave propagation mechanism causes the intensity graph to further deviate from the line. The results also suggest that the effect of nonlinearity in the numerical modeling can be ignored when the transducer was driven at relatively low power in order to reduce computational load and time. For example, the linear analysis may estimate the peak intensity with error less than 1% for power less than 40 W.

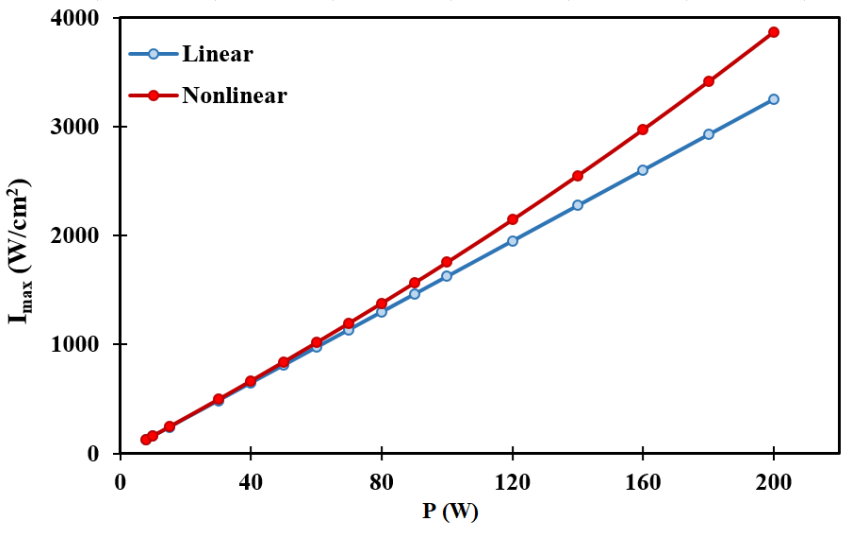

Figure 5-2 Intensity at peak point versus transducer power for linear and nonlinear analyses when the tissue-mimicking phantom was used as the computational domain and the transducer was driven at the frequency of 1.1 MHz.

The results from thermal analysis of HIFU using the numerical simulation are presented in Figure 5-3, which shows the rate of absorbed energy per unit volume along the beam axis (Eq. (3-8)). The diagrams are acquired for the tissue-mimicking phantoms using the linear and nonlinear analyses to show the effects of nonlinearity on the absorption mechanism of acoustic

energy during HIFU. As we can see, the nonlinearity increases the heating rate and corresponding temperature rise at the focused region. Considering the power of 100 W as an example, the nonlinearity causes about 1.4 times more acoustic energy to be converted to heat compared to linear analysis. The increase in the absorption rate of acoustic energy due to the nonlinearity results not only from the production of higher acoustic intensity at the focused area, but also from the generation of higher harmonics of initial frequency during the nonlinear HIFU wave propagation.

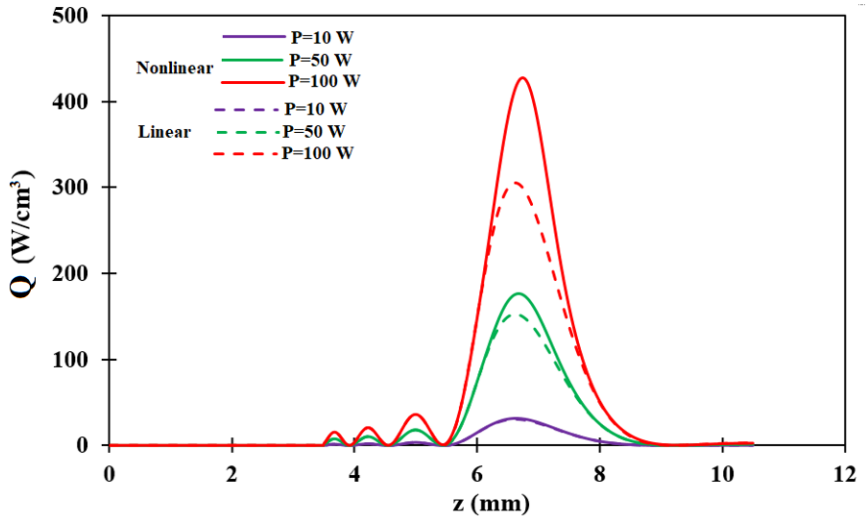

Figure 5-3 Heat absorption profile along the beam axis derived from linear and nonlinear analyses when the tissue-mimicking phantom was used as the computational domain and the transducer was driven at the frequency of 1.1 MHz.

5.1.2. Experimental Results

In this subsection, the temperature profiles for the heating process predicted by the analytical solution (Eq. (3-19)) are presented and compared with the corresponding experimental data achieved from the HIFU experiment, as displayed in Figure 5-4. The results are derived for the tissue-mimicking phantom using an ultrasonic frequency of 1.1 MHz. It can be seen that both analytical and experimental data predicted the same trends during insonation; however, there is an

obvious discrepancy between the experimental and analytical curves. The experimental results show higher temperature at the focal point than for the analytical data. These differences are postulated to be caused by the presence of the thermocouple at the focused area.

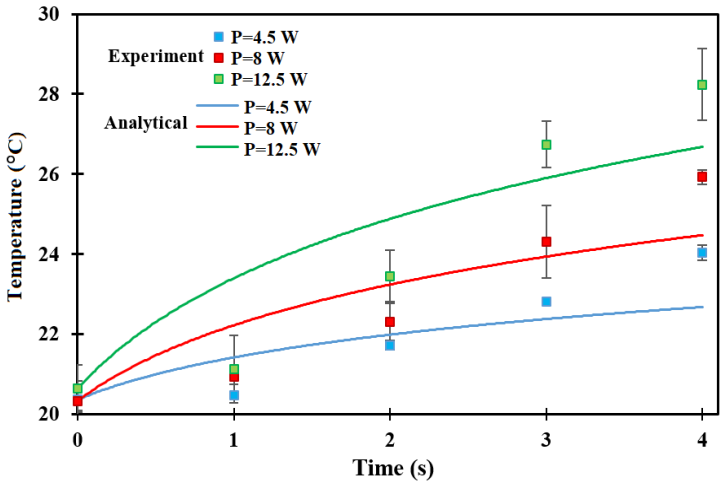

Figure 5-4 Temperature rise of focal point for heating process computed by analytical solution (Eq. (3-19)) and compared with experimental data when the tissue mimicking phantom was used as the computational domain and the transducer was driven at the frequency of 1.1 MHz.

5.2. *NP-Enhanced HIFU*

This section presents the results on the feasibility of using NPs during HIFU, their performance and feature effects on the thermal mechanism of HIFU. Firstly, the experimental observations that show the dose effects of AuNPs when injected locally into the tissue-mimicking phantom and at the focused region are presented. Secondly, the experimental results on the phantoms with uniform distribution of MNPs are provided to show the effects of NP features including the size and volume concentration on the thermal parameters of HIFU. Thirdly, the results form the numerical modeling that predicted the thermal mechanism of HIFU in the presence of NPs are presented and compared with corresponding experiments. Finally, the results achieved from the experimental observations are presented to validate the feasibility of using CNTs as new ultrasound absorption agents during

HIFU, which is followed by discussions on their feature effects on the thermal parameters of HIFU including the absorption rate of acoustic energy and temperature rise.

5.2.1. Dose Effects of AuNPs Under Local Injection

5.2.1.1. Temperature Rise

Figure 5-5 presents the experimental results of temperature profiles at the focal point during the insonation and cooling periods for different doses of AuNPs and powers. All figures demonstrate that the injection of AuNPs significantly enhanced the temperature rise at the focal point during the insonation process. For example, when the power was set at 4.5 W in Figure 5-5(a), the temperature was raised from 20.6 ± 0.7 ℃ to 28.2 ± 1.8 ℃ after 15 second of insonation for the phantom without AuNPs. In comparison, the injection of AuNPs to the focused region increased the temperature rise at the end of insonation by about 1.8 ℃ to 30.1 ± 0.7 ℃ for 0.15 mL dose, and by about 2.2 ℃ to 30.4 ± 0.6 ℃ for 0.3 mL dose. Meanwhile, the comparison between the plots for different powers indicates that the enhancing effects of AuNPs on the temperature rise became more significant as the HIFU transducer was driven at higher powers. More specifically, for the power of 8 W, the enhancements in maximum temperature rise due to AuNPs were about 2.5 ℃ and 4.8 ℃ for the injection dose of 0.15 mL and 0.3 mL, respectively, compared to the case without AuNPs. The temperature rise was even more pronounced for the power of 12.5 W, as shown in Figure 5-5(c), where the injection of 0.15 and 0.3 mL of AuNPs caused the temperature to rise by 9.2 ℃ and 11.8℃, respectively, compared to the case without NPs at the same power.

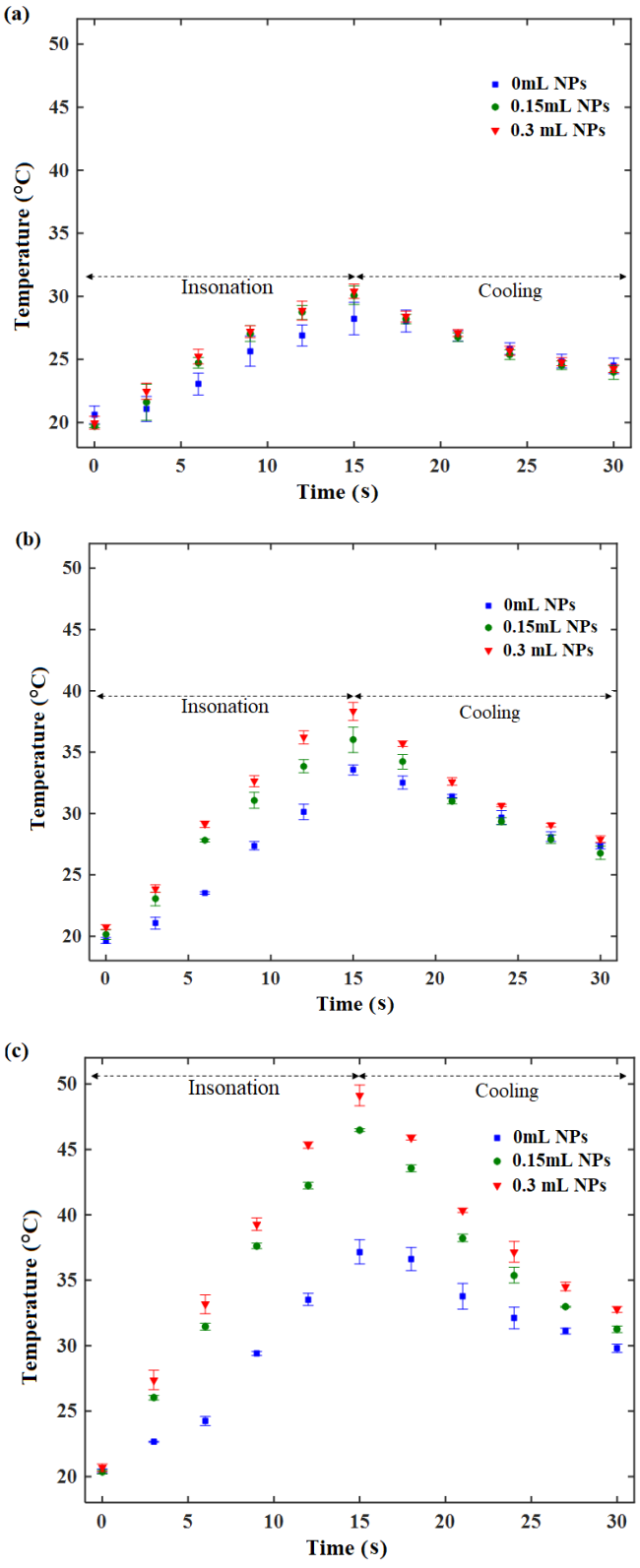

Figure 5-5 Temperature rise diagrams during HIFU with the frequency of 1.1 MHz; and the effects of injected AuNPs at different power levels: **(a)** 4.5 W; **(b)** 8 W; and **(c)** 12.5 W.

5.2.1.2. Absorption Rate

The effects of AuNPs on the heating mechanism of HIFU are provided in more detail in Figure 5-6 which presents the specific absorption rate (SAR) and corresponding maximum temperature rise versus power. Figure 5-6(a) shows that SAR was significantly enhanced by the injection of AuNPs to the focused area for all tested powers. In the case of HIFU driven at the power of 4.5 W, the injection of 0.15 mL of AuNPs enhanced SAR from 584.2 to 2,326.3 W/kg (3.98 times more energy absorption than the case without AuNPs). The trend remained the same as the driving power was increased. Specifically, 2.1 and 2.6 times more acoustic energy were absorbed for the powers of 8 and 12.5 W, respectively, when 0.15 mL dose of AuNPs was injected. Furthermore, the increase of injected dose of AuNPs caused more acoustic energy to be absorbed by the medium. As an example, for the power of 4.5 W, doubling the dose of AuNPs from 0.15 to 0.3 mL induced SAR to increase from 2,326.3 to 3,082.72 W/Kg (1.4 times more acoustic energy was absorbed). Close observation of Figure 5-6(a) also suggests that the injected AuNPs exerted an influence on the trend of SAR with respect to power. In the absence of AuNPs, SAR was increased linearly with the increase of power (blue bars). On the other hand, the injection of AuNPs caused SAR to increase rapidly in a nonlinear manner with the increase of the power (green and red bars). As a result, the effect of AuNPs on temperature rise was expected to become more significant when the HIFU transducer was driven at higher powers. This is indeed corroborated by the plots in Figure 5-6(b) which shows the maximum temperature rise with respect to the driving power. For the phantom without AuNPs, the trend of maximum temperature rise versus the power was almost linear. However, for the injection doses of 0.15 and 0.3 mL of AuNPs, the trend became highly nonlinear.

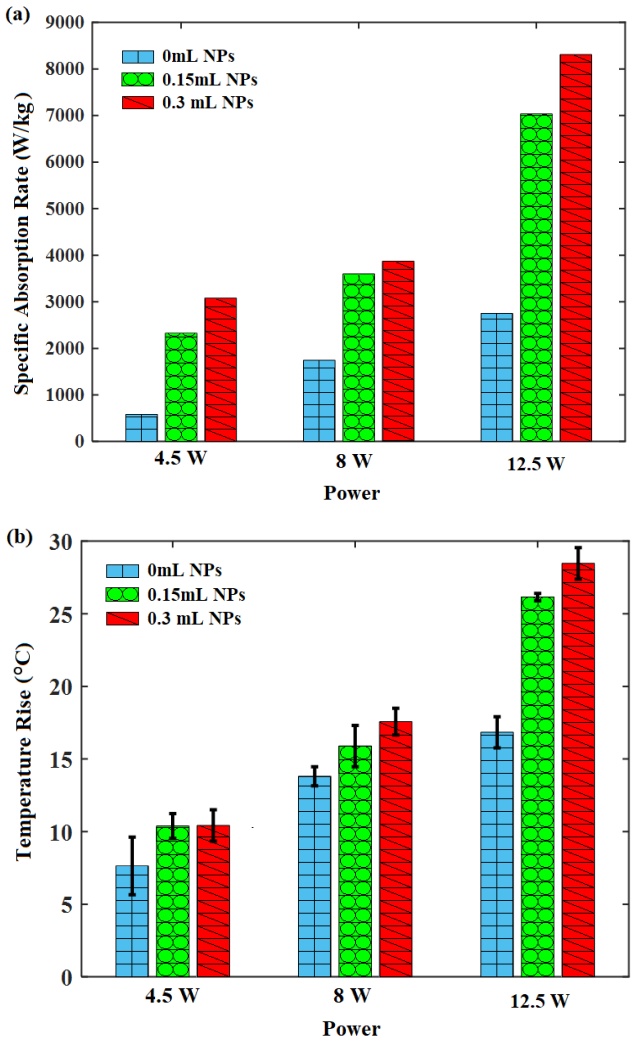

Figure 5-6 Effects of injected AuNPs on heating mechanism: **(a)** specific absorption rate; **(b)** maximum temperature rise at the focal point after 15 seconds of insonation with the frequency of 1.1 MHz.

5.2.2. Effects of NP Features

In this subsection, the effects of NP features including the size and volume concentration on the thermal parameters of HIFU are presented. Here, the results are achieved when the MNPs were used as the nanoscale agents and distributed uniformly in low-absorption phantoms.

5.2.2.1.Temperature Rise

Figure 5-7 shows the effects of MNP size and volume concentration on the temperature rise profile during the HIFU process. The thermal diagrams are provided for different levels of powers with 1.3 MHz ultrasonic frequency. It can be seen from Figure 5-7(a) that for the power of 2 W, the temperature rise profiles are close to each other, although the effects of MNP features are still noticeable. For the phantoms with MNP concentration of 0.5%, the temperature at the focal point was raised by 5.1 ± 0.4 ℃ and 7.8 ± 0.7 ℃ for the MNP sizes of 100 and 200 nm, respectively, after 15 s insonation. Similarly, the temperature rises of 7 ± 0.6 ℃ and 10.6 ± 0.2 ℃ were observed for the MNP sizes of 100 and 200 nm, respectively, when the MNP concentration was 0.75%. It is evident that the heating mechanism was enhanced by increasing the size and volume concentration of MNPs. In addition, a comparison between diagrams with different levels of powers shows that when a higher range of powers was used, the effects of MNPs became more significant. For the power of 4.5 W, as shown in Figure 5-7(b), the peak temperature rises for the phantoms with MNP sizes of 100 and 200 nm, respectively, were 10.2 ± 0.7 ℃ and 15.7 ± 0.6 ℃ for 0.5% MNP concentration, and 15.5 ± 0.6 ℃ and 22 ± 1.2 ℃ for 0.75% MNP concentration. The effects of MNP features were even more pronounced for 8 W (Figure 5-7(c)). By doubling the MNP size from 100 to 200 nm, the peak temperature rise increased from 15.6 ± 1.2 ℃ to 26 ± 1.3 ℃ for 0.5% MNP concentration, and from 22.5 ± 0.7 ℃ to 46 ± 1.3 ℃ for 0.75% concentration.

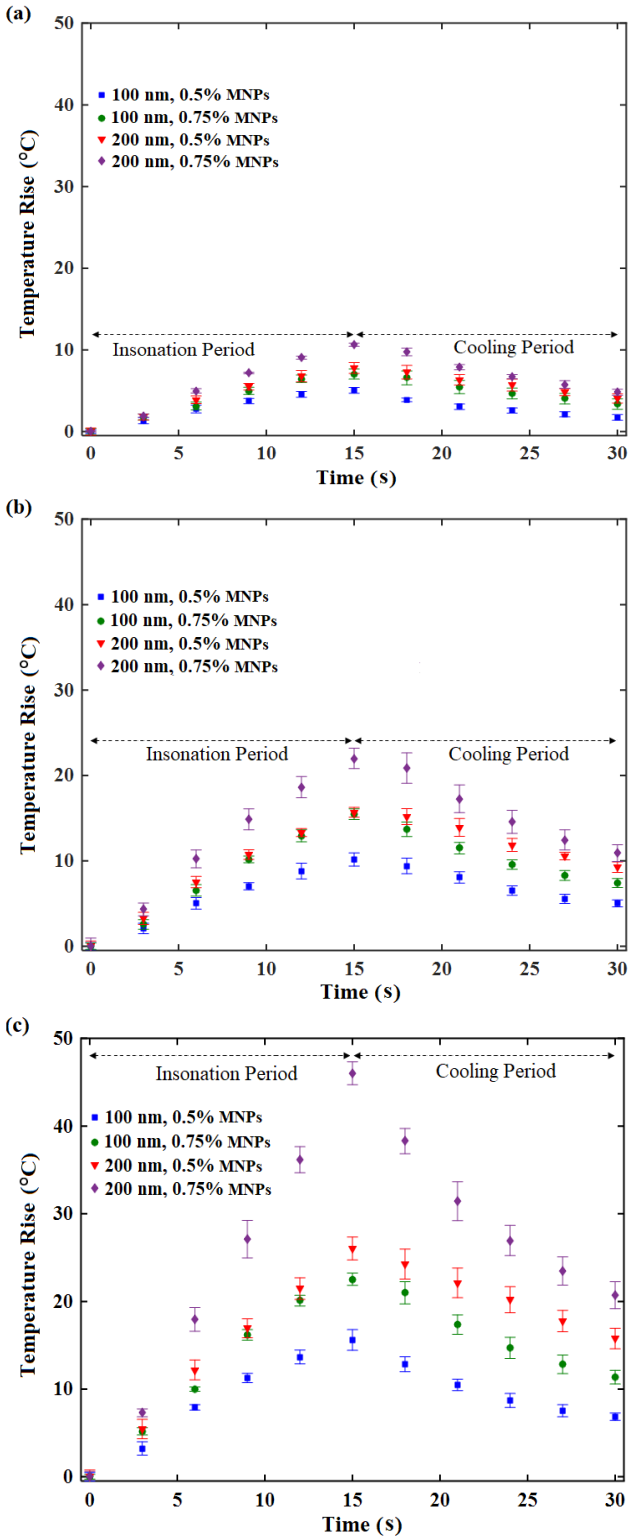

Figure 5-7 Temperature rise profile for phantoms with different concentrations and sizes of MNPs during HIFU for the powers of **(a)** 2 W, **(b)** 4.5 W, and **(c)** 8 W. Ultrasonic frequency was 1.3 MHz.

Figure 5-8 together with Figure 5-7(c) shows the effect of ultrasonic frequency on the performance of MNPs during HIFU when the power of 8 W was used. Figure 5-8(a) indicates that the HIFU insonation for 15 s with the frequency of 1 MHz increased the temperature at the focal point of phantoms with MNPs sizes of 100 and 200 nm, respectively, by 4.8 ± 1.5 ℃ and 9.4 ± 1 ℃ for 0.5% MNP concentrations; by 8.9 ± 1.2 ℃ and 14.8 ± 1.1 ℃ for the concentrations of 0.75%. On the other hand, when the higher frequency of 1.15 MHz was used for the insonation (Figure 5-8(b)), the peak temperature rises for the phantoms with MNP sizes of 100 and 200 nm, respectively, were 9.5 ± 1 ℃ and 14.5 ± 1.6 ℃ for the MNP concentration of 0.5 %; were 13 ± 1.3 ℃ and 19 ± 1.3 ℃ for the concentration of 0.75 %. Overall, the results suggest that the heating mechanism causing temperature rise in MNP-enhanced HIFU process was significantly enhanced by increasing the size and volume concentration of MNPs for all ranges of ultrasonic frequencies; furthermore, when the higher frequencies were used, the effects of MNP features on the heating mechanism became more significant.

5.2.2.2. Absorption Rate

The rate of absorbed energy per unit volume was calculated from the temperature profiles using Eq. (4-2). Figure 5-9(a) presents Q versus power at the ultrasonic frequency of 1.3 MHz. It is evident that Q was enhanced by increasing the power; a close observation suggests a nonlinear trend between the rate of absorbed energy per unit volume and the power in the presence of MNPs. Considering the phantom with 0.75% concentration and 100 nm size of MNPs as an example, the increase of power from 2 to 4.5 W increased Q by 1.4 times, whereas for the power of 8 W, 2 times more energy was converted to heat compared to 4.5 W.

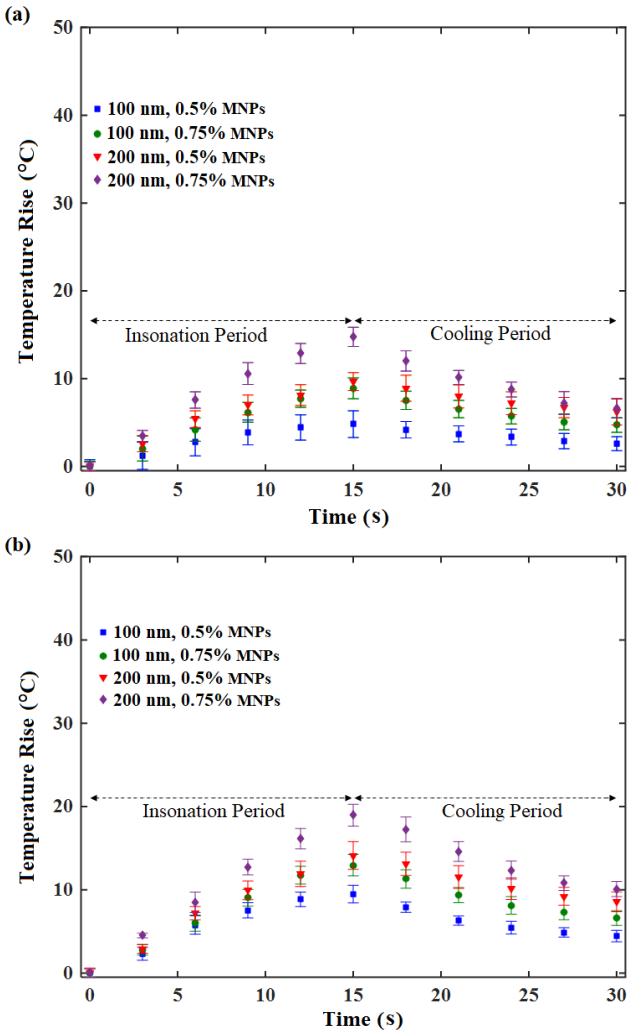

Figure 5-8 Temperature rise profile for phantoms with different concentrations and sizes of MNPs during HIFU using frequency of **(a)** 1 MHz, **(b)** 1.15 MHz. Power was set at 8 W. Refer to Figure 5-7(c) for the frequency of 1.3 MHz.

Similarly, Figure 5-9(b) shows the effect of ultrasonic frequency on the rate of absorbed energy per unit volume when the power was set at 8 W. As expected, Q was enhanced by the increase of ultrasonic frequency for all phantom models. For example, the increase of frequency from 1 to 1.15 and 1.3 MHz caused about 2 and 3 times more acoustic energy to be absorbed by the phantom with MNP size of 100 nm and concentration of 0.5%, respectively. The effects of MNP features on the absorption mechanism of acoustic energy is also evident from Figure 5-9. As

we can see, Q was enhanced by increasing the size and volume concentration of MNPs for all tested ranges of powers and ultrasonic frequencies. As an illustration, about 2 times more energy was converted to heat by the phantom with the MNP size of 200 nm than that with the size of 100 nm, when the MNP concentration was 0.5% and the ultrasonic signal was sent at the frequency of 1.3 MHz and the power of 8 W.

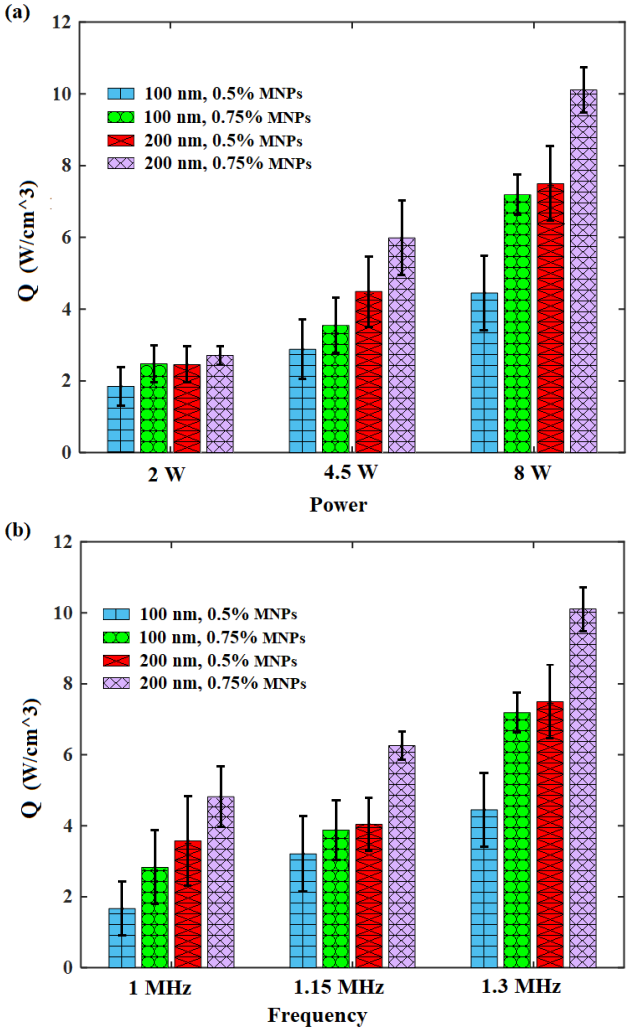

Figure 5-9 Rate of absorbed energy per unit volume for phantoms with different sizes and concentrations of MNPs as a function of: **(a)** power with the ultrasonic frequency of 1.3 MHz; **(b)** ultrasonic frequency with the power of 8 W.

5.2.2.3.Discussion

All of the thermal results have indicated the improving effects of MNPs on the focused ultrasound heating by enhancing the rate of absorbed energy per unit volume and temperature rise. As discussed in subsection 3.2.1, the presence of NPs in a biological tissue can enhance the absorption rate of ultrasonic energy through the viscous and thermal waves mechanisms [35, 103, 108], as illustrated in Figure 3-3. Considering Eq. (3-13), the absorption mechanism of acoustic energy due to the viscous and thermal waves depends on the features of MNPs, including the size and volume concentration. Since both mechanisms occur at the interface of MNPs and suspending medium, the size of MNPs plays a crucial role on the rate of acoustic energy converted to heat. As the MNP radius increases, a larger portion of the particle volume near the surface is involved in the viscous and thermal processes, resulting in higher absorption of the acoustic energy [103, 108]. On the other hand, the increase of MNP concentration enhances the volume of the medium interacting with MNPs, leading to the increase of acoustic energy absorbed in a medium. As a result, it is confirmed that the MNPs with larger size and higher concentration show better performance in enhancing the absorption efficiency of HIFU than those with smaller size and lower concentration, as shown in the experimental results in Figure 5-9.

Due to the increase of absorption rate discussed above and also temperature gradient caused by the interaction between MNPs and ultrasonic waves (Eq. (3-15)), it is expected that the presence of MNPs can significantly enhance the temperature rise profile, as has been supported by the experimental measurement in Figure 5-7 and Figure 5-8. The increase in absorption rate causes more heat to be generated during the HIFU insonation, resulting in a greater temperature rise. Additionally, the temperature gradient due to MNPs' work promotes a rise in the momentum of thermal waves, inducing a heat flow in the direction of ultrasonic waves, and consequently a rise

in temperature profile [103]. Among these two mechanisms involved with temperature rise, the absorption rate is linearly proportional to the power (Eq. (3-12)), while the temperature gradient due to the MNPs' work is related to the square root of power (Eq. (3-15)). As a result, a nonlinear trend between power and the HIFU parameters is expected, as shown in Figure 5-9(a).

Since both the absorption rate and the work done by MNPs increase with the power, it can also be concluded that MNPs show better performance on the heating mechanism when a higher range of powers is applied, as discussed in Figure 5-7 and Figure 5-9(a). In addition to power, the ultrasonic frequency can also affect the performance of MNPs, as the depth of viscous and thermal waves formed around the MNPs can be increased with the frequency (Eq. (3-13)) [108]. As a result, when the acoustic waves are emitted at higher frequency, more acoustic waves are absorbed due to their interactions with thermal and viscous waves, resulting in a higher temperature rise. The enhancing effect of ultrasonic frequency on the performance of MNPs has been shown by experimental results in Figure 5-8 and Figure 5-9(b).

5.2.3. Numerical Modeling

The results of NP-enhanced HIFU predicted by the numerical modeling are presented in this subsection. The thermal diagrams are achieved when the MNPs with the size of 100 nm were used as the nanoscale agents and distributed uniformly in a low-absorption phantom medium.

5.2.3.1. Experimental Validation

First, the results obtained from the numerical simulation were compared with the experimental results to verify the validity of the numerical model. Figure 5-10 shows the temperature rise profiles at the focal point during the insonation for 15 seconds with the power of 8 W and a series of ultrasonic frequencies; continuous lines and markers refer to the simulation and experimental

results, respectively. Generally, both the numerical simulation and the experiment predicted similar trends in all diagrams. Firstly, temperature at the focal point increases with the insonation time in similar nonlinear manners in both results. However, the simulation predicted slightly higher temperature rises than experiments in all profiles, which will be discussed later in this section. Secondly, both results show that the temperature rise during HIFU was enhanced by increasing the MNP concentration, as well as by amplifying the ultrasonic frequency. For the phantom with MNP concentration of 0.5%, the maximum temperature rises of 4.8 ± 1.5 ℃, 9.5 ± 1.1 ℃, and 15.6 ± 1.2 ℃ were observed from the experiments for the ultrasonic frequencies 1, 1.15, and 1.3 MHz, respectively; in comparison, the temperature rises of 6.3 ℃, 9.3 ℃, and 13 ℃ were predicted by the numerical simulation for the corresponding frequencies. Lastly, Figure 5-11 and Figure 5-10(c) suggest that temperature rise was enhanced with the increase of driving power. Considering the phantom with MNP concentration of 0.75%, after 15 second insonation with the powers of 2, 4.5 and 8 W at the frequency of 1.3 MHz, maximum temperature rises of 7.1 ± 0.6 ℃, 15.5 ± 0.6 ℃, and 22.5 ± 0.7 ℃, respectively, were observed from the experiments, whereas the temperature rises of 6.8 ℃, 13.1 ℃, and 21.1 ℃, respectively, were derived from the numerical simulation.

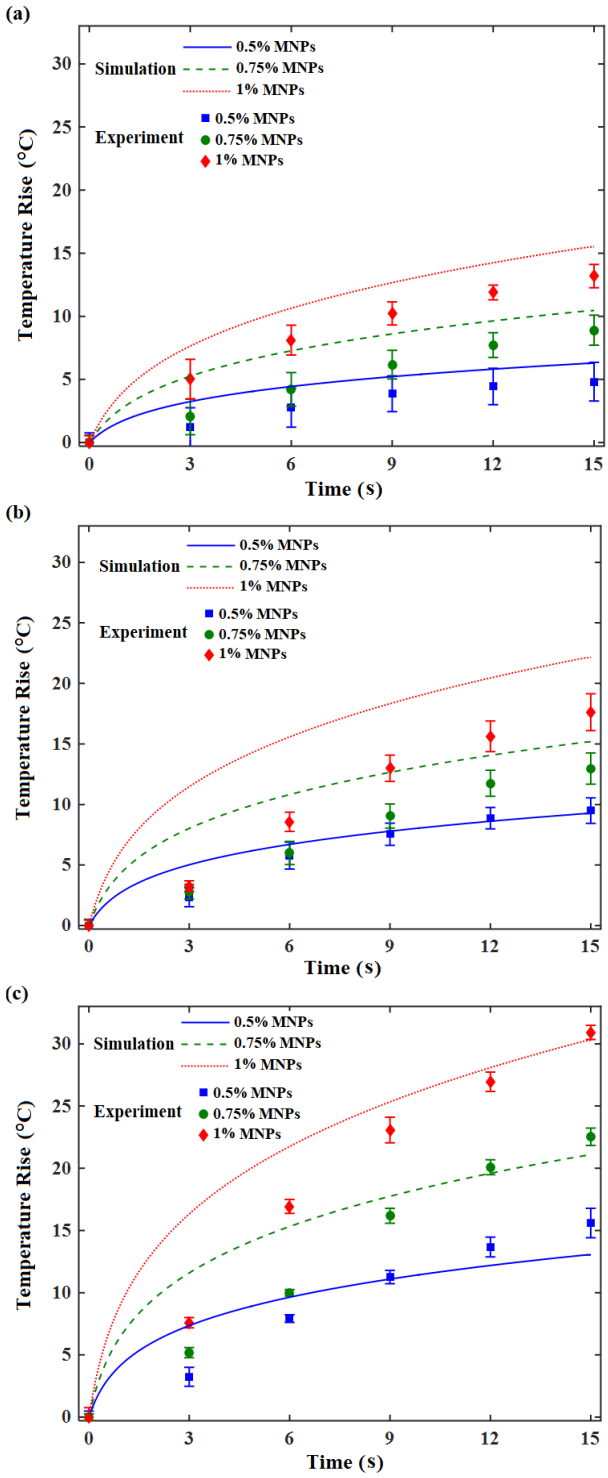

Figure 5-10 Temperature rise profile during HIFU determined by numerical simulation and compared with experimental measurements for phantoms with different concentrations of MNPs, power of 8 W, and frequency of **(a)** 1 MHz, **(b)** 1.15 MHz, **(c)** 1.3 MHz.

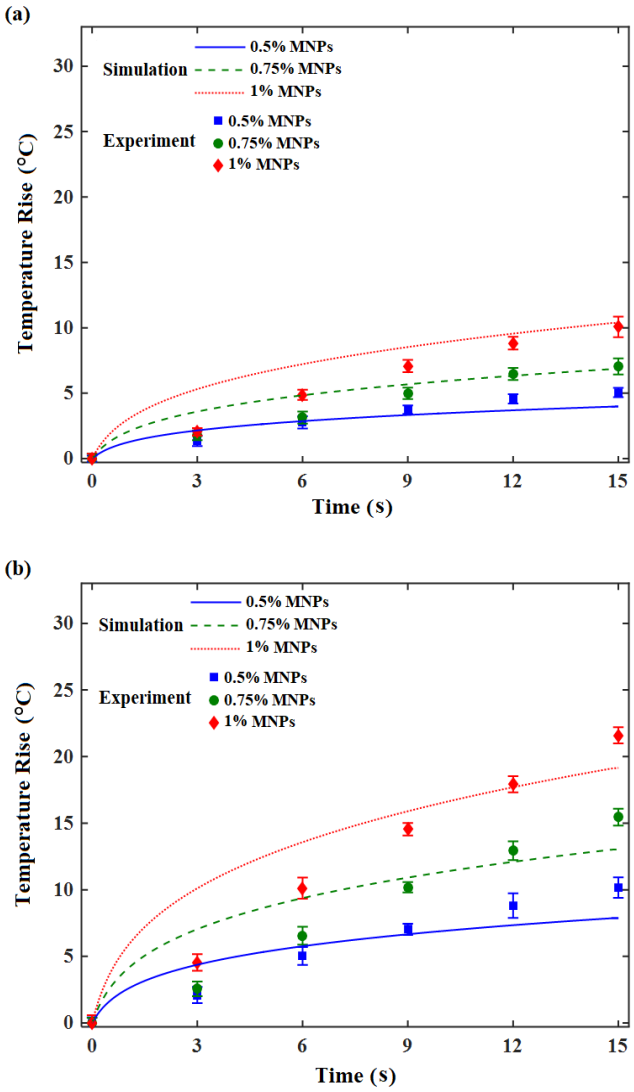

Figure 5-11 Temperature profile during HIFU determined by numerical simulation and compared with experimental measurements for phantoms with different concentrations of MNPs, frequency of 1.3 MHz, and powers of **(a)** 2 W, **(b)** 4.5 W. Please also note Figure 5-10(c) for power of 8 W.

The temperature rise diagrams show a noticeable discrepancy between the numerical results and those measured from the experiments; the numerical modeling predicted higher temperature rises for the HIFU insonation than the experiments, particularly at the beginning of the insonation. This discrepancy might be mainly attributed to the boundary conditions regarding acoustic power used for numerical modeling, as well as the experimental design due to the use of

thermocouple for temperature measurement. In the numerical modeling, the power monitored by the RF amplifier was considered as the acoustic power for the boundary condition in pressure calculation; however, the power generated by RF amplifier circuit was electrical power which was higher than the actual acoustic power emitted from the transducer's surface. In addition, for experiments, a needle-type thermocouple was embedded inside the phantoms to measure the temperature at the focal point which could result in some artificial effects. Firstly, the thermocouple does have higher thermal conductivity and lower thermal capacity than the phantom medium, thus, at the beginning of the insonation, there might be a difference between the actual temperature of the medium and that monitored by the thermocouple. Secondly, the needle thermocouple could only measure the temperature at its tip, thus, a small gap between the tip of thermocouple and the actual focal point, and even a small movement of the thermocouple during the wave propagation could result in some errors during the temperature measurement.

To explore the effects of acoustic power and the position of thermocouple with respect to the focal point on thermal results, the temperature rise profile monitored during an experiment (phantom with 1% volume concentration of MNPs, the power of 8 W and frequency of 1 MHz) is compared with temperature rise profiles for various acoustic powers in Figure 5-12(a) and for various positions of thermocouple in Figure 5-12(b). The result show that a small change in the power or the position of thermocouple can cause a significant change in the results predicted form the numerical modeling, and consequently their difference in respect to the experimental results; specifically, the discrepancy between numerical and experimental results decreases when the lower acoustic powers in comparison to electrical power were used for the numerical modeling.

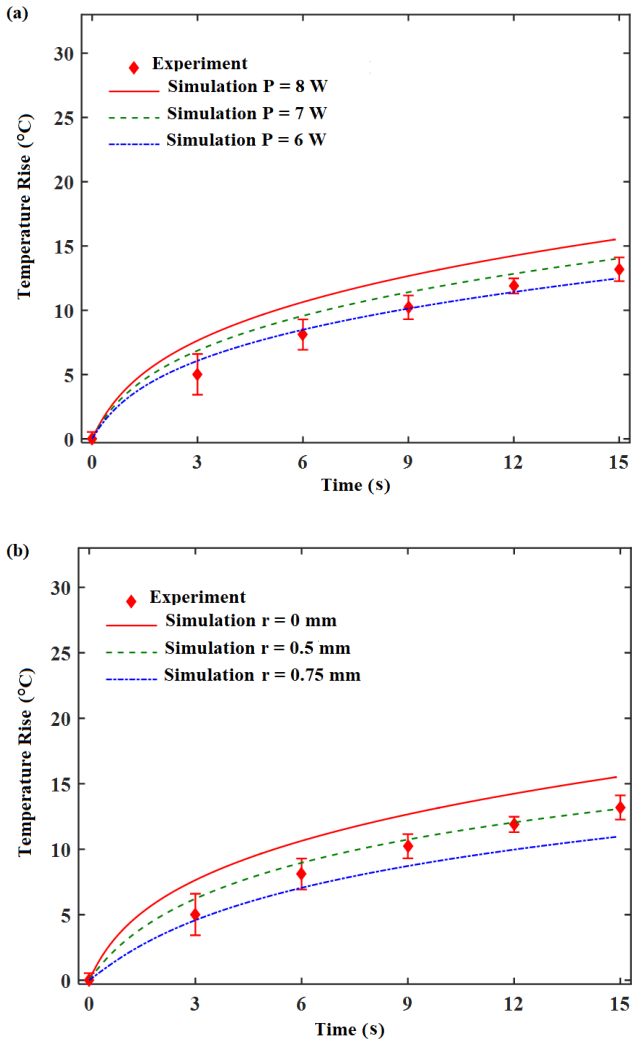

Figure 5-12 The effects of **(a)** acoustic power, and **(b)** the position of thermocouple tip with respect to focal point, on temperature rise profile predicted by numerical modeling in comparison with experimental result when $\varphi = 1\%$, $P = 8\,W$, and $f = 1$ MHz.

5.2.3.2.The NP mechanisms during HIFU

The detailed results of focused ultrasound heating in the presence of NPs are presented in this subsection that show the contribution of each mechanism to the heat generation during the insonation. Figure 5-13 and Figure 5-14 display the diagrams related to the rate of absorbed energy per unit volume and temperature rise, respectively, when the power of 8 W and the ultrasonic

frequency of 1 MHz were applied. The results indicate that the thermal and viscous absorption mechanisms (q_{tv}) which occurs at the interface of MNPs play the major role in converting the acoustic energy to heat, and consequently temperature rise during the HIFU procedure. Considering the computational medium with MNP concentration of 0.5% as an example, about 74% of total wave absorption and 64 % of total temperature rise were caused by q_{tv}. It is also evident that the temperature gradient mechanism caused by the MNPs motion (q_w) plays an active role in generating heat as well as in rising temperature at the focal area. For MNP concentration of 0.5%, nearly 18% of total heat generation and 29% of total temperature rise during the HIFU insonation were attributed to q_w. In addition, the comparison between the diagrams for different volume concentrations shows that the contribution of q_w to the temperature rise become more significant as the concentration of MNPs in the medium is increased. For example, the contribution of q_w on rising temperature was increased to about 39% and 46% for the volume concentrations of 0.75% and 1%, respectively. In the present numerical simulation, the contribution of intrinsic wave absorption (q_i) to the heat generation is minor since the agar gel, used for mimicking the biological tissue and hosting MNPs, have ignorable intrinsic absorption coefficient.

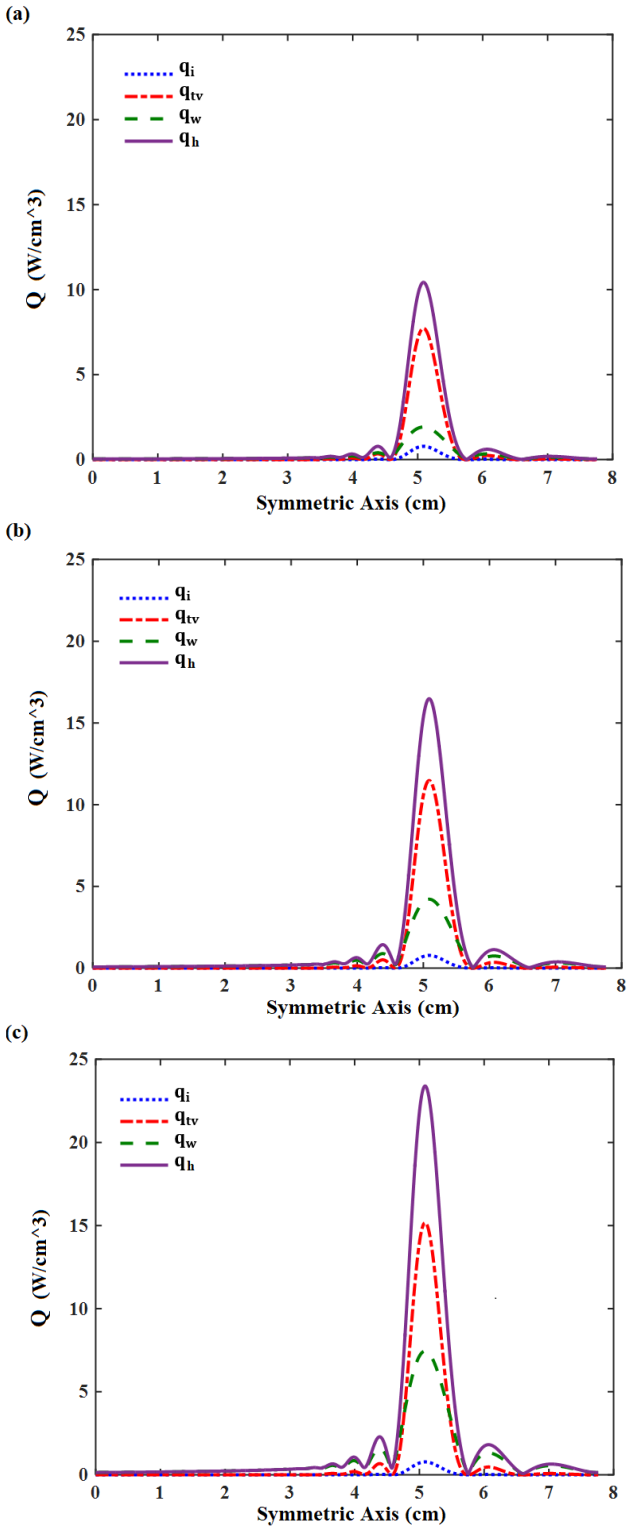

Figure 5-13 Contribution of each mechanism corresponding to NPs on the absorption rate of acoustic energy for phantoms with concentrations of; **(a)** 0.5% MNPs, **(b)** 0.75% MNPs, and **(c)** 1% MNPs; when the power of 8 W and the ultrasonic frequency of 1 MHz were applied

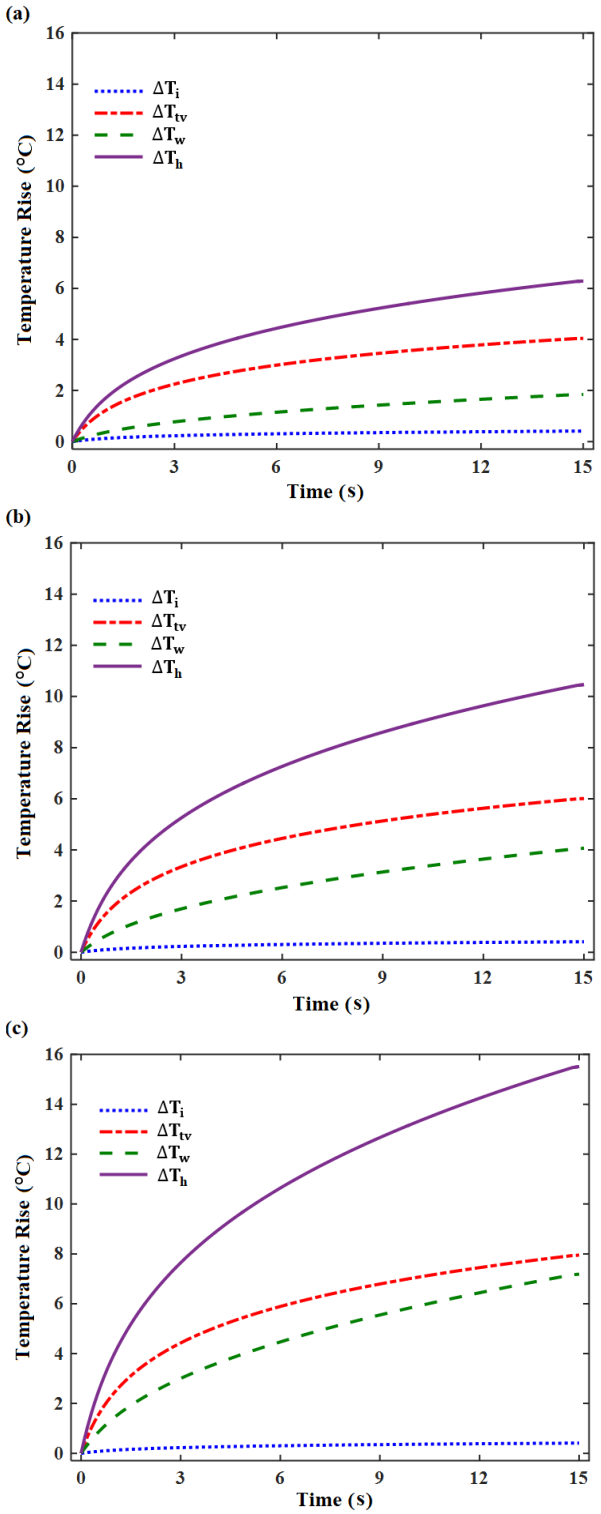

Figure 5-14 Contribution of each mechanism corresponding to NPs on the temperature rise profile for phantoms with concentrations of; **(a)** 0.5% MNPs, **(b)** 0.75% MNPs, and **(c)** 1% MNPs; when the power of 8 W and the ultrasonic frequency of 1 MHz were applied.

5.2.3.3.Temperature rise contour

Figure 5-15 through Figure 5-19 show the temperature rise contours at the focused region, calculated by the numerical simulation for different ultrasonic frequencies and powers, and for media with different MNP concentrations. The numerical simulation predicted a butterfly-shaped distribution of temperature rise profile at the focused region due to the concave geometry of HIFU transducer; no temperature rise was monitored outside the focused region. As we can see from the temperature contours, an increase in MNP concentration resulted in a higher temperature rise at the focused region. For the HIFU insonation with the power of 8 W and ultrasonic frequency of 1 MHz, maximum temperature rises of 6.29 ℃, 10.46 ℃ and 15.51 ℃ were monitored for the MNP concentrations of 0.5%, 0.75%, and 1%, respectively. The numerical simulations also indicate that the temperature rise at the focused region was enhanced by increasing the power; however, the increasing ratio depends on the MNP concentrations. A close observation of temperature contours suggests a nonlinear trend between power and temperature rise. As it can be seen for the numerical medium with MNP concentration of 1% and the ultrasonic frequency of 1.3 MHz, the increase of power from 2 to 4.5 W enhanced the temperature rise 1.8 times (from 10.39 ℃ to 19.15 ℃), whereas the relative enhancement of maximum temperature rise was nearly 1.5 times for the power of 8 W when compared to 4.5 W (30.21 ℃ vs 19.15 ℃). Finally, the enhancement of temperature rise with ultrasonic frequency is also evident from the numerical simulation. Considering the phantom with MNP concentration of 0.75% as an example, the maximum temperature rises of 10.46 ℃, 15.18 ℃, and 21.01 ℃ were computed for the ultrasonic frequencies of 1, 1.15, and 1.3 MHz, respectively.

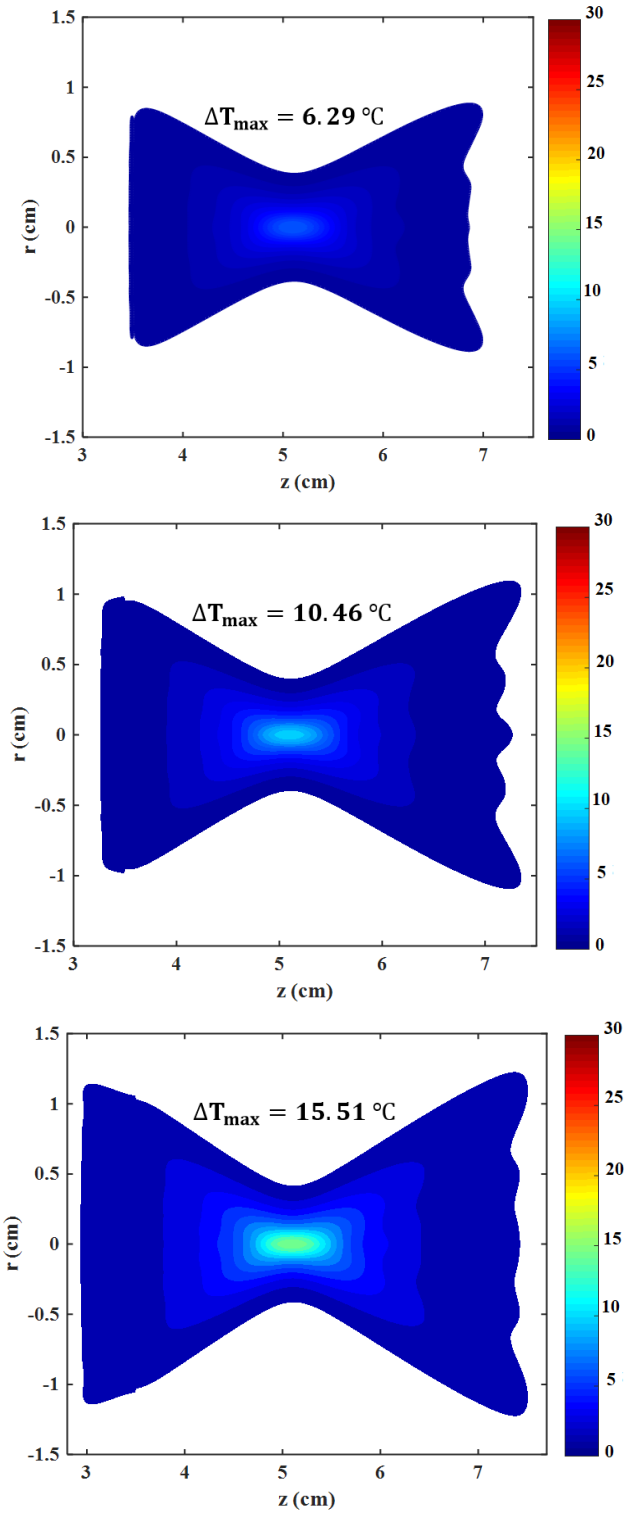

Figure 5-15 Temperature rise contours derived by numerical modelling at the focal region and at the end of insonation for phantoms with different concentrations of MNPs **(a)** 0.5% MNPs, **(b)** 0.75% MNPs, **(c)** 1% MNPs, when $P = 8\,W$ and $f = 1\,MHz$.

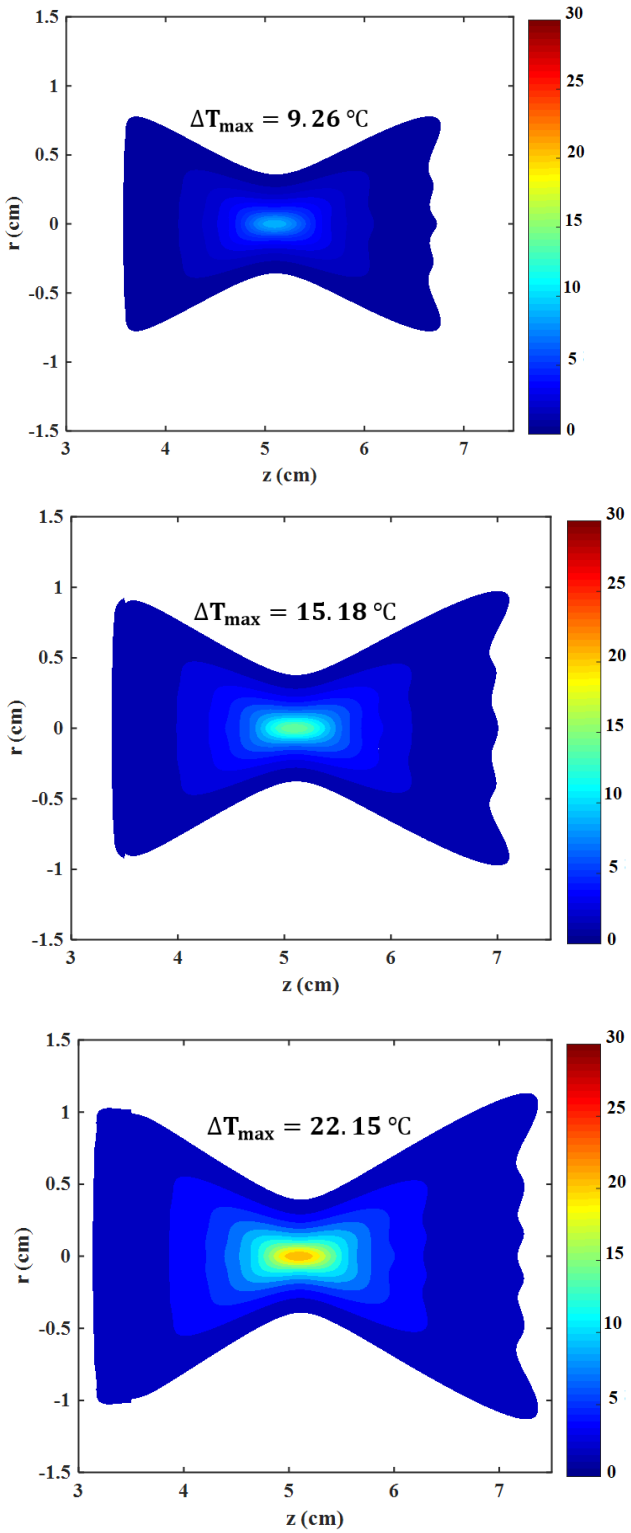

Figure 5-16 Temperature rise contours derived by numerical modelling at the focal region and at the end of insonation for phantoms with different concentrations of MNPs **(a)** 0.5% MNPs, **(b)** 0.75% MNPs, **(c)** 1% MNPs, when $P = 8\,W$ and $f = 1.15\,MHz$.

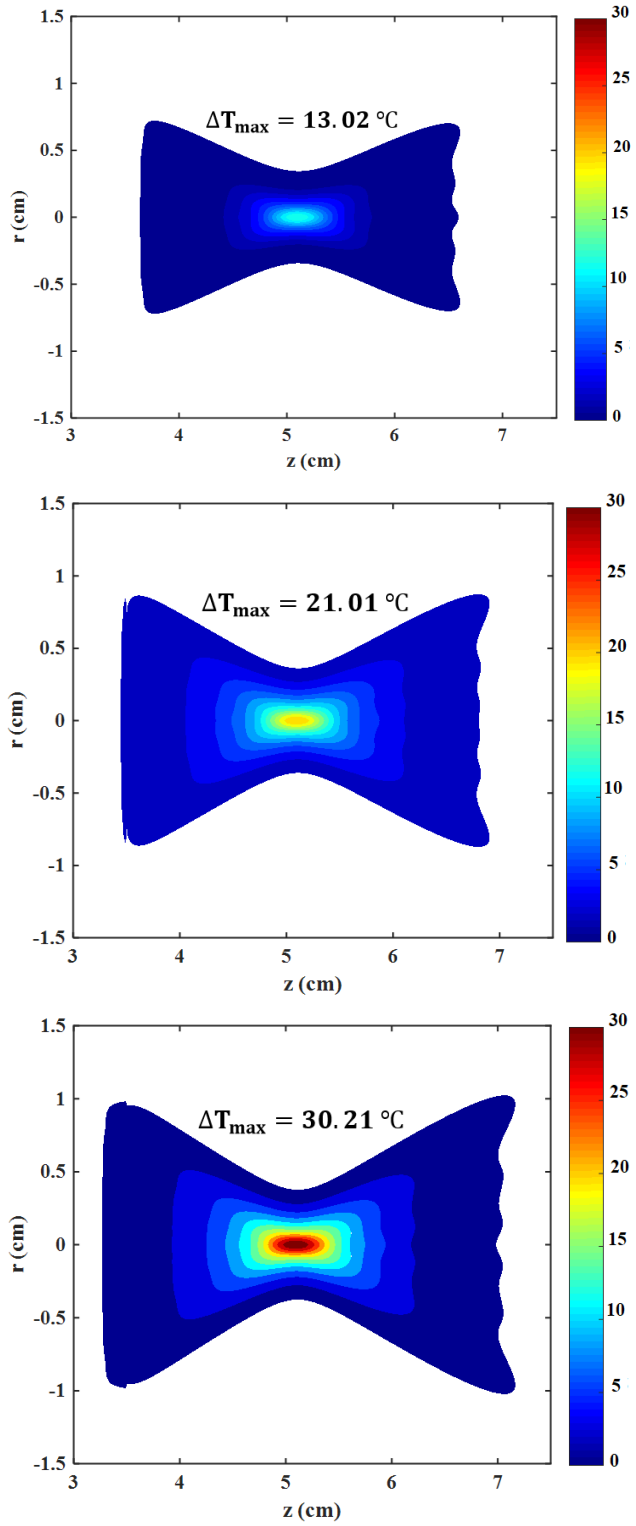

Figure 5-17 Temperature rise contours derived by numerical modelling at the focal region and at the end of insonation for phantoms with different concentrations of MNPs; **(a)** 0.5% MNPs, **(b)** 0.75% MNPs, **(c)** 1% MNPs, when $P = 8\,W$ and $f = 1.3\,MHz$.

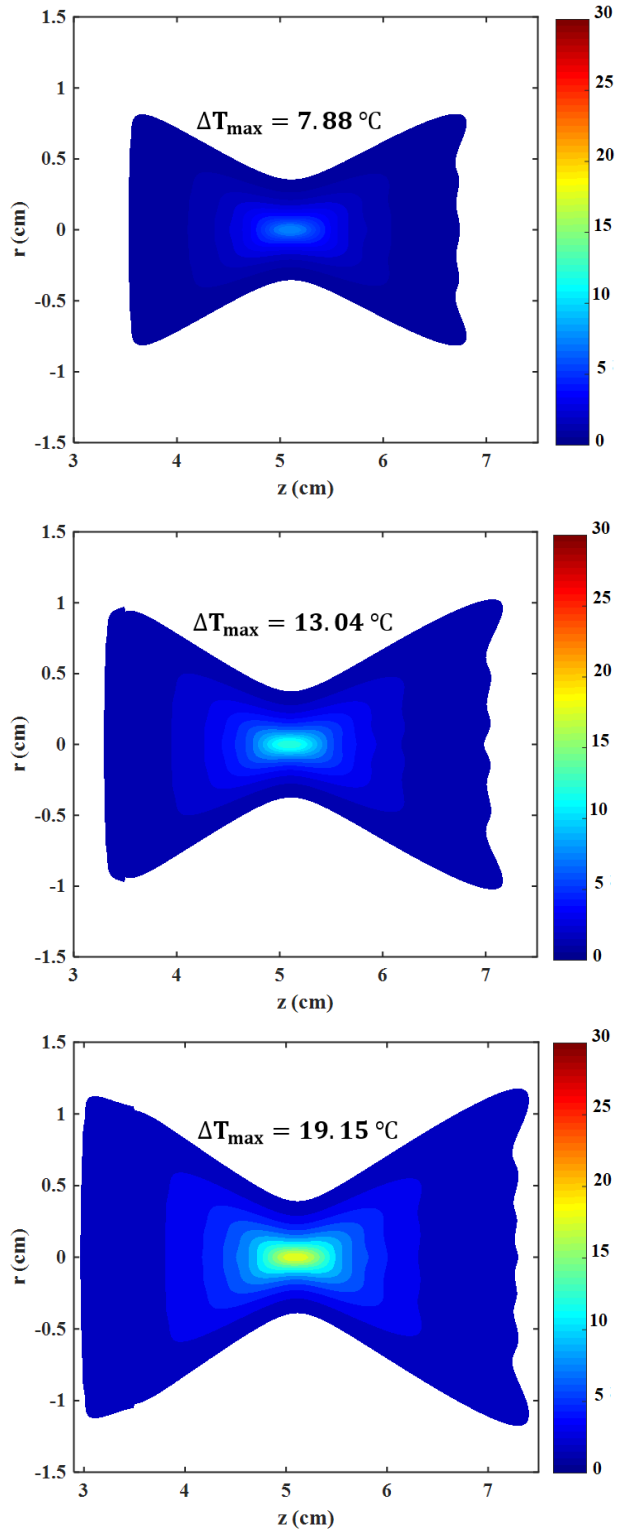

Figure 5-18 Temperature rise contours derived by numerical modelling at the focal region and at the end of insonation for phantoms with different concentrations of MNPs; **(a)** 0.5% MNPs, **(b)** 0.75% MNPs, **(c)** 1% MNPs, when $P = 4.5\ W$ and $f = 1.3\ MHz$.

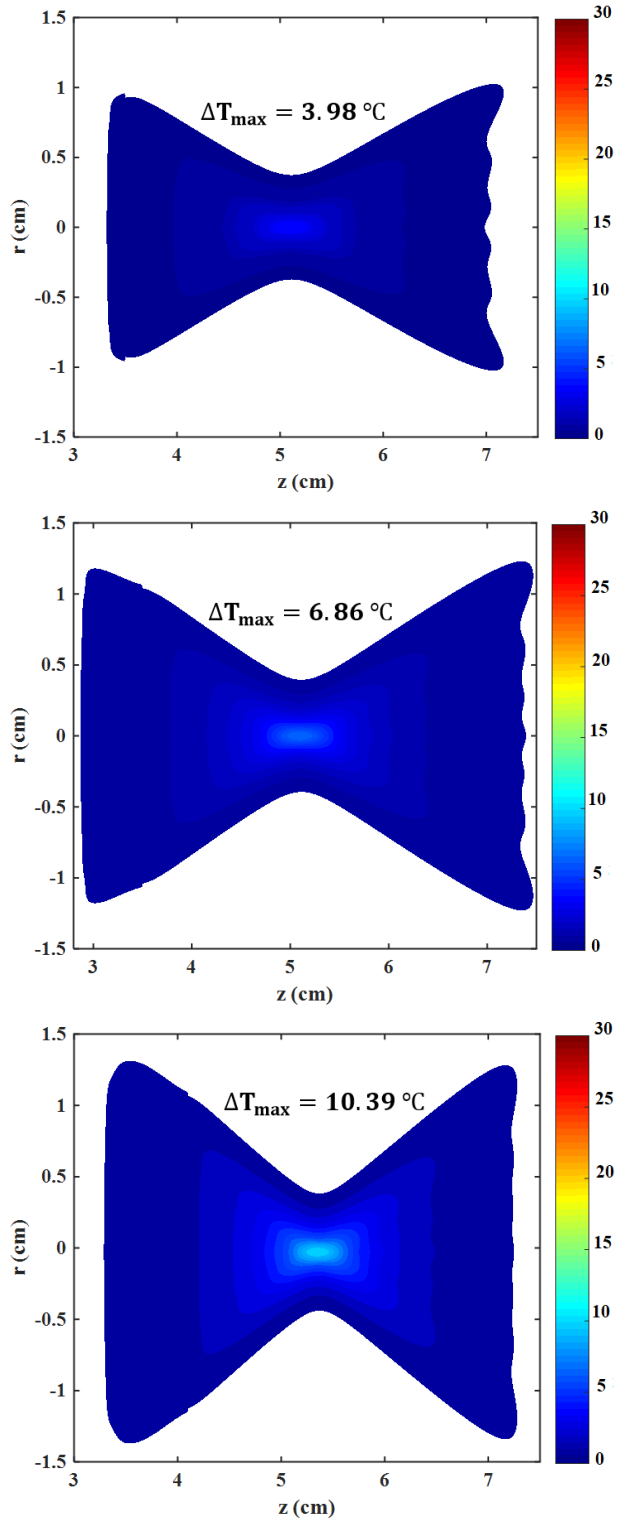

Figure 5-19 Temperature rise contours derived by numerical modelling at the focal region and at the end of insonation for phantoms with different concentrations of MNPs; **(a)** 0.5% MNPs, **(b)** 0.75% MNPs, **(c)** 1% MNPs, when $P = 2\,W$ and $f = 1.3\,MHz$.

5.2.3.4. Size effects of NPs

The size effect of MNPs on the HIFU thermal procedure was also determined using the numerical modeling. Figure 5-20 shows the temperature rise profile during the HIFU insonation for different MNP sizes of 50, 75, and 100 nm. The numerical diagrams were derived for different ranges of frequencies when power was 8 W. It is evident that the temperature rise during the HIFU insonation was enhanced by increasing the MNP size for all ranges of frequencies. Considering Figure 5-20(a) for frequency of 1 MHz as an example, the increase of MNP size from 50 nm to 75 nm and to 100 nm enhanced the temperature rise at the end of insonation by about 3.12 ℃ and 6.84 ℃, respectively. In addition, a comparison between diagrams with different levels of frequencies indicates that the size effect of MNPs became more significant when a higher range of ultrasonic frequencies was used. For the ultrasonic frequency of 1.3 MHz (Figure 5-20(c)), the increase of MNP size from 50 nm to 75 nm and to 100 nm enhanced the maximum temperature rise by about 6.43 ℃ and 14.52 ℃, respectively.

The details on the size effect of NPs are presented in Figure 5-21, which shows the total absorption coefficient of acoustic energy versus the MNP diameter in the range of 10 to 1000 nm for various ultrasonic frequencies. As it can be seen, the total absorption coefficient is increased with the NP size and attained a peak value at a critical diameter. For an example, the peak in total absorption coefficient is observed at the MNP size of 700 nm for the ultrasonic frequency of 1 MHz . The results also show that the critical diameter depends on the ultrasonic frequency in which an increase in frequency tends to shift the peak in attenuation coefficient to occur at lower diameter. As we can see, the increase of ultrasonic frequency from 1 to 1.3 MHz enhanced the peak in attenuation coefficient form 61.01 to 79.29 $\frac{dB}{m}$ and shifted the critical NP size to 600 nm.

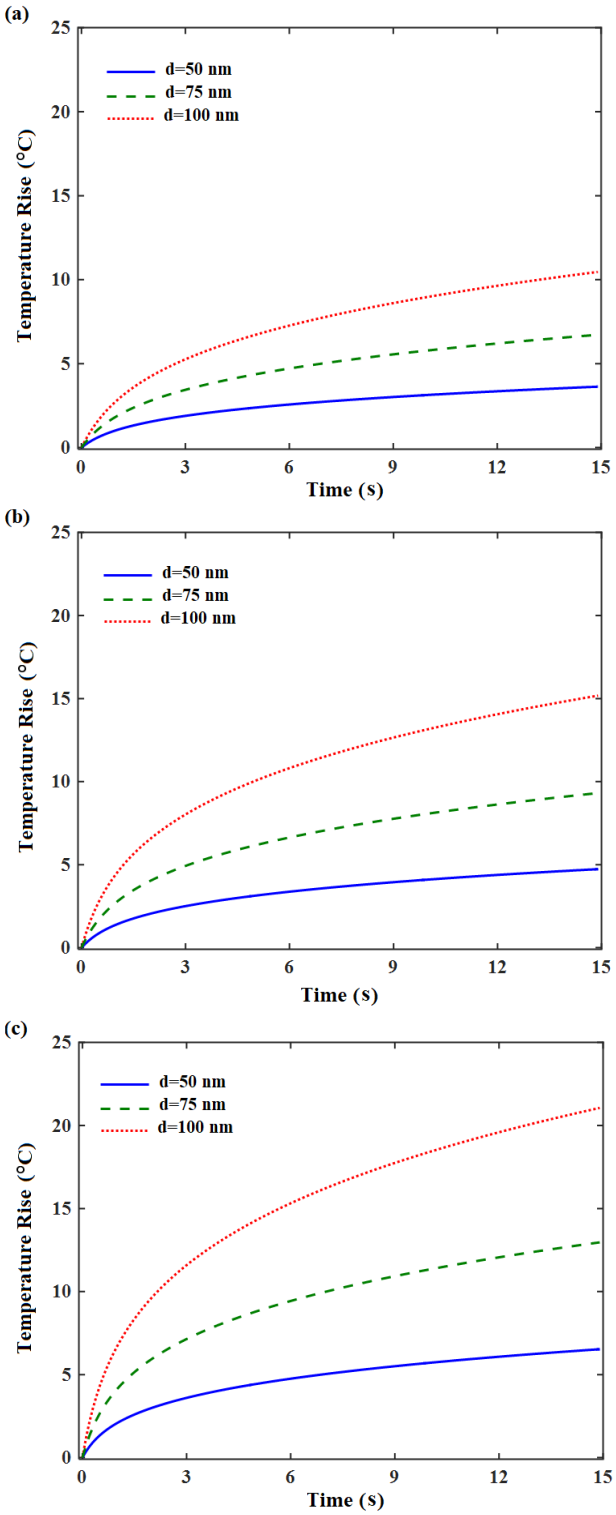

Figure 5-20 Temperature rise profile at focal point for phantoms with different sizes of MNPs derived by numerical modeling when $P = 8\,W$ and ultrasonic frequency was **(a)** $1\,MHz$, **(b)** $1.15\,MHz$, **(c)** $1.3\,MHz$.

Using theoretical models, it can be concluded that the absorption coefficient is maximum when the depths of thermal and shear wave layers generated at the surface of NPs due to their oscillation are equal to the particle size [103, 108].

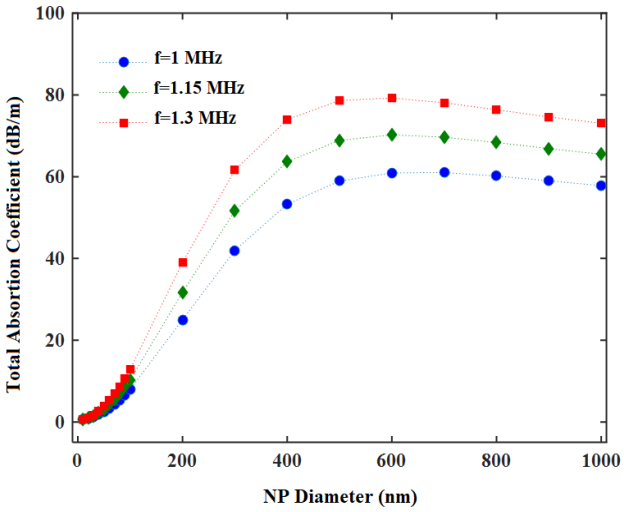

Figure 5-21 Total absorption coefficient versus NP diameter for different ultrasonic frequencies, when volume concentration of 0.75% was used.

5.2.4. CNT-Enhanced HIFU

This subsection presents the results achieved from the experimental observations on the feasibility of using CNTs as ultrasound absorption agents during the HIFU thermal treatment and their effects on the HIFU parameters.

5.2.4.1. Temperature Rise

Figure 5-22 shows the temperature rise profiles at the focal point versus time during the insonation and cooling periods for various concentration of CNTs. As it can be seen from Figure 5-22(a), the HIFU insonation with the ultrasonic field of 4.5 W power and 1.3 MHz frequency induced temperature rises of 2.5 ± 0.3 ℃, 2.8 ± 0.4 ℃, and 4.5 ± 0.4 ℃ for the CNT concentrations of 0.25%, 0.5% and 1%, respectively. It is evident that the enhancing effects of CNTs on rising

temperature was attained by increasing the CNT concentration. From Figure 5-22(b) for the power of 12.5 W and frequency of 1.3 MHz, maximum temperature rises of 6.2 ± 0.2 ℃, 7.9 ± 0.5 ℃, and 11.9 ± 0.2 ℃ were observed for the CNT concentrations of $0.25\%, 0.5\%$ and 1%, respectively. A comparison between Figure 5-22(a) and Figure 5-22(b) shows the enhancing effects of power on the performance of CNTs in rising temperature during the HIFU insonation. Additionally, the thermal diagrams form Figure 5-22(b) and Figure 5-22(c) show the effects of ultrasonic frequency on the performance of CNTs. As we can see, the increase of ultrasonic frequency from 1 to 1.3 MHz enhanced the maximum temperature rise during the insonation by nearly 4.3 ℃, 5.1 ℃, and 7.3 ℃ for the CNT concentrations of $0.25\%, 0.5\%$ and 1%, respectively.

The effects of ultrasonic field during the CNT-enhanced HIFU are presented in Figure 5-23 in more detail. Figure 5-23(a) shows the temperature rise monitored at the end of the insonation versus power for various CNT concentrations when the ultrasonic frequency was set at 1.3 MHz. As we can see, the maximum temperature rise at the focal point was enhanced by increasing the power; a close observation of temperature bars indicates a nonlinear trend between temperature rise and power in the presence of CNTs. Considering the phantom with CNT concentration of 1% as an example, the increase of power from 2 to 4.5 W enhanced the maximum temperature rise 1.5 times, whereas the relative enhancement of temperature rise was about 2.2 times for the power of 8 W when comparing with 4.5 W.

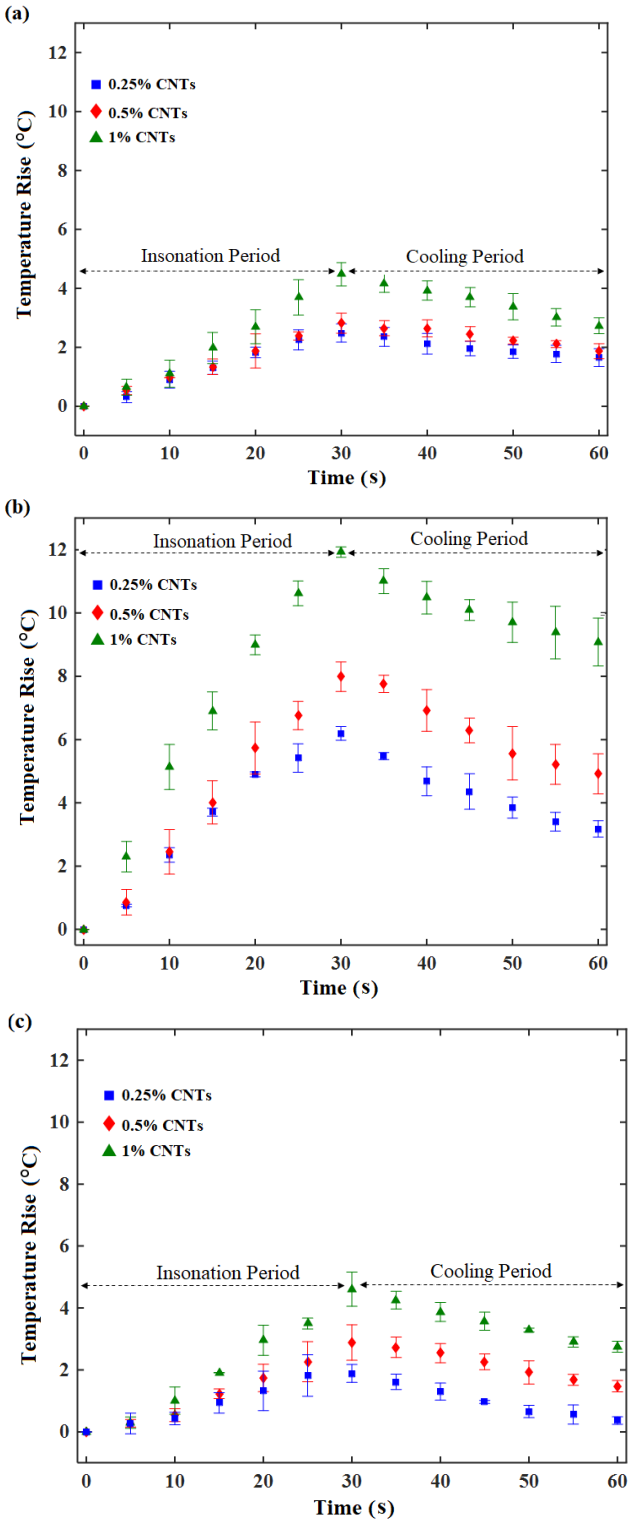

Figure 5-22 Temperature rise diagram during the HIFU insonation for phantoms with different concentrations of CNTs for ultrasonic field of **(a)** $f = 1.3\ MHz, P = 4.5\ W$; **(b)** $f = 1.3\ MHz, P = 12.5\ W$; **(c)** $f = 1\ MHz, P = 12.5\ W$.

Similarly, Figure 5-23(b) displays the maximum temperature rise versus the frequency when the power was 12.5 W. It is evident that the performance of CNTs in rising temperature during HIFU was enhanced by increasing the frequency of ultrasonic field. For example, the maximum temperature rises of 2.8 ± 0.6 ℃, 3.2 ± 0.1 ℃, 4.1 ± 0.7 ℃, and 7.9 ± 0.4 ℃ were monitored at the focal point of phantom with CNT concentration of 0.5% when the frequencies were 1, 1.1, 1.2, and 1.3 MHz, respectively.

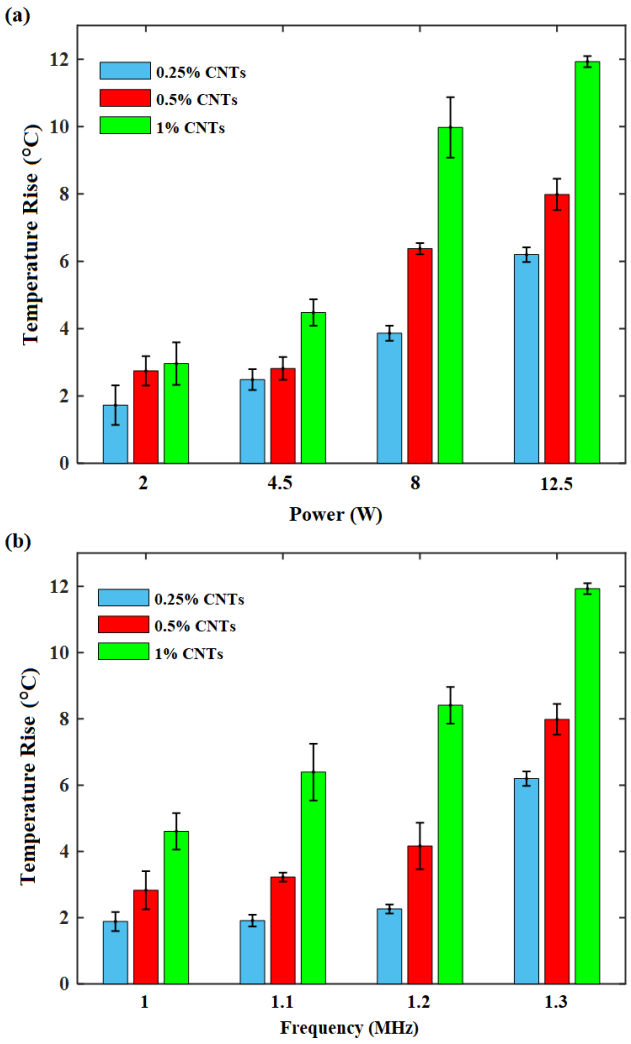

Figure 5-23 Maximum temperature rises versus **(a)** power with the ultrasonic frequency of 1.3 MHz **(b)** ultrasonic frequency with the power of 8 W ; for phantoms with different concentrations of CNTs.

All thermal diagrams have shown the enhancing effects of CNTs on the HIFU thermal treatment by increasing the temperature rise. To examine the performance of CNTs in comparison to MNPs (a well-known effective agents for HIFU), Table 5-1 shows the temperature rise after 15 seconds insonation with respect to the power. The temperature data are presented for various concentrations of CNTs and MNPs when the ultrasonic frequency was set at 1.3 MHz. As it can be seen, CNTs have less effects on rising temperature during the HIFU compared to MNPs for all ranges of powers. Considering the phantoms with concentration of 0.5% as an example, the HIFU insonation with the power of 8 W caused nearly 5 times higher temperature rise in the phantom with MNPs than that with CNTs.

Table 5-1 Temperature rise after 15 seconds of insonation with US frequency of 1.3 MHz for CNTs in comparison with MNPs.

Power (W)	Temperature rise (℃)			
	$\varphi = 0.5\%$		$\varphi = 1\%$	
	MNPs	CNTs	MNPs	CNTs
2	5.05 ± 0.36	1.2 ± 0.48	10.07 ± 0.79	1.78 ± 0.63
4.5	10.16 ± 0.77	1.5 ± 0.28	21.59 ± 0.61	1.98 ± 0.53
8	15.6 ± 1.18	3.20 ± 0.25	30.92 ± 0.57	5.1 ± 0.61

5.2.4.2.Discussion

The enhancing effects of CNTs on the heating mechanism of HIFU might result from the transport processes occurring at the boundaries of CNTs with suspending medium [113–115]. The propagation of ultrasonic waves causes the relative motion of CNTs with respect to the medium's particles, resulting in the generation of shear waves around the CNTs due to the density difference at their boundary and corresponding viscous properties. As a result, the interaction mechanism between ultrasonic and shear waves leads to the higher absorption of acoustic energy through the propagation and consequently higher rise in temperature [114]. In another mechanism, CNTs'

motion results in a temperature gradient around the CNTs due to their oscillation under an acoustic pressure field, causing a heat flux in direction of wave propagation and consequently a rise in temperature. Additionally, the temperature gradient generated at the boundaries of CNTs during HIFU forms thermal waves at that area in which their interaction with ultrasonic waves induces the higher absorption of acoustic energy and consequently higher rise of temperature [114].

These thermal mechanisms which occurs at the boundaries of CNTs depend on the features of CNTs such that the increase of concentration can enhance the conversion rate of acoustic energy to heat and consequent temperature rise at focused region, as also reported in the experimental measurements in Figure 5-23. In addition, the increase of power can enhance the amplitude of acoustic pressure and consequently the oscillating domain of CNTs, resulting in the higher temperature gradient at the boundaries of CNTs. As a result, the enhancing effect of power on the performance of CNTs is expected (Figure 5-22(a) and Figure 5-23(a)). On the other hand, the frequency of ultrasonic field can affect the performance of CNTs, as the depth of thermal and viscous waves generated at the surface of CNTs can be increased with the ultrasonic frequency. As a result, it is expected that when ultrasonic waves are emitted at higher ranges of frequencies, a higher amount of acoustic energy are converted to heat and consequently higher temperature rise are monitored. The enhancing effects of frequency can also be observed from the experimental results (Figure 5-22(b) and Figure 5-23(b)). Finally, the temperature rise induced during the HIFU mediated by CNTs is related to the thermal properties of CNTs and hosting medium. Since CNTs have lower density ($2.3\ \frac{g}{cm^3}$) than MNPs ($5.17\ \frac{g}{cm^3}$), the rate of acoustic energy that absorbed by the medium with CNTs is less than that with MNPs. Therefore, it is expected that in comparison with MNPs, CNTs show less performance in enhancing the HIFU mechanism, as presented in experimental results in Table 5-1.

In addition to the improving effects of CNTs on HIFU's thermal mechanism, reported in the current study, CNTs offer other advantages which make them effective for hyperthermia treatment using HIFU [116, 117]. In fact, it has been proved clinically that the thermal mechanism of HIFU can effectively improve the anti-cancer efficacy of ionizing radiation or systemic chemotherapy regimens [1]. Therefore, HIFU may be used as an auxiliary method for chemotherapy. In addition, due to their potential to enhance the heating mechanism of HIFU, CNTs can be effective agents for carrying chemotherapeutic agents [118, 119].

The geometrical features of CNTs allow them to be used as smart agents on the nanometre scale for carrying anticancer drug, by attaching them to the outer shell or by filling CNTs with them [120]. Clinically, the chemotherapeutic drugs such as cisplatin are delivered intravenously by combining with a solvent before being administered, however, it can cause some additional adverse side effects and damaging the normal cells [121]. CNTs can be beneficial for carrying the anticancer drug because they can provide protection of both (i) a human body against toxic adverse effects from taking the drug, especially for highly toxic drugs such as those used for cancer treatments, and (ii) a chemotherapeutic drug against chemical and biochemical exposure [121]. The clinical and analytical studies have shown the potential of CNTs to transfer all three orientations of cisplatin, as an effective chemotherapeutic agent in treatment of cancer [121]. As a result, CNTs can be considered as affective agents for HIFU when used as therapeutic methods for drug delivery.

Finally, CNTs with ability to enhance the therapeutic mechanism of HIFU, may be employed as thermal sensors on a cellular level that can provide noninvasive temperature control during the HIFU thermal treatment [50, 51]. In practice, it is essential to locally control the temperature during the hyperthermia treatment to avoid ineffective treatment due to the

insufficient heating [122, 123]. In this case, CNTs can be filled with materials showing strong temperature dependencies. The feasibility of different material in conjunction with CNTs such as multi-walled CNT (MWCNT) filled with Co, Fe, CuI and single-walled CNT (SWCNT) filled with AgCl, as sensors for monitoring the temperature is reported in the literature [51].

In summary, although CNTs have not shown the effective performance as MNPs in enhancing the thermal mechanism of HIFU, their benefits for delivery of anticancer drugs and monitoring temperature during hyperthermia may make them potentially effective for the HIFU cancer treatment.

Chapter 6

Conclusion and Future Work

6.1. Summary and Conclusions

High intensity focused ultrasound (HIFU) has gained increasing attention as a noninvasive therapeutic method to treat disordered tissues, such as tumors, through a hyperthermal mechanism using ultrasonic waves. However, long treatment times and collateral damages to healthy tissues due to the use of high powers are still challenges for the clinical application of HIFU. One possible strategy to enhance the deposition efficiency of HIFU at the tumor site is to employ nanoparticles (NPs) as ultrasound absorption agents for the thermal therapy.

During the last decade, a number of studies have shown the utility of MNPs and AuNPs as potential ultrasound agents to enhance the heating mechanism of HIFU, and consequently to reduce its adverse effects. However, the exact interaction mechanism between NPs and ultrasonic waves during the NP-enhanced HIFU, leading to the higher temperature rise, has not been clearly discussed and the effects of important parameters such as NP size that can significantly affect the efficiency of therapy have not been well investigated. This thesis focused on studying the physics of NP-enhanced HIFU and examining the effects of important factors regarding the NP-enhanced focused ultrasound therapy. The main conclusions of this thesis related to NP-enhanced HIFU are as follows:

- An experimental study on tissue mimicking phantoms with similar thermo-acoustic properties to biological tissue was conducted to show the dose effects of AuNPs when injected locally to the targeted area. The results showed that the injection of AuNPs to the

focused region could significantly enhance the heating mechanism of HIFU by increasing the absorption rate of acoustic energy and the temperature rise during the HIFU insonation procedure. The results also indicated that the heating parameters of HIFU were increased with the dose of AuNPs injected to the focused region.

- An experimental analysis using phantoms with uniform distribution of MNPs was performed to examine the effects of MNP features, including the size and volume concentration, on the thermal mechanism of HIFU and to investigate the performance of MNPs when exposed to ultrasonic fields at different ranges of powers and frequencies. A set of thermal parameters including temperature rise and the rate of absorbed energy per unit volume was measured to monitor the mechanism of MNP-enhanced HIFU. Results showed that the MNPs significantly improved the thermal effect of HIFU by enhancing the rate of energy converted to heat and the temperature rise at the focal region. Moreover, it was demonstrated that the increase of MNP size and volume concentration greatly enhanced the HIFU parameters; the effects of MNPs were further improved by increasing the power and frequency of ultrasonic field.
- In an effort to better investigate the heating mechanism of HIFU enhanced by NPs, an analytical and numerical model was developed to simulate the heat transfer induced by the propagation of ultrasonic waves and their interaction with NPs. A set of differential equations governing the temperature variation during HIFU process were derived based on the Kuznetsov, Zabolotskaya and Khokhlov (KZK) equation for nonlinear ultrasound propagation, and the principle of conservation of energy for heat transfer mechanism. The accuracy of numerical model was verified by performing a series of experiments on phantoms embedded with MNPs. Based on the results from the numerical simulation and

experiments, the effects of MNPs features including the size and volume concentration on the HIFU heating mechanism were examined. The results indicated that the transport processes taking place at the boundaries between NPs and surrounding medium play the major role in the temperature rise during HIFU sonication. Besides, the results suggested that the effects of MNPs on rising temperature were improved by amplifying the power and frequency as well as by increasing the MNP concentration and size. Finally, a quantitative comparison with experimental results demonstrated the potential of the numerical model to accurately predict the heating mechanism of HIFU mediated by NPs.

- Finally, an experimental study on tissue phantoms embedded with CNTs was conducted to assess the utility of CNTs during HIFU to enhance heating at low powers, and consequently to reduce its adverse effects. A set of thermal parameters was monitored to examine the performance of CNTs when exposed to ultrasonic fields with different ranges of powers and ultrasonic frequencies. The results showed the improving effects of CNTs on the HIFU thermal ablation by increasing the absorption rate of acoustic energy and temperature rise.

6.2. Research Limitations

In this PhD work, a numerical and experimental study of NP- enhanced HIFU was conducted; however, the current work includes several limitations, listed below:

- The experiments were conducted using in vitro setup using agar-based phantoms which were highly idealized; therefore, the results provided in this work are not directly transferrable to in vivo treatments.
- The numerical modeling was developed based on a simplified model where a homogenous medium was assumed for simulating the biological tissue. Therefore, the developed numerical model is not able to simulate the heating mechanism of HIFU

during clinical applications where medium is inhomogeneous tissue. To this end, exact structure and inhomogeneity of the biological tissue, as well as the distribution of NPs inside the targeted tissue should be well defined to develop the numerical modeling for clinical applications.

- The acoustic properties of the phantom developed for the current studies were not directly measured and calibrated in the lab; instead, the values reported in the literature were used for the numerical modeling.
- In the numerical modeling to simulate the experiments, the power monitored by the amplifier was considered as the acoustic boundary condition in pressure calculation; however, the power generated by RF amplifier circuit was electrical power which is generally higher than the actual acoustic power emitted from the transducer's surface.
- To monitor the thermal mechanism of HIFU in the phantom, an *in situ* temperature measurement using a needle thermocouple was conducted. However, this method might have resulted in some artifact effects and consequently some errors in temperature measurements.

6.3. Future Work

This section proposes the potential directions which can be targeted for further investigations on the topic of this research:

- Studying the effects of NP features including the size and volume concentration on the cavitation mechanism of HIFU by measuring the cavitation threshold, i.e. minimum pressure amplitude required to initiate the cavitation phenomenon.

- Further investigation on the feasibility of using CNTs during the HIFU treatment by examining the effects of CNT features on the thermal and cavitation mechanisms of HIFU.
- Studying the utility of using CNTs filled with the appropriate sensor materials such as Co, Fe, and CuI for monitoring the thermal mechanism of HIFU and examining the performance of those developed nanoscale agents in therapeutic mechanism of HIFU.
- Studying the feasibility of using CNTs in conjunction with HIFU for drug delivery to the brain. In the proposed method for drug delivery, the HIFU mechanism can be employed to open Blood-Brain Barrier (BBB) and CNTs can be used as agents for carrying drugs.

Bibliography

[1] J. E. Kennedy, "High-intensity focused ultrasound in the treatment of solid tumours," *Nat. Rev. Cancer*, vol. 5, no. 4, p. 321, 2005.

[2] H. E. Cline *et al.*, "Focused US system for MR imaging-guided tumor ablation.," *Radiology*, vol. 194, no. 3, pp. 731–737, 1995.

[3] L. Zhang and Z.-B. Wang, "High-intensity focused ultrasound tumor ablation: review of ten years of clinical experience," *Front. Med. China*, vol. 4, no. 3, pp. 294–302, 2010.

[4] V. Frenkel *et al.*, "Pulsed high-intensity focused ultrasound enhances thrombolysis in an in vitro model," *Radiology*, vol. 239, no. 1, pp. 86–93, 2006.

[5] M. J. Stone *et al.*, "Pulsed-high intensity focused ultrasound enhanced tPA mediated thrombolysis in a novel in vivo clot model, a pilot study," *Thromb. Res.*, vol. 121, no. 2, pp. 193–202, 2007.

[6] C. Wright, K. Hynynen, and D. Goertz, "In vitro and in vivo high intensity focused ultrasound thrombolysis," *Invest. Radiol.*, vol. 47, no. 4, p. 217, 2012.

[7] T. Ikeda, S. Yoshizawa, N. Koizumi, M. Mitsuishi, and Y. Matsumoto, "Focused ultrasound and Lithotripsy," in *Therapeutic Ultrasound*, Springer, 2016, pp. 113–129.

[8] T. Ikeda *et al.*, "Cloud cavitation control for lithotripsy using high intensity focused ultrasound," *Ultrasound Med. Biol.*, vol. 32, no. 9, pp. 1383–1397, 2006.

[9] S. Yoshizawa, T. Ikeda, A. Ito, R. Ota, S. Takagi, and Y. Matsumoto, "High intensity focused ultrasound lithotripsy with cavitating microbubbles," *Med. Biol. Eng. Comput.*, vol. 47, no. 8, pp. 851–860, 2009.

[10] A. Burgess, K. Shah, O. Hough, and K. Hynynen, "Focused ultrasound-mediated drug delivery through the blood–brain barrier," *Expert Rev. Neurother.*, vol. 15, no. 5, pp. 477–

491, 2015.

[11] S. Dromi *et al.*, “Pulsed-high intensity focused ultrasound and low temperature–sensitive liposomes for enhanced targeted drug delivery and antitumor effect,” *Clin. cancer Res.*, vol. 13, no. 9, pp. 2722–2727, 2007.

[12] H. Grüll and S. Langereis, “Hyperthermia-triggered drug delivery from temperature-sensitive liposomes using MRI-guided high intensity focused ultrasound,” *J. Control. Release*, vol. 161, no. 2, pp. 317–327, 2012.

[13] > Gail ter Haar and C. Coussios, “High intensity focused ultrasound: physical principles and devices,” *Int. J. Hyperth.*, vol. 23, no. 2, pp. 89–104, 2007.

[14] T. J. Dubinsky, C. Cuevas, M. K. Dighe, O. Kolokythas, and J. H. Hwang, “High-intensity focused ultrasound: current potential and oncologic applications,” *Am. J. Roentgenol.*, vol. 190, no. 1, pp. 191–199, 2008.

[15] A. Blana, B. Walter, S. Rogenhofer, and W. F. Wieland, “High-intensity focused ultrasound for the treatment of localized prostate cancer: 5-year experience,” *Urology*, vol. 63, no. 2, pp. 297–300, 2004.

[16] A. Gelet, J. Y. Chapelon, R. Bouvier, C. Pangaud, and Y. Lasne, “Local control of prostate cancer by transrectal high intensity focused ultrasound therapy: preliminary results,” *J. Urol.*, vol. 161, no. 1, pp. 156–162, 1999.

[17] H. Azzouz and J. De la Rosette, “HIFU: local treatment of prostate cancer,” *eau-ebu Updat. Ser.*, vol. 4, no. 2, pp. 62–70, 2006.

[18] C.-X. Li *et al.*, “Analysis of clinical effect of high-intensity focused ultrasound on liver cancer,” *World J. Gastroenterol.*, vol. 10, no. 15, p. 2201, 2004.

[19] S. Vaezy *et al.*, “Liver hemostasis using high-intensity focused ultrasound,” *Ultrasound*

Med. Biol., vol. 23, no. 9, pp. 1413–1420, 1997.

[20] J. E. Kennedy *et al.*, "High-intensity focused ultrasound for the treatment of liver tumours," *Ultrasonics*, vol. 42, no. 1, pp. 931–935, 2004.

[21] H. Furusawa, "MRI-Guided Focused Ultrasound Surgery of Breast Cancer," in *Non-surgical Ablation Therapy for Early-stage Breast Cancer*, Springer, 2016, pp. 173–181.

[22] H. Furusawa *et al.*, "The evolving non-surgical ablation of breast cancer: MR guided focused ultrasound (MRgFUS)," *Breast cancer*, vol. 14, no. 1, pp. 55–58, 2007.

[23] F. Wu *et al.*, "Extracorporeal high intensity focused ultrasound treatment for patients with breast cancer," *Breast Cancer Res. Treat.*, vol. 92, no. 1, pp. 51–60, 2005.

[24] H. Yang *et al.*, "Non-invasive synergistic treatment of brain tumors by targeted chemotherapeutic delivery and amplified focused ultrasound-hyperthermia using magnetic nanographene oxide," *Adv. Mater.*, vol. 25, no. 26, pp. 3605–3611, 2013.

[25] N. McDannold, G. T. Clement, P. Black, F. Jolesz, and K. Hynynen, "Transcranial magnetic resonance imaging–guided focused ultrasound surgery of brain tumors: initial findings in 3 patients," *Neurosurgery*, vol. 66, no. 2, pp. 323–332, 2010.

[26] Z. Ram *et al.*, "Magnetic resonance imaging-guided, high-intensity focused ultrasound forbrain tumortherapy," *Neurosurgery*, vol. 59, no. 5, pp. 949–956, 2006.

[27] W. Chen *et al.*, "Primary bone malignancy: effective treatment with high-intensity focused ultrasound ablation," *Radiology*, vol. 255, no. 3, pp. 967–978, 2010.

[28] C. Li, W. Zhang, W. Fan, J. Huang, F. Zhang, and P. Wu, "Noninvasive treatment of malignant bone tumors using high-intensity focused ultrasound," *Cancer*, vol. 116, no. 16, pp. 3934–3942, 2010.

[29] M. Huisman *et al.*, "Feasibility of volumetric MRI-guided high intensity focused

ultrasound (MR-HIFU) for painful bone metastases," *J. Ther. ultrasound*, vol. 2, no. 1, p. 16, 2014.

[30] R. O. Illing *et al.*, "The safety and feasibility of extracorporeal high-intensity focused ultrasound (HIFU) for the treatment of liver and kidney tumours in a Western population," *Br. J. Cancer*, vol. 93, no. 8, p. 890, 2005.

[31] J. B. ADAMS, R. G. MOORE, J. H. ANDERSON, J. D. STRANDBERG, F. F. MARSHALL, and L. R. DAVOUSSI, "High-intensity focused ultrasound ablation of rabbit kidney tumors," *J. Endourol.*, vol. 10, no. 1, pp. 71–75, 1996.

[32] M. Marberger, G. Schatzl, D. Cranston, and J. E. Kennedy, "Extracorporeal ablation of renal tumours with high-intensity focused ultrasound," *BJU Int.*, vol. 95, pp. 52–55, 2005.

[33] J. Huang, R. G. Holt, R. O. Cleveland, and R. A. Roy, "Experimental validation of a tractable numerical model for focused ultrasound heating in flow-through tissue phantoms," *J. Acoust. Soc. Am.*, vol. 116, no. 4, pp. 2451–2458, 2004.

[34] M. A. Solovchuk, T. W. H. Sheu, M. Thiriet, and W.-L. Lin, "On a computational study for investigating acoustic streaming and heating during focused ultrasound ablation of liver tumor," *Appl. Therm. Eng.*, vol. 56, no. 1, pp. 62–76, 2013.

[35] S. B. Devarakonda, M. R. Myers, M. Lanier, C. Dumoulin, and R. K. Banerjee, "Assessment of gold nanoparticle-mediated-enhanced hyperthermia using mr-guided high-intensity focused ultrasound ablation procedure," *Nano Lett.*, vol. 17, no. 4, pp. 2532–2538, 2017.

[36] H. Furusawa *et al.*, "Magnetic resonance–guided focused ultrasound surgery of breast cancer: reliability and effectiveness," *J. Am. Coll. Surg.*, vol. 203, no. 1, pp. 54–63, 2006.

[37] J.-J. Li *et al.*, "Complications of high intensity focused ultrasound in patients with

recurrent and metastatic abdominal tumors," *World J. Gastroenterol. WJG*, vol. 13, no. 19, p. 2747, 2007.

[38] K. Kaczmarek, T. Hornowski, M. Kubovčíková, M. Timko, M. Koralewski, and A. Józefczak, "Heating Induced by Therapeutic Ultrasound in the Presence of Magnetic Nanoparticles," *ACS Appl. Mater. Interfaces*, vol. 10, no. 14, pp. 11554–11564, 2018.

[39] D. Kessel, R. Jeffers, J. B. Fowlkes, and C. Cain, "Porphyrin-induced enhancement of ultrasound cytotoxicity," *Int. J. Radiat. Biol.*, vol. 66, no. 2, pp. 221–228, 1994.

[40] S.-Q. Cheng, X.-D. Zhou, Z.-Y. Tang, Y. Yu, S.-S. Bao, and D.-C. Qian, "Iodized oil enhances the thermal effect of high-intensity focused ultrasound on ablating experimental liver cancer," *J. Cancer Res. Clin. Oncol.*, vol. 123, no. 11–12, pp. 639–644, 1997.

[41] Y. Kaneko *et al.*, "Use of a microbubble agent to increase the effects of high intensity focused ultrasound on liver tissue," *Eur. Radiol.*, vol. 15, no. 7, pp. 1415–1420, 2005.

[42] S. A. R. Dibaji, M. F. Al-Rjoub, M. R. Myers, and R. K. Banerjee, "Enhanced heat transfer and thermal dose using magnetic nanoparticles during HIFU thermal ablation—an in-vitro study," *J. Nanotechnol. Eng. Med.*, vol. 4, no. 4, p. 40902, 2013.

[43] E. S. Day, J. G. Morton, and J. L. West, "Nanoparticles for thermal cancer therapy," *J. Biomech. Eng.*, vol. 131, no. 7, p. 74001, 2009.

[44] D. K. Kirui, D. A. Rey, and C. A. Batt, "Gold hybrid nanoparticles for targeted phototherapy and cancer imaging," *Nanotechnology*, vol. 21, no. 10, p. 105105, 2010.

[45] J. R. McLaughlan, D. M. J. Cowell, and S. Freear, "Gold nanoparticle nucleated cavitation for enhanced high intensity focused ultrasound therapy," *Phys. Med. Biol.*, vol. 63, no. 1, p. 15004, 2017.

[46] S. B. Devarakonda, M. R. Myers, and R. K. Banerjee, "Comparison of Heat Transfer

Enhancement Between Magnetic and Gold Nanoparticles During HIFU Sonication," *J. Biomech. Eng.*, vol. 140, no. 8, p. 81003, 2018.

[47] Y. Sun *et al.*, "Evaluation of superparamagnetic iron oxide-polymer composite microcapsules for magnetic resonance-guided high-intensity focused ultrasound cancer surgery," *BMC Cancer*, vol. 14, no. 1, p. 800, 2014.

[48] M. J. Ernsting, M. Murakami, A. Roy, and S.-D. Li, "Factors controlling the pharmacokinetics, biodistribution and intratumoral penetration of nanoparticles," *J. Control. Release*, vol. 172, no. 3, pp. 782–794, 2013.

[49] A. J. Giustini, R. Ivkov, and P. J. Hoopes, "Magnetic nanoparticle biodistribution following intratumoral administration," *Nanotechnology*, vol. 22, no. 34, p. 345101, 2011.

[50] A. Vyalikh *et al.*, "A nanoscaled contactless thermometer for biological systems," *Phys. status solidi*, vol. 244, no. 11, pp. 4092–4096, 2007.

[51] R. Klingeler, S. Hampel, and B. Büchner, "Carbon nanotube based biomedical agents for heating, temperature sensoring and drug delivery," *Int. J. Hyperth.*, vol. 24, no. 6, pp. 496–505, 2008.

[52] M. Thanou and W. Gedroyc, "MRI-guided focused ultrasound as a new method of drug delivery," *J. Drug Deliv.*, vol. 2013, 2013.

[53] J. E. Kennedy, G. R. Ter Haar, and D. Cranston, "High intensity focused ultrasound: surgery of the future?," *Br. J. Radiol.*, vol. 76, no. 909, pp. 590–599, 2003.

[54] S. Vaezy *et al.*, "Real-time visualization of high-intensity focused ultrasound treatment using ultrasound imaging," *Ultrasound Med. Biol.*, vol. 27, no. 1, pp. 33–42, 2001.

[55] G. R. Ter, R. L. Clarke, M. G. Vaughan, and C. R. Hill, "Trackless surgery using focused ultrasound: technique and case report," *Minim. Invasive Ther.*, vol. 1, no. 1, pp. 13–19,

1991.

[56] J. Huang, “Heating in vascular tissue and flow-through tissue phantoms induced by focused ultrasound.” Boston University, 2002.

[57] W.-S. Chen, *Investigations on the destruction of ultrasound contrast agents: Fragmentation thresholds, inertial cavitation, and bioeffects*. 2002.

[58] F. Wu *et al.*, “Circulating tumor cells in patients with solid malignancy treated by high-intensity focused ultrasound,” *Ultrasound Med. Biol.*, vol. 30, no. 4, pp. 511–517, 2004.

[59] S. Li and P.-H. Wu, “Magnetic resonance image-guided versus ultrasound-guided high-intensity focused ultrasound in the treatment of breast cancer,” *Chin. J. Cancer*, vol. 32, no. 8, p. 441, 2013.

[60] F. Wu *et al.*, “Extracorporeal focused ultrasound surgery for treatment of human solid carcinomas: early Chinese clinical experience,” *Ultrasound Med. Biol.*, vol. 30, no. 2, pp. 245–260, 2004.

[61] G. ter Haar, D. Sinnett, and I. Rivens, “High intensity focused ultrasound-a surgical technique for the treatment of discrete liver tumours,” *Phys. Med. Biol.*, vol. 34, no. 11, p. 1743, 1989.

[62] S. Madersbacher, M. Pedevilla, L. Vingers, M. Susani, and M. Marberger, “Effect of high-intensity focused ultrasound on human prostate cancer in vivo,” *Cancer Res.*, vol. 55, no. 15, pp. 3346–3351, 1995.

[63] A. H. Mesiwala *et al.*, “High-intensity focused ultrasound selectively disrupts the blood-brain barrier in vivo,” *Ultrasound Med. Biol.*, vol. 28, no. 3, pp. 389–400, 2002.

[64] E. Martin, D. Jeanmonod, A. Morel, E. Zadicario, and B. Werner, “High-intensity focused ultrasound for noninvasive functional neurosurgery,” *Ann. Neurol.*, vol. 66, no. 6, pp.

858–861, 2009.

[65] D. B. Zippel and M. Z. Papa, “The use of MR imaging guided focused ultrasound in breast cancer patients; a preliminary phase one study and review,” *Breast cancer*, vol. 12, no. 1, p. 32, 2005.

[66] S. Vaezy *et al.*, “Hemostasis of punctured blood vessels using high-intensity focused ultrasound,” *Ultrasound Med. Biol.*, vol. 24, no. 6, pp. 903–910, 1998.

[67] R. W. Wood and A. L. Loomis, “XXXVIII. The physical and biological effects of high-frequency sound-waves of great intensity,” *London, Edinburgh, Dublin Philos. Mag. J. Sci.*, vol. 4, no. 22, pp. 417–436, 1927.

[68] C. H. Johnson, “The lethal effects of ultrasonic radiation,” *J. Physiol.*, vol. 67, no. 4, pp. 356–359, 1929.

[69] E. N. Harvey, “Biological aspects of ultrasonic waves, a general survey,” *Biol. Bull.*, vol. 59, no. 3, pp. 306–325, 1930.

[70] J. G. Lynn and T. J. Putnam, “Histology of cerebral lesions produced by focused ultrasound,” *Am. J. Pathol.*, vol. 20, no. 3, p. 637, 1944.

[71] W. J. Fry, W. H. Mosberg Jr, J. W. Barnard, and F. J. Fry, “Production of focal destructive lesions in the central nervous system with ultrasound,” *J. Neurosurg.*, vol. 11, no. 5, pp. 471–478, 1954.

[72] I. Khan, K. Saeed, and I. Khan, “Nanoparticles: Properties, applications and toxicities,” *Arab. J. Chem.*, 2017.

[73] I. Brigger, C. Dubernet, and P. Couvreur, “Nanoparticles in cancer therapy and diagnosis,” *Adv. Drug Deliv. Rev.*, vol. 64, pp. 24–36, 2012.

[74] L. R. Hirsch *et al.*, “Nanoshell-mediated near-infrared thermal therapy of tumors under

magnetic resonance guidance," *Proc. Natl. Acad. Sci.*, vol. 100, no. 23, pp. 13549–13554, 2003.

[75] L. C. Kennedy *et al.*, "A new era for cancer treatment: gold-nanoparticle-mediated thermal therapies," *Small*, vol. 7, no. 2, pp. 169–183, 2011.

[76] R. Bazak, M. Houri, S. El Achy, W. Hussein, and T. Refaat, "Passive targeting of nanoparticles to cancer: A comprehensive review of the literature," *Mol. Clin. Oncol.*, vol. 2, no. 6, pp. 904–908, 2014.

[77] A. K. Iyer, G. Khaled, J. Fang, and H. Maeda, "Exploiting the enhanced permeability and retention effect for tumor targeting," *Drug Discov. Today*, vol. 11, no. 17–18, pp. 812–818, 2006.

[78] A. Sohail, Z. Ahmad, O. A. Bég, S. Arshad, and L. Sherin, "A review on hyperthermia via nanoparticle-mediated therapy," *Bull. Cancer*, vol. 104, no. 5, pp. 452–461, 2017.

[79] A. Jordan, R. Scholz, P. Wust, H. Fähling, and R. Felix, "Magnetic fluid hyperthermia (MFH): Cancer treatment with AC magnetic field induced excitation of biocompatible superparamagnetic nanoparticles," *J. Magn. Magn. Mater.*, vol. 201, no. 1–3, pp. 413–419, 1999.

[80] S. Laurent, S. Dutz, U. O. Häfeli, and M. Mahmoudi, "Magnetic fluid hyperthermia: focus on superparamagnetic iron oxide nanoparticles," *Adv. Colloid Interface Sci.*, vol. 166, no. 1–2, pp. 8–23, 2011.

[81] G. Vallejo-Fernandez *et al.*, "Mechanisms of hyperthermia in magnetic nanoparticles," *J. Phys. D. Appl. Phys.*, vol. 46, no. 31, p. 312001, 2013.

[82] J.-L. Li and M. Gu, "Gold-nanoparticle-enhanced cancer photothermal therapy," *IEEE J. Sel. Top. quantum Electron.*, vol. 16, no. 4, pp. 989–996, 2009.

[83] G. S. Terentyuk *et al.*, “Laser-induced tissue hyperthermia mediated by gold nanoparticles: toward cancer phototherapy,” *J. Biomed. Opt.*, vol. 14, no. 2, p. 21016, 2009.

[84] N. S. Abadeer and C. J. Murphy, “Recent progress in cancer thermal therapy using gold nanoparticles,” *J. Phys. Chem. C*, vol. 120, no. 9, pp. 4691–4716, 2016.

[85] E. S. Glazer *et al.*, “Noninvasive radiofrequency field destruction of pancreatic adenocarcinoma xenografts treated with targeted gold nanoparticles,” *Clin. Cancer Res.*, vol. 16, no. 23, pp. 5712–5721, 2010.

[86] K. P. Tamarov *et al.*, “Radio frequency radiation-induced hyperthermia using Si nanoparticle-based sensitizers for mild cancer therapy,” *Sci. Rep.*, vol. 4, no. 1, pp. 1–7, 2014.

[87] M. J. Smith, V. H. B. Ho, N. J. Darton, and N. K. H. Slater, “Effect of magnetite nanoparticle agglomerates on ultrasound induced inertial cavitation,” *Ultrasound Med. Biol.*, vol. 35, no. 6, pp. 1010–1014, 2009.

[88] V. H. B. Ho, M. J. Smith, and N. K. H. Slater, “Effect of magnetite nanoparticle agglomerates on the destruction of tumor spheroids using high intensity focused ultrasound,” *Ultrasound Med. Biol.*, vol. 37, no. 1, pp. 169–175, 2011.

[89] Y. Sun *et al.*, “Superparamagnetic PLGA-iron oxide microcapsules for dual-modality US/MR imaging and high intensity focused US breast cancer ablation,” *Biomaterials*, vol. 33, no. 24, pp. 5854–5864, 2012.

[90] Y. You *et al.*, “Nanoparticle-enhanced synergistic HIFU ablation and transarterial chemoembolization for efficient cancer therapy,” *Nanoscale*, vol. 8, no. 7, pp. 4324–4339, 2016.

[91] D. Coluccia *et al.*, “Enhancing glioblastoma treatment using cisplatin-gold-nanoparticle conjugates and targeted delivery with magnetic resonance-guided focused ultrasound,” *Nanomedicine Nanotechnology, Biol. Med.*, vol. 14, no. 4, pp. 1137–1148, 2018.

[92] W. J. Fry and R. B. Fry, “Determination of absolute sound levels and acoustic absorption coefficients by thermocouple probes—Theory,” *J. Acoust. Soc. Am.*, vol. 26, no. 3, pp. 294–310, 1954.

[93] W. J. Fry and R. B. Fry, “Determination of absolute sound levels and acoustic absorption coefficients by thermocouple probes—experiment,” *J. Acoust. Soc. Am.*, vol. 26, no. 3, pp. 311–317, 1954.

[94] P. P. Lele, “A simple method for production of trackless focal lesions with focused ultrasound: physical factors,” *J. Physiol.*, vol. 160, no. 3, pp. 494–512, 1962.

[95] K. J. Parker, “Effects of heat conduction and sample size on ultrasonic absorption measurements,” *J. Acoust. Soc. Am.*, vol. 77, no. 2, pp. 719–725, 1985.

[96] H. H. Pennes, “Analysis of tissue and arterial blood temperatures in the resting human forearm,” *J. Appl. Physiol.*, vol. 1, no. 2, pp. 93–122, 1948.

[97] S. Weinbaum, L. M. Jiji, and D. E. Lemons, “Theory and experiment for the effect of vascular microstructure on surface tissue heat transfer—Part I: Anatomical foundation and model conceptualization,” 1984.

[98] H. Arkin, L. X. Xu, and K. R. Holmes, “Recent developments in modeling heat transfer in blood perfused tissues,” *IEEE Trans. Biomed. Eng.*, vol. 41, no. 2, pp. 97–107, 1994.

[99] J. Crezee and J. J. W. Lagendijk, “Experimental verification of bioheat transfer theories: measurement of temperature profiles around large artificial vessels in perfused tissue,” *Phys. Med. Biol.*, vol. 35, no. 7, p. 905, 1990.

[100] E. G. Moros, A. W. Dutton, R. B. Roemer, M. Burton, and K. Hynynen, “Experimental evaluation of two simple thermal models using hyperthermia in muscle in vivo,” *Int. J. Hyperth.*, vol. 9, no. 4, pp. 581–598, 1993.

[101] M. C. Kolios, M. D. Sherar, and J. W. Hunt, “Blood flow cooling and ultrasonic lesion formation,” *Med. Phys.*, vol. 23, no. 7, pp. 1287–1298, 1996.

[102] F. P. Curra, P. D. Mourad, V. A. Khokhlova, R. O. Cleveland, and L. A. Crum, “Numerical simulations of heating patterns and tissue temperature response due to high-intensity focused ultrasound,” *IEEE Trans. Ultrason. Ferroelectr. Freq. Control*, vol. 47, no. 4, pp. 1077–1089, 2000.

[103] C. Bera, S. B. Devarakonda, V. Kumar, A. K. Ganguli, and R. K. Banerjee, “The mechanism of nanoparticle-mediated enhanced energy transfer during high-intensity focused ultrasound sonication,” *Phys. Chem. Chem. Phys.*, vol. 19, no. 29, pp. 19075–19082, 2017.

[104] T. G. Leighton, “What is ultrasound?,” *Prog. Biophys. Mol. Biol.*, vol. 93, no. 1–3, pp. 3–83, 2007.

[105] L. E. Kinsler, A. R. Frey, A. B. Coppens, and J. V Sanders, “Fundamentals of acoustics,” *Fundam. Acoust. 4th Ed. by Lawrence E. Kinsler, Austin R. Frey, Alan B. Coppens, James V. Sanders, pp. 560. ISBN 0-471-84789-5. Wiley-VCH, December 1999.*, p. 560, 1999.

[106] V. F. Humphrey, “Ultrasound and matter—Physical interactions,” *Prog. Biophys. Mol. Biol.*, vol. 93, no. 1–3, pp. 195–211, 2007.

[107] M. F. Hamilton and D. T. Blackstock, *Nonlinear acoustics*, vol. 1. Academic press San Diego, 1998.

[108] J. R. Allegra and S. A. Hawley, “Attenuation of sound in suspensions and emulsions:

Theory and experiments," *J. Acoust. Soc. Am.*, vol. 51, no. 5B, pp. 1545–1564, 1972.

[109] F. P. Incropera, A. S. Lavine, T. L. Bergman, and D. P. DeWitt, *Fundamentals of heat and mass transfer*. Wiley, 2007.

[110] J. E. Soneson, "A user-friendly software package for HIFU simulation," in *AIP Conference Proceedings*, 2009, vol. 1113, no. 1, pp. 165–169.

[111] C. R. Dillon, U. Vyas, A. Payne, D. A. Christensen, and R. B. Roemer, "An analytical solution for improved HIFU SAR estimation," *Phys. Med. Biol.*, vol. 57, no. 14, p. 4527, 2012.

[112] K. Hynynen, C. J. Martin, D. J. Watmough, and J. R. Mallard, "Errors in temperature measurement by thermocouple probes during ultrasound induced hyperthermia," *Br. J. Radiol.*, vol. 56, no. 672, pp. 969–970, 1983.

[113] M. Ayub, A. C. Zander, C. Q. Howard, and B. S. Cazzolato, "A review of acoustic absorption mechanisms of nanoscopic fibres," *Proc. Acoust. 2011*, pp. 2–4, 2011.

[114] M. Ayub, A. C. Zander, D. M. Huang, C. Q. Howard, and B. S. Cazzolato, "Molecular dynamics simulations of acoustic absorption by a carbon nanotube," *Phys. Fluids*, vol. 30, no. 6, p. 66101, 2018.

[115] M. Ayub *et al.*, "Acoustic absorption behaviour of carbon nanotube arrays," in *Inter-noise and Noise-Con congress and conference proceedings*, 2014, vol. 249, no. 7, pp. 929–938.

[116] R. Singh and S. V Torti, "Carbon nanotubes in hyperthermia therapy," *Adv. Drug Deliv. Rev.*, vol. 65, no. 15, pp. 2045–2060, 2013.

[117] C. Iancu and L. Mocan, "Advances in cancer therapy through the use of carbon nanotube-mediated targeted hyperthermia," *Int. J. Nanomedicine*, vol. 6, p. 1675, 2011.

[118] T. A. Hilder and J. M. Hill, "Carbon nanotubes as drug delivery nanocapsules," *Curr.*

Appl. Phys., vol. 8, no. 3–4, pp. 258–261, 2008.

[119] L. Lacerda, S. Raffa, M. Prato, A. Bianco, and K. Kostarelos, "Cell-penetrating CNTs for delivery of therapeutics," *Nano Today*, vol. 2, no. 6, pp. 38–43, 2007.

[120] Z. Liu, S. Tabakman, K. Welsher, and H. Dai, "Carbon nanotubes in biology and medicine: in vitro and in vivo detection, imaging and drug delivery," *Nano Res.*, vol. 2, no. 2, pp. 85–120, 2009.

[121] T. A. Hilder and J. M. Hill, "Modelling the encapsulation of the anticancer drug cisplatin into carbon nanotubes," *Nanotechnology*, vol. 18, no. 27, p. 275704, 2007.

[122] N. McDannold, K. Hynynen, and F. Jolesz, "MRI monitoring of the thermal ablation of tissue: effects of long exposure times," *J. Magn. Reson. Imaging*, vol. 13, no. 3, pp. 421–427, 2001.

[123] L. Curiel, R. Chopra, and K. Hynynen, "In vivo monitoring of focused ultrasound surgery using local harmonic motion," *Ultrasound Med. Biol.*, vol. 35, no. 1, pp. 65–78, 2009.